

Copyright © by

Hwei-Kwan Hong

1970

I. ELECTRONIC STATES OF HEAVILY-DOPED
MOLECULAR CRYSTALS--NAPHTHALENE

I. THEORETICAL

II. EXPERIMENTAL

II. LOWEST SINGLET AND TRIPLET EXCITED
STATES OF PYRAZINE

Thesis by

Hwei-Kwan Hong

In Partial Fulfillment of the Requirements

For the Degree of

Doctor of Philosophy

California Institute of Technology

Pasadena, California

1970

(Submitted October 6, 1969)

For My Parents and
My Wife

ACKNOWLEDGMENTS

I wish to express my sincere thanks to Professor G. Wilse Robinson, my research advisor, for his continuous guidance and encouragement during the course of this research. His insistence on academic excellency and his creative approach to science have been a constant source of inspiration. I am especially thankful for the freedom he provides in allowing me to pursue my own interests and the compassion he shows when things get out of hand.

Discussions with other members of the group are always enjoyable. Many fruitful hours have been spent with Don Burland, Eldon Priestley, George Castro, Dave Hanson, Elliot Bernstein and last, but not least, Steve Colson. Steve and Elliot gave me my first lesson on experimental spectroscopy. Without their help, this work could never have been done.

I am also grateful to my parents and my wife who took pains to see that my studies were not interrupted by other non-scientific matters.

Members of the chemistry machine shop and glass-blowing shop were especially helpful. Special thanks go to Learco Minghetti and Erich Siegel who are always available when help is needed.

I would also like to thank Mrs. Adria Larson who typed the first draft of this manuscript. Her secretarial skill has been one of the delights of working in this group.

Financial supports from the California Institute of Technology, Army Research Office and National Science Foundation are gratefully acknowledged.

ABSTRACT

PART I

The energy spectrum of heavily-doped molecular crystals was treated in the Green's function formulation. The mixed crystal Green's function was obtained by averaging over all possible impurity distributions. The resulting Green's function, which takes the form of an infinite perturbation expansion, was further approximated by a closed form suitable for numerical calculations. The density-of-states functions and optical spectra for binary mixtures of normal naphthalene and deuterated naphthalene were calculated using the pure crystal density-of-states functions. The results showed that when the trap depth is large, two separate energy bands persist, but when the trap depth is small only a single band exists. Furthermore, in the former case it was found that the intensities of the outer Davydov bands are enhanced whereas the inner bands are weakened. Comparisons with previous theoretical calculations and experimental results are also made.

PART II

The energy states and optical spectra of heavily-doped mixed crystals are investigated. Studies are made for the following binary systems: (1) naphthalene- \underline{h}_8 and \underline{d}_8 , (2) naphthalene- \underline{h}_8 and $\alpha\underline{d}_4$, and (3) naphthalene- \underline{h}_8 and $\beta\underline{d}_1$, corresponding to strong, medium and weak perturbations. In addition to ordinary absorption spectra at 4° K,

band-to-band transitions at both 4° K and 77° K are also analyzed with emphasis on their relations to cooperative excitation and overall density-of-states functions for mixed crystals. It is found that the theoretical calculations presented in a previous paper agree generally with experiments except for cluster states observed in system (1) at lower guest concentrations. These features are discussed semi-quantitatively. As to the intermolecular interaction parameters, it is found that experimental results compare favorably with calculations based on experimental density-of-states functions but not with those based on octopole interactions or charge-transfer interactions. Previous experimental results of Sheka and the theoretical model of Broude and Rashba are also compared with present investigations.

PART III

The phosphorescence, fluorescence and absorption spectra of pyrazine- \underline{h}_4 and \underline{d}_4 have been obtained at 4° K in a benzene matrix. For comparison, those of the isotopically mixed crystal pyrazine- \underline{h}_4 in \underline{d}_4 were also taken. All these spectra show extremely sharp and well-resolved lines and reveal detailed vibronic structure.

The analysis of the weak fluorescence spectrum resolves the long-disputed question of whether one or two transitions are involved in the near-ultraviolet absorption of pyrazine. The "mirror-image relationship" between absorption and emission shows that the lowest singlet state is an allowed transition, properly designated as ${}^1B_{3u} \leftarrow {}^1A_{1g}$. The forbidden component ${}^1B_{2g}$, predicted by both

"exciton" and MO theories to be below the allowed component, must lie higher. Its exact location still remains uncertain.

The phosphorescence spectrum when compared with the excitation phosphorescence spectra, indicates that the lowest triplet state is also symmetry allowed, showing a strong 0-0 band and a "mirror-image relationship" between absorption and emission. In accordance with previous work, the triplet state is designated as ${}^3B_{3u}$.

The vibronic structure of the phosphorescence spectrum is very complicated. Previous work on the analysis of this spectrum all concluded that a long progression of ν_{6a} exists. Under the high resolution attainable in our work, the supposed ν_{6a} progression proves to have a composite triplet structure, starting from the second member of the progression. Not only is the ν_{9a} hydrogen-bending mode present as shown by the appearance of the C-D bending mode in the \underline{d}_4 spectrum, but a band of 1207 cm^{-1} in the pyrazine in benzene system and 1231 cm^{-1} in the mixed crystal system is also observed. This band is assigned as $2\nu_{6b}$ and of a_{1g} symmetry. Its anonymously strong intensity in the phosphorescence spectrum is interpreted as due to the Fermi resonance with the $2\nu_{6a}$ and ν_{9a} band.

To help resolve the present controversy over the crystal phosphorescence spectrum of pyrazine, detailed vibrational analyses of the emission spectra were made. The fluorescence spectrum has essentially the same vibronic structure as the phosphorescence spectrum.

TABLE OF CONTENTS

ACKNOWLEDGMENTS	iii
ABSTRACT	iv
PART	PAGE
I ELECTRONIC STATES OF HEAVILY-DOPED MOLECULAR CRYSTALS--NAPHTHALENE.	
I. THEORETICAL	1
1. INTRODUCTION	2
2. THEORY	6
A. Perturbation Method for Isotopically- Mixed Crystals	6
B. The Green's Function Method	14
C. The Average Green's Function	19
D. Approximate Green's Function and the Calculation of the Naphthalene Mixed Crystal Energy Spectrum	35
3. RESULTS AND DISCUSSION	40
A. Calculations Based on Experimental Density-of-States Function.	40
B. Calculations Based on the Octopole Model	49
C. Some Comments of Broude and Rashba's Model Sheka's Experiments	53
ACKNOWLEDGMENTS	55

PART	PAGE
REFERENCES	56
FIGURES	60
II ELECTRONIC STATES OF HEAVILY-DOPED MOLECULAR CRYSTALS--NAPHTHALENE.	
II. EXPERIMENTAL	96
1. INTRODUCTION	97
2. EXPERIMENTAL	99
3. RESULTS AND DISCUSSION	101
A. Absorption	101
Naphthalene- \underline{h}_8 and Naphthalene- \underline{d}_8	101
Naphthalene- \underline{h}_8 and Naphthalene- $\alpha\underline{d}_4$	110
Naphthalene- \underline{h}_8 and Naphthalene- $\beta\underline{d}_1$	114
B. Band-to-Band Transitions	116
General Discussion	116
Naphthalene- \underline{h}_8 and \underline{d}_8	120
Naphthalene- \underline{h}_8 and Naphthalene- $\alpha\underline{d}_4$	126
Naphthalene- \underline{h}_8 and Naphthalene- $\beta\underline{d}_1$	129
4. CONCLUSIONS	131
REFERENCES	132
TABLE	136
FIGURES	138
III LOWEST SINGLET AND TRIPLET EXCITED STATES OF PYRAZINE	164
1. INTRODUCTION	165

PART	PAGE
2. EXPERIMENTAL	166
3. DISCUSSION	168
A. Singlet-Triplet System	169
Position of the 0-0 Band	169
Vibrational Analysis	172
B. Singlet-Singlet System	179
REFERENCES	184
TABLES	188
FIGURES	205
PROPOSITIONS	211

PART I
ELECTRONIC STATES OF HEAVILY-DOPED
MOLECULAR CRYSTALS--NAPHTHALENE
I. THEORETICAL

(Accepted for publication in J. Chem. Phys.)

1. INTRODUCTION

The quantum states of solids are characterized by energy bands. The periodicity of the lattice requires the stationary state wavefunctions to transform like the representations of the translational group, each associated with the reduced vector \underline{k} . Solid state phenomena such as excitons,^{1, 2} phonons,³ and magnons⁴ are conveniently described within this group theoretical framework. In each case, the quasimomentum $\hbar\underline{k}$ is always a good quantum number and is suitable for the description of energy systematics. On the other hand, many important physical systems, such as doped molecular crystals, alloys, copolymers, and some important biological macromolecules do not possess translational symmetry. The studies of their physical properties are usually hindered by the lack of symmetry. However, when the system does not deviate too much from a periodic system, theoretical analysis can usually be carried out by setting up the stationary state wavefunctions for the periodic system and, then, allowing them to mix when the imperfection is introduced. One of the simplest systems for which this perturbation technique can be utilized is the system of isotopically mixed molecular crystals.

In the discussion of mixed molecular crystals, two different cases can be distinguished: (a) infinitely-dilute mixed crystals and (b) heavily-doped mixed crystals. Case (a) has been studied extensively during the last decade both in theory and experiment. Experiments have been performed to study exciton trapping,^{5, 6} exciton migration,⁷ and, more fundamentally, the intermolecular interactions

that are responsible for the entire exciton band structure.⁸ Considerable theoretical work,⁹⁻¹⁹ mostly based on Koster and Slater's²⁰⁻²² formulation, was also carried out. This study was facilitated by the fact that, at very low concentrations of impurities, guest-guest interactions can be neglected. In the absence of such interactions, the exact site occupied by the impurity need not be specified and thus the disorder is actually minimized in this case.

For case (b), the designation of guest and host is no longer very meaningful. Interactions between like molecules must now be taken into account. The situation is further complicated by the fact that the Hamiltonian of the system is only defined in an average sense. The ordering of the guests (or conversely, the ordering of the hosts) affects the energy spectrum of the system. A complete analysis would have to involve a statistical averaging of all the possible configurations.

Previous work on case (b) is rather limited compared with case (a). Broude and Rashba's method,²³ which is based on the assumption that like molecules at like sites have the same excitation amplitude is expected to be useful only for equimolecular admixtures. Craig and Philpott's¹³⁻¹⁵ super-lattice method, while mathematically more manageable, is limited by the size of the super-cell that can be handled. Since a finite number of molecules are treated, a finite number of states are obtained. In addition only discrete compositions can be considered. In order to approach the true situation, the super-cell has to be enormously large. The most serious drawback to the latter approach seems to rest with the basic assumption that impurities are arranged on a super-lattice in translationally equivalent sets. This

immediately leaves out all the aperiodic distributions in the averaging process. When attempts are made to remedy this situation, and bigger cells are chosen, the problem becomes computationally intractable. In actual numerical calculations, Craig and Philpott calculated only the $\underline{k} = \underline{0}$ component of the density of states for naphthalene- \underline{h}_8 and \underline{d}_8 . They did not treat spectra involving shallower energy gaps.

The only experiments to date on concentrated mixed crystals have been those of Broude and Rashba²³ and Sheka^{24, 25} on benzenes and naphthalenes, respectively. Sheka's experiments were carried out at 22° K. The spectra obtained were rather broad and some of the fine structure caused by "cluster states" typically observed in the spectra of certain mixed crystals became obscure. Furthermore, in this work weighed samples with known concentrations were not used. Rather Broude and Rashba's approximate formula was fit to the spectra in order to determine the concentrations. Thus, on the experimental side, additional work using weighed samples at lower temperatures seems desirable.

In Part I of this series, we consider the general formulation for isotopically-mixed crystals with various compositions, using the Green's function method. Exact expressions for the mixed crystal Green's function are presented in terms of an infinite perturbation expansion. An approximate formula in closed form suitable for actual numerical calculations is also given and applied specifically to the mixed crystals of naphthalenes with different trap depths. Density-of-states functions and optical spectra for the mixed crystals were calculated using two different sets of pure crystal density-of-states functions,

one based on Craig and Walmsley's²⁶ octopole model and the other experimentally determined by Colson et al.²⁷ In Part II new experimental data on the absorption spectra and emission spectra at different temperatures will be analyzed and discussed in the light of the theoretical model.

The purpose of the present work is many-fold: (a) As a prototype of disordered systems, heavily-doped mixed crystals present a physically amenable system for more or less exact treatment. Understanding the electronic states of this system is the first step toward the understanding of more complicated disordered systems. (b) A unified theory connecting the electronic states and optical properties of pure crystals on the one hand and infinitely-dilute mixed crystals on the other is long overdue. The present investigation will, hopefully, help fill the gap. (c) Heavily-doped mixed crystals provide additional detailed information concerning the guest-guest interactions in molecular crystals. An exact theoretical analysis of this system not only provides a check on the gross density-of-states function but also allows the individual pairwise interactions to be determined. (d) These studies also provide answers to the question of whether Davydov splitting is primarily due to symmetry relations or resonance coupling, as raised frequently by some of the workers in this field.^{2b, 16}

Among the general theories of disordered solids, the multiple-scattering formulation of Lax²⁸ has been the most successful. This pioneering work was followed by the elegant mathematical analysis of Yonezawa and Matsubara²⁹ (YM). The present theoretical development

parallels closely YM's work except that their theory is generalized to the case of multiple-branched exciton bands and particularized to the problem of isotopically mixed crystals.

2. THEORY

A. Perturbation Method for Isotopically-Mixed Crystals

The system under discussion consists of two types of molecules with different excitation energies. For dilute mixed crystals, it is common practice to denote the major component as the host and the minor component as the guest. However, in the case of heavily-doped mixed crystals, the distinction between the host and the guest is not very meaningful. We will simply refer to them as the A-component and the B-component. We take the A-component to have the higher excitation energy (e. g., naphthalene with a higher degree of deuteration).

We start with the total Hamiltonian of a pure crystal composed of A-molecules.

$$H^0 = \sum_i H_i^A + \sum_{i>j} \sum V_{ij}^{AA} , \quad (1)$$

where H_i^A = the Hamiltonian of an A-molecule at site i , and V_{ij}^{AA} = the interaction between an A-molecule at site i and an A-molecule at site j .

When the B-component is introduced as an impurity, the Hamiltonian

becomes

$$H' = \sum_i H_i^A + \sum_p H_p^B + \sum_{i>j} \sum V_{ij}^{AA} + \sum_{p>q} V_{pq}^{BB} + \sum_i \sum_p V_{ip}^{AB}, \quad (2)$$

where H_i^A = the Hamiltonian of an A-molecule at site i

H_p^B = the Hamiltonian of a B-molecule at site p

V_{ij}^{AA} = the interaction between an A-molecule at site i
and an A-molecule at site j

V_{pq}^{BB} = the interaction between a B-molecule at site p
and a B-molecule at site q.

V_{ip}^{AB} = the interaction between an A-molecule at site i
and a B-molecule at site p.

We limit our discussion to the case of isotopically-mixed crystals. In this case, all the interactions between A and A, B and B, and A and B can be assumed to be equal, hence:

$$H' = \sum_i H_i^A + \sum_p H_p^B + \sum_{n>m} \sum V_{nm}, \quad (3)$$

where V_{nm} is the interaction between molecules without making a distinction between A and B.

The mixed crystal Hamiltonian can be expressed in terms of the pure crystal Hamiltonian and a perturbation:

$$H' = H^0 + \sum_p t_p, \quad (4)$$

where $t_p = H_p^B - H_p^A$ is the localized perturbation acting only on the p^{th} site occupied by the B-molecule. For isotopically-mixed crystals, the t_p 's arise primarily from the change in nuclear kinetic energy as a result of isotopic substitution. Explicitly,

$$t_p = -\frac{\hbar^2}{2} \left(\frac{1}{m_B} - \frac{1}{m_A} \right) \sum_{ip} \frac{\partial^2}{\partial x_{ip}^2}, \quad (5)$$

where m_B and m_A are the masses of isotopes (either hydrogen or deuterium) in the B-molecule and the A-molecule, respectively. The x_{ip} 's run over all the coordinates of the substituted nuclei of the molecule at site p .

In the present discussion, the zero-zero band of an electronic transition is considered as an isolated Frenkel exciton band. It has been shown¹³ that under the assumption of a localized perturbation, which is implied in Eq. (4), the introduction of isotopic impurities does not cause the mixing between different excited states if initially they are constructed properly to include possible configurational interactions. The existence of vibrational sublevels in a particular electronic state also has little effect on the pure electronic transition. In the limit of weak coupling, the vibrational spacings are certainly larger than the exciton bandwidth. Within this limit it was pointed out by several authors^{13, 16} that the one-band approximation is very likely adequate for most purposes.

The eigenfunctions of the pure crystal Hamiltonian can be constructed from site functions with Bloch symmetry:³⁰

$$\Psi(\underline{k}) = \sum_i e^{i\underline{k} \cdot \underline{R}_i} \Phi_i,$$

where $\Phi_i = \prod_{j \neq i} \phi_j^*$ is the wavefunction corresponding to the excitation localized at site i . There are as many such "site functions" as the number of molecules per unit cell. These site functions reduce the Hamiltonian matrix to small blocks characterized by their wave vectors. Further reduction within the block is not possible except in some special cases, for example, the $\underline{k} = \underline{0}$ block. However, in the limit of short-range interactions such as those encountered in molecular crystals of benzene and naphthalene, Colson et al.³⁰ have shown that the factor group operations can be applied to all the \underline{k} -blocks, and simple linear combinations of site functions can be used for all the \underline{k} -states. The approximation greatly simplifies the theoretical derivations, as will be seen later in Section 2. C. Using this approximation for the lowest excited singlet state (${}^1B_{2u}$) of the naphthalene crystal (two molecules per unit cell) the two site-functions are,³¹

$$\begin{aligned} \Psi_{A_u}(\underline{k}) &= \frac{1}{\sqrt{N}} [\Psi_\alpha(\underline{k}) + \Psi_\beta(\underline{k})] = \frac{1}{\sqrt{N}} \left[\sum_\alpha e^{i\underline{k} \cdot \underline{R}_\alpha} |\alpha\rangle + \sum_\beta e^{i\underline{k} \cdot \underline{R}_\beta} |\beta\rangle \right] \\ \Psi_{B_u}(\underline{k}) &= \frac{1}{\sqrt{N}} [\Psi_\alpha(\underline{k}) - \Psi_\beta(\underline{k})] = \frac{1}{\sqrt{N}} \left[\sum_\alpha e^{i\underline{k} \cdot \underline{R}_\alpha} |\alpha\rangle - \sum_\beta e^{i\underline{k} \cdot \underline{R}_\beta} |\beta\rangle \right] \end{aligned} \quad (6)$$

where $|\alpha\rangle$ is the wavefunction corresponding to the excitation at α -sites, and $|\beta\rangle$ is the wavefunction corresponding to the excitation at β -sites;

and the summation is carried over all the α -sites and all the β -sites.

The corresponding energies are found to be

$$\begin{aligned} E_{A_u}(\underline{k}) &= \epsilon_A + I_{\alpha\alpha}(\underline{k}) + I_{\alpha\beta}(\underline{k}) \\ E_{B_u}(\underline{k}) &= \epsilon_A + I_{\alpha\alpha}(\underline{k}) - I_{\alpha\beta}(\underline{k}) \quad , \end{aligned} \quad (7)$$

where $I_{\alpha\alpha}$ and $I_{\alpha\beta}$ are the modulated sums^{2a} of translationally equivalent and inequivalent interactions, respectively. ϵ_A corresponds to the mean of the exciton band. It is also equal to the gas phase transition energy minus the site shift that is caused by the static interactions between the molecule and its environment.

We now expand the mixed crystal wavefunctions in terms of the complete set of pure crystal wavefunctions

$$\psi = \sum_{\underline{k}^+} f(\underline{k}^+) |\underline{k}^+\rangle + \sum_{\underline{k}^-} f(\underline{k}^-) |\underline{k}^-\rangle \quad , \quad (8)$$

where $|\underline{k}^+\rangle = \Psi_{A_u}(\underline{k})$

and $|\underline{k}^-\rangle = \Psi_{B_u}(\underline{k})$.

For convenience we have put $\underline{k} = \underline{k}^+$ for A_u states and $\underline{k} = \underline{k}^-$ for B_u states. As a vector, \underline{k}^+ may be equal to \underline{k}^- but $|\underline{k}^+\rangle$ is uniquely different from $|\underline{k}^-\rangle$. The corresponding energies for the \underline{k}^+ and \underline{k}^- states are

$$\begin{aligned} E_{\underline{k}^+} &= \epsilon_A + \epsilon(\underline{k}^+) \\ E_{\underline{k}^-} &= \epsilon_A + \epsilon(\underline{k}^-) \quad , \end{aligned} \quad (9)$$

with $\epsilon(\underline{k}^+) = I_{\alpha\alpha} + I_{\alpha\beta}$ and $\epsilon(\underline{k}^-) = I_{\alpha\alpha} - I_{\alpha\beta}$.

In the derivation of secular equations, we note that t_p acts only on the nuclear part of the Born-Oppenheimer wavefunctions. The following expressions can be easily obtained,

$$\begin{aligned} \langle \Phi_i | t_p | \Phi_j \rangle &= 0 \quad \text{if } i \neq j \\ \langle \Phi_i | t_p | \Phi_i \rangle &= (\Delta^* - \Delta^0) \delta_{ip} + \Delta^0 \\ \Delta^* &= \langle \chi^* | t | \chi^* \rangle \\ \Delta^0 &= \langle \chi^0 | t | \chi^0 \rangle \quad , \end{aligned} \tag{10}$$

where χ^* and χ^0 are the nuclear wavefunctions for the excited and ground states, respectively, of the A-molecule. We drop the site index because the expressions are independent of site. Δ^* corresponds to the first-order value of the zero-point energy difference between A and B in the excited state, and Δ^0 corresponds to the same quantity at the ground state. Since the wavefunctions for A and B are expected to be very similar we can assume that the first-order correction is adequate and set $\Delta^* - \Delta^0$ equal to $E_B - E_A$, i. e., the difference in excitation energies or simply the trap depth Δ .

Notice that if the site shift does not depend on isotopic substitution, which is the case in naphthalene⁸ but not in benzene,³² we can set $\Delta = \epsilon_B - \epsilon_A$, where ϵ_B is the mean of the exciton band for the B-molecule.

With the aid of Eq. (10), the secular equations are found to be

$$\begin{aligned}
(E + N_B \Delta^0 - E_{\underline{k}^+}) f(\underline{k}^+) &= \frac{\Delta}{N} \left\{ \sum_{\underline{k}'^+} f(\underline{k}'^+) [\rho_\alpha(\underline{k}^+ - \underline{k}'^+) + \rho_\beta(\underline{k}^+ - \underline{k}'^+)] \right. \\
&\quad \left. + \sum_{\underline{k}'^-} f(\underline{k}'^-) [\rho_\alpha(\underline{k}^+ - \underline{k}'^-) - \rho_\beta(\underline{k}^+ - \underline{k}'^-)] \right\}
\end{aligned} \tag{11a}$$

$$\begin{aligned}
(E + N_B \Delta^0 - E_{\underline{k}^-}) f(\underline{k}^-) &= \frac{\Delta}{N} \left\{ \sum_{\underline{k}'^+} f(\underline{k}'^+) [\rho_\alpha(\underline{k}^- - \underline{k}'^+) - \rho_\beta(\underline{k}^- - \underline{k}'^+)] \right. \\
&\quad \left. + \sum_{\underline{k}'^-} f(\underline{k}'^-) [\rho_\alpha(\underline{k}^- - \underline{k}'^-) + \rho_\beta(\underline{k}^- - \underline{k}'^-)] \right\} ,
\end{aligned} \tag{11b}$$

where

$$\rho_\alpha(\underline{k} - \underline{k}') = \sum_{\alpha} e^{-i(\underline{k} - \underline{k}') \cdot \underline{R}_\alpha}$$

$$\rho_\beta(\underline{k} - \underline{k}') = \sum_{\beta} e^{-i(\underline{k} - \underline{k}') \cdot \underline{R}_\beta}$$

N_B = total number of B-molecules.

The summations \sum_{α} and \sum_{β} are carried out over all α -sites and β -sites occupied by the B-molecules. If we use the mixed crystal ground state as the energy zero, $N_B \Delta^0$ terms can be dropped. The solutions of Eqs. (11) would correspond to the exact excitation energies in mixed crystals.

Several features of the secular equations can be noted.

1. The introduction of impurities not only causes the mixing among the \underline{k}^+ states and the \underline{k}^- states, but it also causes the mixing between \underline{k}^+ states and \underline{k}^- states. For a multiple-branched exciton band, the full interaction matrix must be used to calculate the perturbed energy states.

2. It is apparent that for a single impurity molecule there is no need to specify whether the impurity occupies the α - or β -site. However, when more than one impurity is present, the energy states depend on the exact sites occupied by the impurities. This is manifested by the fact that the coupling matrix elements among all \underline{k} -states depend on whether the impurities occupy α - or β -sites.

We have derived the secular equations using a delocalized representation. For dilute mixed crystals, the corresponding equations can be converted to a localized set. This is essentially the method of Koster and Slater.²⁰⁻²² For example, the energy matrix for dimers is found to be

$$\left| \begin{array}{cc} 1 - \frac{\Delta}{N} \sum_{\text{all } \underline{k}} \frac{1}{E - E_{\underline{k}}} & - \frac{\Delta}{N} \left(\sum_{\underline{k}^+} \frac{e^{i\underline{k}^+ \cdot \underline{R}}}{E - E_{\underline{k}^+}} \pm \sum_{\underline{k}^-} \frac{e^{i\underline{k}^- \cdot \underline{R}}}{E - E_{\underline{k}^-}} \right) \\ - \frac{\Delta}{N} \left(\sum_{\underline{k}^+} \frac{e^{-i\underline{k}^+ \cdot \underline{R}}}{E - E_{\underline{k}^+}} \pm \sum_{\underline{k}^-} \frac{e^{-i\underline{k}^- \cdot \underline{R}}}{E - E_{\underline{k}^-}} \right) & 1 - \frac{\Delta}{N} \sum_{\text{all } \underline{k}} \frac{1}{E - E_{\underline{k}}} \end{array} \right| = 0.$$

The upper sign must be used for translationally equivalent dimers, and the lower sign must be used for translationally inequivalent dimers.

\underline{R} is the distance between the impurities. Similar expressions were obtained by Craig and Philpott.¹⁴

In the next section we will use the secular equations (11a) and (11b) to derive the Green's function. By solving the Green's function we can calculate the density-of-states function and also the optical absorption spectrum for heavily-doped mixed crystals.

B. The Green's Function Method

A Green's function is conveniently defined by the operator equation:

$$G = (E - H')^{-1} , \quad (12)$$

where H' is the Hamiltonian of the system. In terms of any complete orthonormal set $\{\underline{k}\}$, Eq. (12) can be written in a matrix representation:

$$\sum_{\underline{k}''} (E - H')_{\underline{k}\underline{k}''} G_{\underline{k}''\underline{k}'} = \delta_{\underline{k}\underline{k}'} . \quad (13a)$$

It follows immediately that

$$G_{\underline{k}\underline{k}'} = \sum_n \frac{f_n^*(\underline{k})f_n(\underline{k}')}{E - E_n} , \quad (13b)$$

where E_n is an eigenvalue of H' , and $f_n(\underline{k})$ is the expansion coefficient of the eigenstate $|n\rangle$ on to the basis state $|\underline{k}\rangle$, or equivalently $f_n(\underline{k}) = \langle \underline{k} | n \rangle$.

Following Goodings and Mozer,³³ we define a weighted density-of-states function:

$$g_{\underline{k}\underline{k}'}(E) = \sum_n f_n^*(\underline{k})f_n(\underline{k}')\delta(E - E_n) . \quad (14)$$

Equation (13b) can then be written in an integral form,

$$G_{\underline{k}\underline{k}'}(E) = \int \frac{g_{\underline{k}\underline{k}'}(E')dE'}{E - E'} .$$

Using the symbolic identity

$$(E + i\epsilon - E')^{-1} = p(E - E')^{-1} + i\pi\delta(E - E') \quad ,$$

the Green's function can be separated into a real part and an imaginary part:

$$\text{Re } G_{\underline{k}\underline{k}'}(E + i\epsilon) = p \int \frac{\underline{g}_{\underline{k}\underline{k}'}(E')dE'}{E - E'} \quad (15a)$$

$$\text{Im } G_{\underline{k}\underline{k}'}(E + i\epsilon) = \pi \underline{g}_{\underline{k}\underline{k}'}(E) \quad . \quad (15b)$$

The energy states of the condensed system can be best described by a normalized density-of-states function $D(E)$ defined as the fraction of states per unit energy or

$$D(E) = \frac{1}{N} \sum_n \delta(E - E_n) \quad .$$

Through Eqs. (14) and (15), $D(E)$ is related to the Green's function by the expression

$$D(E) = \frac{1}{N} \text{Trace } \underline{g} = \frac{1}{N\pi} \text{Im Trace } \underline{G}(E + i\epsilon) \quad . \quad (16)$$

If we identify the $\{\underline{k}\}$ set as the delocalized basis set in Eq. (6), the familiar $\underline{k} = \underline{0}$ selection rule implies that the transition probability to an eigenstate $|n\rangle$ is equal to the square of its projection onto the $\underline{k} = \underline{0}$ state times the square of the transition moment of the $\underline{k} = \underline{0}$ state. Since two Davydov components exist, we define two optical absorption functions $I_{A_u}(E)$ and $I_{B_u}(E)$ as

$$I_{A_u}(E) = \sum_n f_n^*(\underline{k}^+ = \underline{0}) f_n(\underline{k}^+ = \underline{0}) \delta(E - E_n) \quad (17)$$

$$I_{B_u}(E) = \sum_n f_n^*(\underline{k}^- = \underline{0}) f_n(\underline{k}^- = \underline{0}) \delta(E - E_n) .$$

The product of $I(E)$ and the square of the transition moment will yield the actual spectrum. Using Eqs. (14) and (15), the $I(E)$'s are related to Green's function by the expressions

$$I_{A_u}(E) = \frac{1}{\pi} \text{Im} G_{\underline{k}^+ = \underline{0}, \underline{k}^+ = \underline{0}}(E + i\epsilon) \quad (18)$$

$$I_{B_u}(E) = \frac{1}{\pi} \text{Im} G_{\underline{k}^- = \underline{0}, \underline{k}^- = \underline{0}}(E + i\epsilon) .$$

$I_{A_u}(E)$ and $I_{B_u}(E)$ will give the "normalized" spectra of mixed crystals polarized along \underline{b} and \underline{ac} , respectively.

The foregoing expressions with the exception of Eqs. (17) and (18) are quite general. $\{\underline{k}\}$ can be any basis set, either localized or delocalized, and H' can be any Hamiltonian, either for a pure or a mixed crystal. Now we are in a position to use the result and to apply it to our problem. We can easily recognize that the secular equations (11a) and (11b) involve nothing but the inverse of the Green's function in a \underline{k} -representation. These equations can be rewritten as

$$\sum_{\underline{k}'} (E - H')_{\underline{k}\underline{k}'} f(\underline{k}') = 0$$

$$\text{or} \quad \sum_{\underline{k}'} G_{\underline{k}\underline{k}'}^{-1} f(\underline{k}') = 0 ,$$

where
$$G_{\underline{k}\underline{k}'}^{-1} = (E - E_{\underline{k}})\delta_{\underline{k}\underline{k}'} - \Delta_{\underline{k}\underline{k}'} \quad , \quad (19)$$

with
$$\Delta_{\underline{k}^+ \underline{k}'^+} = \Delta_{\underline{k}^- \underline{k}'^-} = \frac{\Delta}{N} [\rho_{\alpha}(\underline{k} - \underline{k}') + \rho_{\beta}(\underline{k} - \underline{k}')]$$

$$\Delta_{\underline{k}^- \underline{k}'^+} = \Delta_{\underline{k}^+ \underline{k}'^-} = \frac{\Delta}{N} [\rho_{\alpha}(\underline{k} - \underline{k}') - \rho_{\beta}(\underline{k} - \underline{k}')] \quad ,$$

and the summations are over all \underline{k}' of both exciton branches. Substituting Eq. (9) into Eq. (19), we have

$$G_{\underline{k}\underline{k}'}^{-1} = [E - \epsilon_A - \epsilon(\underline{k})]\delta_{\underline{k}\underline{k}'} - \Delta_{\underline{k}\underline{k}'} \quad . \quad (20)$$

We further define

$$G_{\underline{k}\underline{k}'}^0 = \frac{\delta_{\underline{k}\underline{k}'}}{E - \epsilon_A - \epsilon(\underline{k})} = G_0(\underline{k})\delta_{\underline{k}\underline{k}'} \quad . \quad (21)$$

It can be noted that $G_0(\underline{k})$ is the Green's function for a pure crystal consisting of A only. Such a crystal possesses periodicity, i. e., the quasimomentum $\hbar\underline{k}$ is a good quantum number. Mixing between the \underline{k} -states then comes from the perturbation $\Delta_{\underline{k}\underline{k}'}$. Equation (20) can be converted by matrix inversion to yield the true Green's function. With the aid of Eq. (21), we find

$$G_{\underline{k}\underline{k}'} = G_0(\underline{k})\delta_{\underline{k}\underline{k}'} + G_0(\underline{k}) \sum_{\underline{k}''} \Delta_{\underline{k}\underline{k}''} G_{\underline{k}''\underline{k}'} \quad . \quad (22)$$

This is exactly the matrix form of the operator equation:

$$\frac{1}{E-H'} = \frac{1}{E-H^0} + \frac{1}{E-H^0} \Delta \frac{1}{E-H'} \quad .$$

Equation (22) can now be solved by iteration, and we have

$$\begin{aligned} G_{\underline{k}\underline{k}'} &= G_0(\underline{k})\delta_{\underline{k}\underline{k}'} + \frac{\Delta}{N} G_0(\underline{k})\rho(\underline{k}-\underline{k}')G_0(\underline{k}') \\ &+ \left(\frac{\Delta}{N}\right)^2 G_0(\underline{k}) \sum_{\underline{k}''} \rho(\underline{k}-\underline{k}'')G_0(\underline{k}'')\rho(\underline{k}''-\underline{k}')G_0(\underline{k}') \\ &+ \left(\frac{\Delta}{N}\right)^3 G_0(\underline{k}) \sum_{\underline{k}''} \sum_{\underline{k}'''} \rho(\underline{k}-\underline{k}'')G_0(\underline{k}'')\rho(\underline{k}''-\underline{k}''') \\ &\times G_0(\underline{k}''')\rho(\underline{k}'''-\underline{k}')G_0(\underline{k}') + \dots \quad , \end{aligned} \quad (23)$$

where $\rho(\underline{k}-\underline{k}') = \rho_\alpha(\underline{k}-\underline{k}') + \rho_\beta(\underline{k}-\underline{k}')$

or $\phantom{\rho(\underline{k}-\underline{k}') = \rho_\alpha(\underline{k}-\underline{k}') + \rho_\beta(\underline{k}-\underline{k}')} = \rho_\alpha(\underline{k}-\underline{k}') - \rho_\beta(\underline{k}-\underline{k}') \quad ,$

depending upon whether $|\underline{k}\rangle$, $|\underline{k}'\rangle$ belong to the same branch or not.

At this point, it is necessary to average over all impurity distributions to obtain an average Green's function. It is exactly this complication that makes the heavily-doped mixed crystal much more involved. Similar problems involving the electronic states of a random lattice occupied by two types of atoms have been taken up by Yonezawa and Matsubara.^{29a} The corresponding problem for lattice vibrations was also treated by Leath and Goodman³⁴ using essentially the same formulation. However, only a simple lattice with but one molecule per unit cell was considered in any of these papers. For most organic

solids of interest the very existence of multiple excitation branches deserves more careful consideration. In the following section we will proceed with the averaging process to see what complications, if any, arise for the case of multiple exciton branches.

C. The Average Green's Function

To find the average Green's function, it is necessary to evaluate the s-moments of the ρ 's defined as

$$M_s(\underline{p}_1, \underline{p}_2, \underline{p}_3, \dots, \underline{p}_s) = \langle \rho(\underline{p}_1)\rho(\underline{p}_2)\rho(\underline{p}_3)\dots\rho(\underline{p}_s) \rangle_{\text{avg}} \quad (24)$$

with $\underline{p}_1 = \underline{k} - \underline{k}'$, $\underline{p}_2 = \underline{k}' - \underline{k}''$, $\underline{p}_3 = \underline{k}'' - \underline{k}'''$, etc.

In terms of these moments, the average Green's function $\langle G_{\underline{k}\underline{k}'} \rangle$ is found from Eq. (23) to be:

$$\begin{aligned} \langle G_{\underline{k}\underline{k}'} \rangle &= G_0(\underline{k}) \delta_{\underline{k}\underline{k}'} + \frac{\Delta}{N} G_0(\underline{k}) M_1(\underline{k} - \underline{k}') G_0(\underline{k}') \\ &+ \left(\frac{\Delta}{N} \right)^2 G_0(\underline{k}) \sum_{\underline{k}''} M_2(\underline{k} - \underline{k}'', \underline{k}'' - \underline{k}') G_0(\underline{k}'') G_0(\underline{k}') \\ &+ \left(\frac{\Delta}{N} \right)^3 G_0(\underline{k}) \sum_{\underline{k}''} \sum_{\underline{k}'''} M_3(\underline{k} - \underline{k}''', \underline{k}''' - \underline{k}'', \underline{k}'' - \underline{k}') \\ &G_0(\underline{k}''') G_0(\underline{k}'') G_0(\underline{k}') + \dots \quad (25) \end{aligned}$$

The average over all impurity distributions can be effected by replacing the sum over all impurity sites by the sum over all lattice sites multiplied by the impurity concentration:

$$\sum_{\{\ell\}} \rightarrow C_B \sum_n ,$$

where $\{\ell\}$ means the average over all possible distributions of ℓ impurities. In doing this, we must take special care in the cases where impurity sites coincide in the summation of Eq. (24). We will evaluate directly some moments of ρ to illustrate the general approach to this problem.

For $s = 1$, two cases can be distinguished:

I. $|\underline{k}\rangle, |\underline{k}'\rangle$ belong to the same exciton branch,

$$M_1(\underline{p}_1) = \left\langle \sum_{\ell_\alpha} \exp(-i\underline{p}_1 \cdot \underline{R}_{\ell_\alpha}) + \sum_{m_\beta} \exp(-i\underline{p}_1 \cdot \underline{R}_{m_\beta}) \right\rangle_{\text{avg}} ,$$

where ℓ impurities occupy α -sites and m impurities occupy β -sites with $\ell + m = C_B N$, the total number of impurities. Replacing the impurity sum by a lattice sum, we have

$$M_1(\underline{p}_1) = C_B \left[\sum_{n_\alpha} \exp(-i\underline{p}_1 \cdot \underline{R}_{n_\alpha}) + \sum_{n_\beta} \exp(-i\underline{p}_1 \cdot \underline{R}_{n_\beta}) \right] ,$$

where n_α and n_β run over all α -sites and β -sites. Therefore,

$$M_1(\underline{p}_1) = C_B N \delta(\underline{p}_1) . \quad (26a)$$

II. $|\underline{k}\rangle, |\underline{k}'\rangle$ belong to different branches

$$\begin{aligned} M_1(\underline{p}_1) &= \left\langle \sum_{\ell_\alpha} \exp(-i\underline{p}_1 \cdot \underline{R}_{\ell_\alpha}) - \sum_{m_\beta} \exp(-i\underline{p}_1 \cdot \underline{R}_{m_\beta}) \right\rangle_{\text{avg}} \\ &= C_B \left[\sum_{n_\alpha} \exp(-i\underline{p}_1 \cdot \underline{R}_{n_\alpha}) - \sum_{n_\beta} \exp(-i\underline{p}_1 \cdot \underline{R}_{n_\beta}) \right] = 0 . \quad (26b) \end{aligned}$$

Similarly, for $s = 2$ we have three cases:

I. $|\underline{k}\rangle$, $|\underline{k}'\rangle$, and $|\underline{k}''\rangle$ all belong to the same branch

$$\begin{aligned}
M_2(\underline{p}_1, \underline{p}_2) &= \left\langle \left[\sum_{\underline{\ell}_\alpha} \exp(-i\underline{p}_1 \cdot \underline{R}_{\underline{\ell}_\alpha}) + \sum_{\underline{m}_\beta} \exp(-i\underline{p}_1 \cdot \underline{R}_{\underline{m}_\beta}) \right] \left[\sum_{\underline{\ell}'_\alpha} \exp(i\underline{p}_2 \cdot \underline{R}_{\underline{\ell}'_\alpha}) \right. \right. \\
&\quad \left. \left. + \sum_{\underline{m}'_\beta} \exp(-i\underline{p}_2 \cdot \underline{R}_{\underline{m}'_\beta}) \right] \right\rangle_{\text{avg}} \\
&= \left\langle \sum_{\underline{\ell}_\alpha} \exp[-i(\underline{p}_1 + \underline{p}_2) \cdot \underline{R}_{\underline{\ell}_\alpha}] + \sum_{\underline{m}_\beta} \exp[-i(\underline{p}_1 + \underline{p}_2) \cdot \underline{R}_{\underline{m}_\beta}] \right\rangle_{\text{avg}} \\
&\quad + \left\langle \sum_{\underline{\ell}_\alpha \neq \underline{\ell}'_\alpha} \sum \exp[-i(\underline{p}_1 \cdot \underline{R}_{\underline{\ell}_\alpha} + \underline{p}_2 \cdot \underline{R}_{\underline{\ell}'_\alpha})] \right\rangle \\
&\quad + \sum_{\underline{\ell}_\alpha} \sum_{\underline{m}_\beta} \exp[-i(\underline{p}_1 \cdot \underline{R}_{\underline{\ell}_\alpha} + \underline{p}_2 \cdot \underline{R}_{\underline{m}_\beta})] + \sum_{\underline{m}_\beta \neq \underline{m}'_\beta} \sum \exp[-i(\underline{p}_1 \cdot \underline{R}_{\underline{m}_\beta} \\
&\quad + \underline{p}_2 \cdot \underline{R}_{\underline{m}'_\beta})] + \sum_{\underline{\ell}_\alpha} \sum_{\underline{m}_\beta} \exp[-i(\underline{p}_1 \cdot \underline{R}_{\underline{m}_\beta} + \underline{p}_2 \cdot \underline{R}_{\underline{\ell}_\alpha})] \right\rangle_{\text{avg}} .
\end{aligned}$$

Replacing the impurity sum by a lattice sum,

$$\begin{aligned}
M_2(\underline{p}_1, \underline{p}_2) &= C_B \left\{ \sum_{\underline{n}_\alpha} \exp[-i(\underline{p}_1 + \underline{p}_2) \cdot \underline{R}_{\underline{n}_\alpha}] + \sum_{\underline{n}_\beta} \exp[-i(\underline{p}_1 + \underline{p}_2) \cdot \underline{R}_{\underline{n}_\beta}] \right\} \\
&\quad + C_B^2 \left\{ \sum_{\underline{n}_\alpha \neq \underline{n}'_\alpha} \sum \exp[-i(\underline{p}_1 \cdot \underline{R}_{\underline{n}_\alpha} + \underline{p}_2 \cdot \underline{R}_{\underline{n}'_\alpha})] + \sum_{\underline{n}_\alpha} \sum_{\underline{n}_\beta} \exp[-i(\underline{p}_1 \cdot \underline{R}_{\underline{n}_\alpha} \right. \\
&\quad \left. + \underline{p}_2 \cdot \underline{R}_{\underline{n}_\beta})] + \sum_{\underline{n}_\beta \neq \underline{n}'_\beta} \sum \exp[-i(\underline{p}_1 \cdot \underline{R}_{\underline{n}_\beta} + \underline{p}_2 \cdot \underline{R}_{\underline{n}'_\beta})] \right\} \\
&\quad + \sum_{\underline{n}_\beta} \sum_{\underline{n}_\alpha} \exp[-i(\underline{p}_1 \cdot \underline{R}_{\underline{n}_\beta} + \underline{p}_2 \cdot \underline{R}_{\underline{n}_\alpha})] \left. \right\} .
\end{aligned}$$

Using the equality:

$$\begin{aligned}
& \left[\sum_{n_\alpha} \exp(-i\hat{p}_1 \cdot \hat{R}_{n_\alpha}) + \sum_{n_\beta} \exp(-i\hat{p}_1 \cdot \hat{R}_{n_\beta}) \right] \left[\sum_{n_\alpha} \exp(-i\hat{p}_2 \cdot \hat{R}_{n_\alpha}) \right. \\
& \qquad \qquad \qquad \left. + \sum_{n_\beta} \exp(-i\hat{p}_2 \cdot \hat{R}_{n_\beta}) \right] \\
& = \sum_{n_\alpha} \exp[-i(\hat{p}_1 + \hat{p}_2) \cdot \hat{R}_{n_\alpha}] + \sum_{n_\beta} \exp[-i(\hat{p}_1 + \hat{p}_2) \cdot \hat{R}_{n_\beta}] \\
& \quad + \sum_{n_\alpha \neq n'_\alpha} \sum_{\alpha} \exp[-i(\hat{p}_1 \cdot \hat{R}_{n_\alpha} + \hat{p}_2 \cdot \hat{R}_{n'_\alpha})] + \sum_{n_\alpha n_\beta} \exp[-i(\hat{p}_1 \cdot \hat{R}_{n_\alpha} + \hat{p}_2 \cdot \hat{R}_{n_\beta})] \\
& \quad + \sum_{n_\beta \neq n'_\beta} \sum_{\beta} \exp[-i(\hat{p}_1 \cdot \hat{R}_{n_\beta} + \hat{p}_2 \cdot \hat{R}_{n'_\beta})] + \sum_{n_\beta n_\alpha} \exp[-i(\hat{p}_1 \cdot \hat{R}_{n_\beta} + \hat{p}_2 \cdot \hat{R}_{n_\alpha})] ,
\end{aligned}$$

we have

$$\begin{aligned}
M_2(\hat{p}_1, \hat{p}_2) &= C_B N \delta(\hat{p}_1 + \hat{p}_2) + C_B^2 [N \delta(\hat{p}_1) N \delta(\hat{p}_2) - N \delta(\hat{p}_1 + \hat{p}_2)] \\
&= C_B^2 N^2 \delta(\hat{p}_1) \delta(\hat{p}_2) + (C_B - C_B^2) N \delta(\hat{p}_1 + \hat{p}_2) \tag{27a}
\end{aligned}$$

II. $|\underline{k}\rangle$, $|\underline{k}'\rangle$ belong to the same branch and $|\underline{k}''\rangle$ belongs to the other

$$\begin{aligned}
M_2(\hat{p}_1, \hat{p}_2) &= \left\langle \left[\sum_{\ell_\alpha} \exp(-i\hat{p}_1 \cdot \hat{R}_{\ell_\alpha}) + \sum_{m_\beta} \exp(-i\hat{p}_1 \cdot \hat{R}_{m_\beta}) \right] \right. \\
& \quad \left. \left[\sum_{\ell_\alpha} \exp(-i\hat{p}_2 \cdot \hat{R}_{\ell_\alpha}) - \sum_{m_\beta} \exp(-i\hat{p}_2 \cdot \hat{R}_{m_\beta}) \right] \right\rangle_{\text{avg}} .
\end{aligned}$$

Using the same method, we find that

$$M_2(\hat{p}_1, \hat{p}_2) = 0 . \tag{27b}$$

III. $|\underline{k}\rangle$, $|\underline{k}''\rangle$ belong to the same branch, and $|\underline{k}'\rangle$ belongs to the other

$$\begin{aligned}
 M_2(\underline{p}_1, \underline{p}_2) &= \left\langle \left[\sum_{\ell_\alpha} \exp(-i\underline{p}_1 \cdot \underline{R}_{\ell_\alpha}) - \sum_{m_\beta} \exp(-i\underline{p}_1 \cdot \underline{R}_{m_\beta}) \right] \right. \\
 &\quad \left. \left[\sum_{\ell_\alpha} \exp(-i\underline{p}_2 \cdot \underline{R}_{\ell_\alpha}) - \sum_{m_\beta} \exp(-i\underline{p}_2 \cdot \underline{R}_{m_\beta}) \right] \right\rangle_{\text{avg}} \\
 &= (C_B - C_B^2) N \delta(\underline{p}_1 + \underline{p}_2) \quad . \quad (27c)
 \end{aligned}$$

It is clear that these expressions can be combined into a single formula if we define the delta function in a broader sense. As an example, take the case of the naphthalene pure crystal where the eigenstates in the A_u branch can have the same \underline{k} as the eigenstates in the B_u branch. In the normal sense $\delta(\underline{k} - \underline{k}') = 1$ if $\underline{k} = \underline{k}'$ no matter whether $|\underline{k}\rangle$, $|\underline{k}'\rangle$ belong to the same branch or not. Using this notation, we will have to treat all possible cases separately as we did above. However, we can define our delta function as

$$\delta(\underline{p}_1 + \underline{p}_2 + \underline{p}_3 + \cdots + \underline{p}_S) \Rightarrow \delta(\underline{p}_1 + \underline{p}_2 + \underline{p}_3 + \cdots + \underline{p}_S) H[(-1)^n] \quad , \quad (28)$$

where $H[(-1)^n]$ is the Heaviside step function and n is the number of \underline{p} 's that connect \underline{k} in one branch and \underline{k}' in the other; so

$$\begin{aligned}
 H[(-1)^n] &= 0 && \text{if } n = \text{odd} \\
 H[(-1)^n] &= 1 && \text{if } n = \text{even} \quad .
 \end{aligned}$$

By this definition, we can combine Eqs. (26a), (26b), (27a), (27b), and (27c) to yield a simple expression for M_1 and M_2 ,

$$M_1(\underline{p}_1) = C_B N \delta(\underline{p}_1) \quad (29a)$$

$$M_2(\underline{p}_1, \underline{p}_2) = C_B^2 N^2 \delta(\underline{p}_1) \delta(\underline{p}_2) + (C_B - C_B^2) N \delta(\underline{p}_1 + \underline{p}_2) \quad (29b)$$

It can be seen that M_2 in case (II) is equal to zero because $\delta(\underline{p}_2) = 0$, $\delta(\underline{p}_1 + \underline{p}_2) = 0$, and M_2 in case (III) is equal to $N(C_B - C_B^2) \delta(\underline{p}_1 + \underline{p}_2)$ because $\delta(\underline{p}_1) = \delta(\underline{p}_2) = 0$.

Formally, Eqs. (29a) and (29b) are analogous to the expressions obtained by YM for the electronic state of binary solids composed of two types of atoms. Physically, we can say that the existence of two branches of exciton states increases the number of intermediate states to which the exciton under scattering can go. Furthermore, in addition to the normal conservation of momentum for the simple case of one molecule per unit cell, the factor-group symmetry must also be retained (vide infra). In Fig. 1, we illustrate all these different situations diagrammatically by drawing the possible scattering routes. The correspondence between systems with one exciton branch and two exciton branches can be readily seen.

To proceed with the general s-moment, we follow YM^{29a} and define a "restricted" lattice average as

$$\begin{aligned} & \langle Y(\underline{p}_1) Y(\underline{p}_2) Y(\underline{p}_3) \cdots Y(\underline{p}_s) \rangle_{\text{avg}} \\ &= \sum_{\mathbf{n}_1 \neq \mathbf{n}_2 \neq \mathbf{n}_3 \cdots \neq \mathbf{n}_s} (\pm) \exp \left(-i \sum_{t=1}^s \underline{p}_t \cdot \underline{R}_{\mathbf{n}_t} \right), \quad (30) \end{aligned}$$

where $\mathbf{n}_1 \neq \mathbf{n}_2 \neq \mathbf{n}_3 \cdots \neq \mathbf{n}_s$ means that all \mathbf{n}_t 's are different from one another. Two possible forms of Y's are involved

$$Y^+(\underline{p}) = \sum_{\underline{n}_\alpha} \exp(-i\underline{p} \cdot \underline{R}_{\underline{n}_\alpha}) + \sum_{\underline{n}_\beta} \exp(-i\underline{p} \cdot \underline{R}_{\underline{n}_\beta})$$

$$Y^-(\underline{p}) = \sum_{\underline{n}_\alpha} \exp(-i\underline{p} \cdot \underline{R}_{\underline{n}_\alpha}) - \sum_{\underline{n}_\beta} \exp(-i\underline{p} \cdot \underline{R}_{\underline{n}_\beta}) ,$$

depending upon whether $|\underline{k}\rangle$, $|\underline{k}'\rangle$ belong to the same branch ($\underline{p} = \underline{k} - \underline{k}'$). The signs in front of the exponential depend on whether $\underline{R}_{\underline{n}_t}$ is \underline{R}_α or \underline{R}_β . They also depend on whether Y is Y^+ or Y^- .

This definition immediately yields the following relation:

$$\exp_L \left[\sum_j \alpha_j \langle Y(\underline{p}_j) \rangle_{\text{avg}} \right]$$

$$= \langle \exp_L \left[\sum_i \alpha_i Y(\underline{p}_i) + \sum_{i \neq j} \sum \alpha_i \alpha_j Y(\underline{p}_i + \underline{p}_j) + \dots \right] \rangle_{\text{avg}} \quad (31)$$

where \exp_L is the "leveled exponential" introduced by Kubo,³⁵

$$\exp_L \left(\sum_i x_i \right) = 1 + x_1 + x_2 + \dots$$

$$+ x_1 x_2 + x_2 x_3 + \dots \quad (32)$$

$$+ x_1 x_2 x_3 + \dots ,$$

with each term containing only the first power of any x_j . Equation (31) enables us to express the s -moment of Y ($s > 1$) by a sum over various products of the first moment of Y . The result is

$$\langle Y(\underline{p}_1) Y(\underline{p}_2) \dots Y(\underline{p}_s) \rangle_{\text{avg}}$$

$$= (-1)^s \sum_{\{m\}} \prod_m [-(i_m - 1)!] Y_1^m(\underline{p}_{1m} + \underline{p}_{2m} + \underline{p}_{3m} + \dots + \underline{p}_{1m}), \quad (33)$$

where Y_1^m is the first moment of Y with its argument equal to the sum

of the i_m p's in the m^{th} compartment of a particular partition. $\sum_{\{m\}}$ is carried over all the possible partitions $\{m\}$. Notice that $\sum_m i_m = s$. Careful examination of the Y_1^m 's results in the following conclusions:

- (i) If there is an even number of \underline{p} 's connecting \underline{k} in one branch and \underline{k}' in the other,

$$\begin{aligned} Y_1^m &= \sum_{n_\alpha} \exp \left[-i \left(\underline{p}_{1m} + \underline{p}_{2m} + \underline{p}_{3m} + \cdots + \underline{p}_{im} \right) \cdot \underline{R}_{n_\alpha} \right] \\ &\quad + \sum_{n_\beta} \exp \left[-i \left(\underline{p}_{1m} + \underline{p}_{2m} + \underline{p}_{3m} + \cdots + \underline{p}_{im} \right) \cdot \underline{R}_{n_\beta} \right] \\ &= N \delta \left(\underline{p}_{1m} + \underline{p}_{2m} + \underline{p}_{3m} + \cdots + \underline{p}_{im} \right) . \end{aligned}$$

- (ii) If there is an odd number of \underline{p} 's connecting \underline{k} in one branch and \underline{k}' in the other,

$$\begin{aligned} Y_1^m &= \sum_{n_\alpha} \exp \left[-i \left(\underline{p}_{1m} + \underline{p}_{2m} + \underline{p}_{3m} + \cdots + \underline{p}_{im} \right) \cdot \underline{R}_{n_\alpha} \right] \\ &\quad - \sum_{n_\beta} \exp \left[-i \left(\underline{p}_{1m} + \underline{p}_{2m} + \underline{p}_{3m} + \cdots + \underline{p}_{im} \right) \cdot \underline{R}_{n_\beta} \right] \\ &= 0 . \end{aligned}$$

If we again define the delta function in a broader sense as in Eq. (28), we can use a single formula for all the cases,

$$Y_1^m = N \delta \left(\underline{p}_{1m} + \underline{p}_{2m} + \underline{p}_{3m} + \cdots + \underline{p}_{im} \right) . \quad (34)$$

Formally this is again equivalent to the results of YM. ^{29a}

A comment should be made at this point. Although the present discussions are limited to the case of two molecules per unit cell, with

special reference to the naphthalene singlet, the results we have obtained so far can be extended to more complicated systems such as benzene with four molecules per unit cell. The crucial assumption that has to be made is the one we used in Section 2. A; namely, that the exact crystal wavefunctions can be approximated by a simple linear combination of site functions as a result of weak translationally equivalent interactions. It can be noted that the first factor on the right-hand side of Eq. (28) has to do with the translational symmetry of the lattice, while the second factor has to do with the interchange symmetry of the lattice. In the "restricted" Frenkel limit,³⁰ the basis functions in Eq. (6) are constructed so that they belong to the irreducible representations of both the translational group and the interchange group. Equation (28) simply states that a scattering route is allowed if the product of the characters of these irreducible representations (or states involved in the scattering processes), i. e., $\Gamma(\underline{k})\Gamma^*(\underline{k}')\Gamma(\underline{k}'')\Gamma^*(\underline{k}''')\dots$ contains the characters of the totally symmetric representations of both the translational group (i. e., $\underline{p} = \underline{k} - \underline{k}' + \underline{k}'' - \underline{k}''' \dots = \underline{0}$) and the interchange group (i. e., $n = \text{even}$). This is a general rule and is suitable for all the multiple-branched exciton bands.

For molecular crystals that do have strong translationally equivalent interactions, the assumption that factor group operations can be applied to all the \underline{k} -states is no longer valid. The wavefunctions would be (for two molecules per unit cell)

$$\Psi_j(\underline{k}) = \frac{1}{\sqrt{N}} [A(\underline{k}, j)\Psi_\alpha(\underline{k}) + B(\underline{k}, j)\Psi_\beta(\underline{k})] \quad ,$$

where the j 's denote different exciton branches. Although the formula-
tion presented so far would still be applicable, the lattice sum now
takes the following form:

$$Y_1^m(\underline{p}_{1m} + \underline{p}_{2m} + \cdots + \underline{p}_{im}) = \left\{ \sum_{n_\alpha} A(\underline{k}, j) A(\underline{k}', j') A(\underline{k}'', j'') \cdots \right. \\ \exp \left[-i(\underline{p}_{1m} + \underline{p}_{2m} + \cdots + \underline{p}_{im}) \cdot \underline{R}_{n_\alpha} \right] + \sum_{n_\beta} B(\underline{k}, j) B(\underline{k}', j') B(\underline{k}'', j'') \cdots \\ \left. \exp \left[-i(\underline{p}_{1m} + \underline{p}_{2m} + \cdots + \underline{p}_{im}) \cdot \underline{R}_{n_\beta} \right] \right\} .$$

No simple expressions can be written. The $A(\underline{k}, j)$'s and $B(\underline{k}, j)$'s would
have to be evaluated in order to do further calculations. Fortunately,
most low-lying states of molecular crystals seem not to fall into such
categories.

To relate the moments of ρ to the moments of Y , we further
define,

$$\langle X(\underline{p}_1) X(\underline{p}_2) X(\underline{p}_3) \cdots X(\underline{p}_s) \rangle_{\text{avg}} \\ = \sum_{l_1 \neq l_2 \neq \cdots \neq l_s} (\pm) \exp \left(-i \sum_{t=1}^s \underline{p}_t \cdot \underline{R}_{l_t} \right) , \quad (35)$$

where \sum_l is the sum over all impurity sites and $l_1 \neq l_2 \cdots l_s$ means that
all \underline{R}_{l_t} 's are different.

The relation between the moments of X and the moments of Y
can be easily established:

$$\langle X(\underline{p}_1) X(\underline{p}_2) \cdots X(\underline{p}_s) \rangle_{\text{avg}} = C_B^s \langle Y(\underline{p}_1) Y(\underline{p}_2) \cdots Y(\underline{p}_s) \rangle_{\text{avg}} . \quad (36)$$

An expression similar to Eq. (31) now relates the moments of ρ to the moments of X :

$$\begin{aligned} \langle \exp_L \left[\sum_j \alpha_j \rho(\underline{p}_j) \right] \rangle_{\text{avg}} & \\ & = \langle \exp_L \left[\sum_j \alpha_j X(\underline{p}_j) + \sum_{i \neq j} \alpha_i \alpha_j X(\underline{p}_i + \underline{p}_j) + \dots \right] \rangle_{\text{avg}} . \end{aligned} \quad (37)$$

Equations (33) through (37) would enable us to evaluate the various moments and the average Green's function. The final expressions of the moments can be conveniently given in terms of the cumulants^{29a} through the following equations:

$$\langle \exp_L \sum_j \alpha_j \rho(\underline{p}_j) \rangle_{\text{avg}} = \exp_L \left[\langle \exp_L \left\{ \sum_j \alpha_j \rho(\underline{p}_j) \right\} - 1 \rangle_c \right] . \quad (38a)$$

The s -cumulant is, in turn, given as

$$\langle \rho(\underline{p}_1) \rho(\underline{p}_2) \dots \rho(\underline{p}_s) \rangle_c = P_s(C_B) N \delta(\underline{p}_1 + \underline{p}_2 + \dots + \underline{p}_s) , \quad (38b)$$

where $P_s(C_B)$ is given by a generating function

$$\log[1 - C_B + C_B \exp(x)] = \sum_{s=1}^{\infty} P_s(C_B) x^s / s! , \quad (38c)$$

for example,

$$P_1(C_B) = C_B$$

$$P_2(C_B) = C_B - C_B^2$$

$$P_3(C_B) = C_B - 3C_B^2 + 2C_B^3$$

$$P_4(C_B) = C_B - 7C_B^2 + 12C_B^3 - 6C_B^4, \text{ etc.}$$

The function $P_s(C_B)$ can be viewed as a probabilistic weighting function and the delta functions contain the "selection rules" of scattering. As shown in the earlier sections, for multiple-branched exciton bands in the "restricted" Frenkel limit, no complications involving the P_s 's result; however, the delta functions will have to be modified to account for the conservation of factor group symmetries. Using these equations, the average Green's function is found to be:

$$\begin{aligned}
\langle G_{\underline{k}\underline{k}'} \rangle &= G_0(\underline{k}) \delta_{\underline{k}\underline{k}'} + \left(\frac{\Delta}{N} \right) \delta_{\underline{k}\underline{k}'} NP_1(C_B) G_0(\underline{k}) G_0(\underline{k}') \\
&+ \left(\frac{\Delta}{N} \right)^2 \delta_{\underline{k}\underline{k}'} \left\{ N^2 P_1^2(C_B) G_0(\underline{k}) G_0(\underline{k}) G_0(\underline{k}') \right. \\
&\quad \left. + NP_2(C_B) G_0(\underline{k}) \sum_{\underline{k}''} G_0(\underline{k}'') G_0(\underline{k}') \right\} \\
&+ \left(\frac{\Delta}{N} \right)^3 \delta_{\underline{k}\underline{k}'} \left\{ N^3 P_1^3(C_B) G_0(\underline{k}) G_0(\underline{k}) G_0(\underline{k}) G_0(\underline{k}') \right. \\
&\quad + N^2 P_1(C_B) P_2(C_B) G_0(\underline{k}) \sum_{\underline{k}''} G_0(\underline{k}) G_0(\underline{k}'') G_0(\underline{k}') \\
&\quad + N^2 P_1(C_B) P_2(C_B) G_0(\underline{k}) \sum_{\underline{k}''} G_0(\underline{k}'') G_0(\underline{k}') G_0(\underline{k}') \\
&\quad + N^2 P_1(C_B) P_2(C_B) G_0(\underline{k}) \sum_{\underline{k}''} G_0(\underline{k}'') G_0(\underline{k}'') G_0(\underline{k}') \\
&\quad \left. + NP_3(C_B) G_0(\underline{k}) \sum_{\underline{k}''} \sum_{\underline{k}'''} G_0(\underline{k}'') G_0(\underline{k}''') G_0(\underline{k}') \right\} + \dots \quad (39)
\end{aligned}$$

Notice that any summation $\sum_{\underline{k}}$ includes all the \underline{k} -states in all the branches.

A diagrammatic method in which each expansion term is represented by a diagram drawn in momentum space has been developed by Edwards³⁶ and Klauder.³⁷ Equation (39) is depicted diagrammatically in Fig. 2. We have represented the true Green's function by a heavy horizontal line and the free propagator G_0 by a thinner line. Each vertex is associated with a polynomial $P_{\underline{s}}(C_{\mathbf{B}})$, where \underline{s} equals the number of interaction lines connecting the impurity (represented by a cross) and the exciton line. Each interaction line is associated with a momentum transfer $\underline{p} = \underline{k}_1 - \underline{k}_2$, and since the net momentum transfer to a single impurity is zero, each vertex also carries a delta function $N\delta(\underline{p}_1 + \underline{p}_2 + \cdots + \underline{p}_s)$. The expansion can thus be written down easily by enumerating all the possible diagrams.

These diagrams have the general form of an exciton line with a series of self-energy parts. At this point we define a "proper" self-energy part to be a self-energy part that cannot be split into two parts by cutting the exciton line once. It can be shown that by replacing the last free propagator G_0 with the true propagator $\langle G \rangle$, it is now only necessary to sum over all proper self-energy parts. This is demonstrated diagrammatically in Fig. 3. Further simplification can be achieved if all but the first free propagator G_0 in each term is replaced by the true $\langle G \rangle$. All the proper self-energy parts that can be broken down into two proper self-energy parts by a closed line cutting through the exciton line twice can be eliminated. This is again shown in Fig. 4. Equation (39) now takes the simpler form

$$\langle G(\underline{k}) \rangle = G_0(\underline{k}) + G_0(\underline{k})\Sigma^*(\underline{k})\langle G(\underline{k}) \rangle \quad . \quad (40)$$

This is the familiar Dyson equation.³⁸ $\Sigma^*(\underline{k})$ denotes the sum of all the irreducible proper self-energy parts and is called the exciton self-energy. Alternately, we can rewrite Eq. (40) as

$$\langle G(\underline{k}, E) \rangle = \frac{1}{G_0^{-1}(\underline{k}, E) - \Sigma^*(\underline{k}, E)} \quad (41)$$

The argument E is introduced here to denote the E -dependence.

In order to obtain expressions that are more symmetric with respect to both components, the first constant term in the self-energy can be absorbed into $G_0^{-1}(\underline{k}, E)$. If we define

$$\Sigma(\underline{k}, E) = \Sigma^*(\underline{k}, E) - \Delta C_B \quad ,$$

Eq. (41) now becomes

$$\langle G(\underline{k}, E) \rangle = \frac{1}{E - C_A \epsilon_A - C_B \epsilon_B - \epsilon(\underline{k}) - \Sigma(\underline{k}, E)} \quad . \quad (42a)$$

The self-energy, thus defined, can be obtained from Fig. 4 by removing the first diagram from the summation:

$$\begin{aligned} \Sigma(\underline{k}, E) = & \left(\frac{\Delta}{N}\right)^2 NP_2(C_B) \sum_{\underline{k}'} \langle G(\underline{k}', E) \rangle \\ & + \left(\frac{\Delta}{N}\right)^3 NP_3(C_B) \sum_{\underline{k}'} \sum_{\underline{k}''} \langle G(\underline{k}', E) \rangle \langle G(\underline{k}'', E) \rangle \\ & + \left(\frac{\Delta}{N}\right)^4 NP_4(C_B) \sum_{\underline{k}'} \sum_{\underline{k}''} \sum_{\underline{k}'''} \langle G(\underline{k}', E) \rangle \langle G(\underline{k}'', E) \rangle \langle G(\underline{k}''', E) \rangle \end{aligned}$$

$$\begin{aligned}
& + \left(\frac{\Delta}{N}\right)^4 N^2 P_2^2(C_B) \sum_{\underline{k}'} \sum_{\underline{k}''} \sum_{\underline{k}'''} \delta(\underline{k} - \underline{k}' + \underline{k}'' - \underline{k}''') \\
& \delta(\underline{k}' - \underline{k}'' + \underline{k}''' - \underline{k}) \langle G(\underline{k}', E) \rangle \langle G(\underline{k}'', E) \rangle \langle G(\underline{k}''', E) \rangle + \dots \quad . \quad \left. \vphantom{\sum_{\underline{k}'''} } \right\} (42b)
\end{aligned}$$

We have thus extended YM's results to more complicated systems using a physically reasonable approximation, namely the neglect of all but short-range forces in the molecular crystal. Equations (42a) and (42b) then become the master equations with which the energy spectrum of mixed crystals can be calculated. It can be seen that the self-energy includes terms that arise from multiple scattering by a single impurity [such as the first, second and third terms in Eq. (42b)] and also terms that arise from interference scattering by the multiple centers [such as the fourth term in Eq. (42b)]. The former bear no explicit \underline{k} -dependence and hence can be calculated if the density-of-states function is known, whereas the latter have to be evaluated from the dispersion relation. A word of caution has to be made about the fourth term and similar terms associated with two impurities in the expansion. According to our definition of the delta function we draw all the possible scattering routes in Fig. 5. Terms to be included in the sum are those given in Fig. 5a and terms to be excluded are those in Fig. 5b. (We assume $\underline{k} = \underline{k}^+$.) If we define

$$\begin{aligned}
f_1(E, \underline{R}) &= \sum_{\underline{k}^+} e^{i\underline{k}^+ \cdot \underline{R}} \langle G(\underline{k}^+, E) \rangle + \sum_{\underline{k}^-} e^{i\underline{k}^- \cdot \underline{R}} \langle G(\underline{k}^-, E) \rangle \\
f_2(E, \underline{R}) &= \sum_{\underline{k}^+} e^{i\underline{k}^+ \cdot \underline{R}} \langle G(\underline{k}^+, E) \rangle - \sum_{\underline{k}^-} e^{i\underline{k}^- \cdot \underline{R}} \langle G(\underline{k}^-, E) \rangle \quad ,
\end{aligned}$$

we can rewrite the fourth term as

$$\begin{aligned}
& \left(\frac{\Delta}{N}\right)^4 N^2 P_2^2(C_B) \sum_{\underline{k}'} \sum_{\underline{k}''} \sum_{\underline{k}'''} \delta(\underline{k}-\underline{k}'+\underline{k}''-\underline{k}''') \delta(\underline{k}'-\underline{k}''+\underline{k}'''-\underline{k}) \\
& \qquad \qquad \qquad \langle G(\underline{k}', E) \rangle \langle G(\underline{k}'', E) \rangle \langle G(\underline{k}''', E) \rangle \\
& = \left(\frac{\Delta}{N}\right)^4 N^2 P_2^2(C_B) \frac{1}{N} \left[\sum_{\underline{R}_e} e^{i\underline{k} \cdot \underline{R}_e} f_1(E, \underline{R}_e) |f_1(E, \underline{R}_e)|^2 \right. \\
& \qquad \qquad \qquad \left. + \sum_{\underline{R}_i} e^{i\underline{k} \cdot \underline{R}_i} f_2(E, \underline{R}_i) |f_2(E, \underline{R}_i)|^2 \right] ,
\end{aligned}$$

where \underline{R}_e is the separation between two translationally equivalent impurities and \underline{R}_i is the separation between two translationally inequivalent impurities. The necessity of using two f-functions to associate with dimers is rather unique for multiple-branch exciton bands. As has been shown in Section 2. A, energy expressions for translationally equivalent dimers and translationally inequivalent dimers are different. The way we define our delta function will automatically take care of this.

YM^{29b} have obtained the second-order self-energy by summing all the diagrams associated with two impurities. They also showed that at low concentrations the second-order self-energy gives the energies of dimers with variable separations consistent with the Koster-Slater equations. A parallel treatment of the present problem would lead to the same conclusion, both the translationally equivalent

dimers and inequivalent dimers being obtained in the same limit. Expressions similar to those we have derived in Section 2. A can be shown to be included in the second-order self-energy.

Although the exact expression of the average Green's function can be written down in an expansion, no closed form has yet been obtained. This is quite expected in view of the fact that we are trying to describe a highly discontinuous function by an analytical expression. In the next section, we will derive an approximation for the average Green's function and apply it to actual numerical calculations.

D. Approximate Green's Function and the Calculation of the Naphthalene Mixed Crystal Energy Spectrum

If We substitute the expressions for the P_s 's in terms of C_A and C_B into Eq. (42b), we have

$$\begin{aligned}
 \Sigma(\underline{k}, E) &= \Delta^2 C_A C_B \left[\frac{1}{N} \sum_{\underline{k}'} \langle G(\underline{k}', E) \rangle \right] + \Delta^3 C_A C_B (C_A - C_B) \\
 &\quad \left[\frac{1}{N} \sum_{\underline{k}'} \langle G(\underline{k}', E) \rangle \right]^2 \\
 &\quad + \Delta^4 C_A C_B (1 - 6C_A C_B) \left[\frac{1}{N} \sum_{\underline{k}'} \langle G(\underline{k}', E) \rangle \right]^3 \\
 &\quad + \frac{\Delta^4 (C_A C_B)^2}{N^2} \left[\sum_{\underline{k}'} \sum_{\underline{k}''} \sum_{\underline{k}'''} \delta(\underline{k} - \underline{k}' + \underline{k}'' - \underline{k}''') \delta(\underline{k}' - \underline{k}'' + \underline{k}''' - \underline{k}) \right. \\
 &\quad \quad \left. \langle G(\underline{k}', E) \rangle \langle G(\underline{k}'', E) \rangle \langle G(\underline{k}''', E) \rangle \right] \\
 &= \Delta^2 C_A C_B \langle G(E) \rangle [1 - \Delta(C_B - C_A) \langle G(E) \rangle + \dots] \quad , \quad (43)
 \end{aligned}$$

where

$$\langle G(E) \rangle = \frac{1}{N} \sum_{\underline{k}'} \langle G(\underline{k}', E) \rangle = \frac{1}{N} \sum_{\underline{k}'} \frac{1}{E - C_A \epsilon_A - C_B \epsilon_B - \epsilon(\underline{k}') - \Sigma(\underline{k}', E)} . \quad (44)$$

This suggests an approximate closed form of the following type:

$$\Sigma(\underline{k}, E) = \frac{C_A C_B \Delta^2}{\langle G(E) \rangle^{-1} + (C_B - C_A) \Delta + \xi} \quad (45)$$

If we investigate the asymptotic behavior of the self-energy, we find that in the limit of zero bandwidth [$\epsilon(\underline{k}) = 0$], the exact self-energy is given by

$$\Sigma(E) = \frac{C_A C_B \Delta^2}{E - C_A \epsilon_A - C_B \epsilon_B + (C_B - C_A) \Delta} \quad (46)$$

To compare Eq. (45) with Eq. (46), we have to assume that the self-energy is \underline{k} -independent. Then, when $\epsilon(\underline{k}) = 0$, $\langle G(E) \rangle^{-1} = E - C_A \epsilon_A - C_B \epsilon_B - \Sigma(E)$. It follows immediately that $\xi = \Sigma(E)$. An approximate self-energy is then obtained:

$$\Sigma(E) = \frac{C_A C_B \Delta^2}{\langle G(E) \rangle^{-1} + (C_B - C_A) \Delta + \Sigma(E)} \quad (47a)$$

With this approximate self-energy, Eq. (44) now becomes

$$\langle G(E) \rangle = \frac{1}{N} \sum_{\underline{k}'} \frac{1}{E - C_A \epsilon_A - C_B \epsilon_B - \epsilon(\underline{k}') - \Sigma(E)} . \quad (47b)$$

Equation (47) has been derived by Taylor³⁹ for the lattice vibration of mixed crystals with mass defects. It was also obtained by Onodera and Toyozawa⁴⁰ for the corresponding electron problem. YM^{29c} also showed that when the first-order self-energy was expressed as a continued fraction, the lowest approximation agreed with Eq. (47a).

Some features of Eq. (47) can be noted.

- (i) It satisfies the dual symmetry, i. e., the equation is unchanged under the transformation: $C_A \leftrightarrow C_B$, $\Delta \leftrightarrow -\Delta$, $\epsilon_A \leftrightarrow \epsilon_B$.
- (ii) The mixed crystal problem can be solved if the density-of-states function is known. The dispersion relation is not needed in this approximation.
- (iii) It is exact when $\epsilon(\underline{k}) = 0$ and also when $\Delta = 0$.
- (iv) It is exact when $C_B \rightarrow 0$. In this limit

$$\Sigma(E) = \frac{C_B \Delta^2}{\langle G(E) \rangle^{-1} - \Delta} .$$

There is a pole that corresponds to isolated impurities given by the following relation:

$$\frac{1}{N} \sum_{\underline{k}'} \frac{1}{E - \epsilon_A - \epsilon(\underline{k}')} - (\epsilon_B - \epsilon_A)^{-1} = 0 .$$

Our problem now is to solve simultaneously Eqs. (47a) and (47b). Putting $\langle G(E) \rangle = a + bi$ and $\Sigma(E) = c + di$, we obtain four equations:

$$a = \sum_{E'} \frac{D^0(E')(E - C_A \epsilon_A - C_B \epsilon_B - E' - c)}{(E - C_A \epsilon_A - C_B \epsilon_B - E' - c)^2 + d^2} \quad (48a)$$

$$b = \sum_{E'} \frac{D^0(E')d}{(E - C_A \epsilon_A - C_B \epsilon_B - E' - c)^2 + d^2} \quad (48b)$$

$$a = \frac{-cx - dy}{x^2 + y^2} \quad (48c)$$

$$b = \frac{-dx + cy}{x^2 + y^2} , \quad (48d)$$

where $D^0(E')$ is the density-of-states function for a pure crystal and

$$x = c[(C_B - C_A)\Delta + c] - d^2 - C_A C_B \Delta^2$$

$$y = d[(C_B - C_A)\Delta + 2c] .$$

Two sets of $D^0(E')$ are used, one obtained by Craig and Walmsley²⁶ and the other by Colson et al.²⁷ They are shown in Figs. 6 and 7. Notice that the Davydov components are located -77 cm^{-1} and 81 cm^{-1} from the mean of the exciton band according to Colson et al. and -103 cm^{-1} and 53 cm^{-1} according to Craig and Walmsley. To solve Eqs. (48), a trial and error method was used. A set of trial values for c and d were inserted into Eqs. (48) and using Newton's method, a new set of values for c and d were obtained. The iterations were carried on until these values converged. Using the results obtained in Section 2. B, the density-of-states function and the optical

spectrum were calculated from the following expressions:

$$D(E) = \frac{1}{\pi} \text{Im} \langle G(E) \rangle = \frac{b}{\pi}$$

$$\begin{aligned} I(E) &= \frac{1}{\pi} \text{Im} \langle G_{00}(E) \rangle \\ &= \frac{1}{\pi} \frac{\text{Im} \Sigma(E)}{[E - C_A \epsilon_A - C_B \epsilon_B - E_0 - \text{Re} \Sigma(E)]^2 + [\text{Im} \Sigma(E)]^2} \\ &= \frac{1}{\pi} \frac{d}{(E - C_A \epsilon_A - C_B \epsilon_B - E_0 - c)^2 + d^2} \quad , \end{aligned}$$

where the E_0 's correspond to the energies of the Davydov components.

We have assumed that the two Davydov components are infinitely sharp. In reality, it is observed that the \underline{b} -component is somewhat broad. This has not been taken into account in our calculation. The actual spectrum may be obtained by incorporating the actual line shape of the pure crystal into the calculated spectrum.

The exact $I(E)$, $D(E)$ must satisfy some important sum rules.

They are

$$\int_{-\infty}^{\infty} I(E) dE = 1 \quad (49a)$$

$$\int_{-\infty}^{\infty} EI(E) dE = C_A \epsilon_A + C_B \epsilon_B + E_0 \quad (49b)$$

and

$$\int_{-\infty}^{\infty} D(E) dE = 1 \quad (49c)$$

$$\int_{-\infty}^{\infty} ED(E)dE = C_A \epsilon_A + C_B \epsilon_B \quad (49d)$$

It is easy to show that our approximation $I(E)$, $D(E)$ also satisfy these sum rules. Equations (49a) and (49b) state that the approximate $I(E)$ and $D(E)$ are correctly normalized and Eqs. (49b) and (49d) state that they satisfy the "rule of the lever."

3. RESULTS AND DISCUSSION

A. Calculations Based on Experimental

Density-of-States Functions

As we have discussed in Section 2. D, the mixed crystal density-of-states function and optical spectrum are completely determined in the first approximation by the overall density-of-states function (including both exciton branches) and energy gap. The assumption that self-energy does not depend on \underline{k} has the effect of smearing out the density-of-states function that would otherwise be very irregular due to the existence of cluster states.⁴⁰ This approximation would suffer severely if the energy gaps were large. For isotopic substitution, the largest possible energy gap is 115 cm^{-1} corresponding to the case of naphthalene- \underline{h}_8 and \underline{d}_8 . Since the bandwidth is known to be of the same order of magnitude, all the isotopic mixed crystals fall within the limit of shallow traps. The approximation is, therefore, expected to be good.

In Figs. 8, 9, 10, and 11, we show the results of our

calculations for different energy gaps, using the experimental density-of-states function by Colson *et al.*²⁷ Here the density-of-states function is taken as a 186-point histogram. Each energy interval corresponds to 1 cm^{-1} . At fixed energy gap and concentration a particular energy, usually chosen close to ϵ_A or ϵ_B , is used as a starting point. After the values of c and d were calculated from Eqs. (48) by iterations for that energy, they are corrected for energy change and used as the trial values for the next energy interval both higher and lower by 1 cm^{-1} . Using this procedure, we can scan the whole region where the density-of-states is non-vanishing. In situations such as naphthalene- \underline{h}_8 in \underline{d}_8 , two bands exist and two starting points are needed to cover both domains; otherwise one would be sufficient. The convergence is excellent except at band edges. This was also noted by Taylor.³⁹ However, we did not use his procedure and stopped wherever the density-of-states was sufficiently small.

In Fig. 8, where the energy gap corresponds to that for C_8H_{10} - C_8D_{10} mixed crystals, we notice that for all concentrations the eigenstates of the mixed crystal are grouped into two bands. This is due to the moderately large energy gap involved. Each component forms its own exciton band with little disturbance from the other. Davydov splittings similar to those of the pure crystal arise naturally as a result of interactions between like molecules. The density-of-states attributable to each component is such that the integrated area is equal to the concentration of the component.³⁹ This is consistent with the fact that the total number of states is not altered by a unitary

transformation. Since the shapes of the density-of-states functions in Fig. 8 are all quite similar, the bandwidth increases with concentration, bearing roughly a \sqrt{C} -dependence similar to the findings of Onodera and Toyozawa⁴⁰ and Taylor.³⁹ It can also be noted that the mean of the individual exciton bands is shifted relative to the mean energies ϵ_A and ϵ_B of the pure crystal exciton bands, indicating the existence of a "repulsive interaction" between the bands. Eventually as $C \rightarrow 0$, these interactions will move the ideal mixed crystal level to the isolated impurity level causing the quasisonance shift.⁸

Lifshitz¹⁸ has recently given an extensive discussion of the systematics of the energy levels and behavior of band edges in disordered systems. In particular, he predicted that when the perturbation is strong enough to split a state from the main band to form a localized impurity state, the edge of the main band will move to higher energies as more impurities are introduced. This prediction is in agreement with our results.

The Davydov components are seen to be broadened by disordering. For the inner bands, the broadening is much larger due to the proximity of the top of the lower band and the bottom of the upper band. Since the $\underline{a_c}$ component is assumed to be at the bottom of the band, it is broadened to only one side whereas the \underline{b} component, which is inside the band, is seen to be broadened on both sides with more broadening on the side that has larger density-of-states. Recently Sommer and Jortner¹⁶ have suggested looking for the background absorption in the main band induced by isolated impurities as a means of monitoring the

band structure. It would appear from Fig. 8 (and the later figures as well) that little can be learned about the overall band structure by looking at disorder-induced spectra even at high impurity concentrations.

If we turn our attention now to the intensity distribution of the Davydov components, we observe that the outer bands are enhanced and the inner bands weakened. This agrees qualitatively with Sheka's²⁵ experiment and Broude and Rashba's²³ approximate formula. The integrated absorption intensity attributable to each component divided by its concentration is plotted in Fig. 12. It can be seen that these values converge nicely to the corresponding values for dilute mixed crystals (as $C \rightarrow 0$) as given by Rashba's⁹ equation:

$$I = \left[\frac{1}{E - E(0)} \right]^2 \left[\frac{1}{N} \sum_{\underline{k}} \frac{1}{[E - \epsilon(\underline{k})]^2} \right]^{-1}$$

$$= \left[\frac{1}{E - E(0)} \right]^2 \left[\sum_{E'} \frac{D^0(E')}{(E - E')^2} \right]^{-1} .$$

The fact that the outer bands are stronger and sharper indicates that they are relatively undistributed by the presence of the impurities. This, of course, is due to the large energy difference between the perturbing and the perturbed states. As the bandwidth increases so does the Davydov splitting until it reaches the limit of full Davydov splitting manifested by the pure crystal. According to the density-of-states function of Colson et al.,²⁷ the Davydov

components are located near the bottom and the top of the band. This results in a near \sqrt{C} -dependence for the Davydov splittings. Broude and Rashba's allegation that the sum of the Davydov splittings must be equal to the Davydov splitting of the pure crystal is certainly not consistent with the present calculations. In fact, we will show in Part II of this series that our experimental results agree with our calculation rather than with Broude and Rashba's.

Notice that at low concentrations both the theoretical optical spectrum and the density-of-states function are rather structureless. This is probably the most vulnerable region as far as the applicability of the theory is concerned. Experimental data also indicate that although the theory predicts a reasonably good band edge it does not, as expected, show the fine structure observed in the optical spectrum.

Finally, our numerical results indicate that the calculated $I(E)$ and $D(E)$ remain correctly renormalized and their first moments equal to $C_A \epsilon_A + C_B \epsilon_B + E_0$ and $C_A \epsilon_A + C_B \epsilon_B$, respectively, within a few wavenumbers. Thus the sum rules in Eqs. (49) are satisfied. This provides a good check on the iteration.

Proceeding now to shallower trap depths, we show in Fig. 9 our calculated results for naphthalene- \underline{h}_8 and $\beta\underline{d}_4$. The energy gap in this case is 74 cm^{-1} . It can be seen that two bands attributable to naphthalene- \underline{h}_8 and $\beta\underline{d}_4$ merge together when the \underline{h}_8 concentration is larger than 30%, and are barely separated at lower concentrations. The \underline{p} -polarized absorption has a peak in the region $300 \text{ cm}^{-1} \sim 350 \text{ cm}^{-1}$, which is reminiscent of the \underline{p} -polarized absorption of $\beta\underline{d}_4$; but it also

extends throughout the entire band and shows a small hump in the \underline{h}_8 region, roughly corresponding to the \underline{b} -polarized absorption of \underline{h}_8 . The \underline{ac} -polarized absorption behaves quite similarly. Compared with the results of \underline{h}_8 in \underline{d}_8 , the inner components are here weaker and broader while the outer components are stronger.

If we use Izyumov's¹⁹ method to calculate the isolated impurity states, we find that $E_r = 180 \text{ cm}^{-1}$ for \underline{h}_8 in $\beta\underline{d}_4$ and $E_r = 291 \text{ cm}^{-1}$ for $\beta\underline{d}_4$ in \underline{h}_8 . (The energy reference is the same as in Fig. 9.) The former corresponds to a bound state and the latter to a virtual state. It is interesting to note that, as the concentration of \underline{h}_8 is lowered to less than 10%, the \underline{h}_8 band tends to separate from the $\beta\underline{d}_4$ band and to form a bound state. On the contrary, when the concentration of $\beta\underline{d}_4$ is lower than 10%, the entire $\beta\underline{d}_4$ band will be embedded into the \underline{h}_8 band and produce a virtual state. The last graph in Fig. 9 is quite similar to Fig. 6 of Sommer and Jortner's paper¹⁶ except that here we are talking about virtual states involving large impurity concentrations. The behavior of the spectrum at lower concentrations of $\beta\underline{d}_4$ is such that the peak at 305 cm^{-1} will move to lower energy and converge to 291 cm^{-1} (a virtual state), and the peak at 265 cm^{-1} will move to 277 cm^{-1} (the \underline{b} -component of \underline{h}_8). Virtual states are frequently difficult to locate. Our calculation suggests that by following the \underline{b} -component of the $\beta\underline{d}_4$, which is relatively strong, and extrapolating to $C \rightarrow 0$, we can locate the virtual state. Of course, this depends on the accurate determination of the band position, which may not be so easy for the naphthalene \underline{b} -component due to its inherent broadness.

As we proceed to a smaller energy gap, we find that the inner Davydov components almost disappear. For naphthalene- \underline{h}_8 and $\alpha\underline{d}_4$ with $\Delta = 51 \text{ cm}^{-1}$, only two absorption peaks are apparent in Fig. 10. The assignment of each peak to each component has to be made very carefully. We first examine the isolated impurity states. They are found to be 169 cm^{-1} for \underline{h}_8 in $\alpha\underline{d}_4$ and 267 cm^{-1} for $\alpha\underline{d}_4$ in \underline{h}_8 . The former is a bound state being only 1 cm^{-1} from the main band edge; the latter is a virtual state lower in energy than the \underline{b} -component of \underline{h}_8 (277 cm^{-1}). With this in mind, we can start interpreting the first and the last graphs in Fig. 10. In the first graph, the sharp \underline{b} -polarized absorption is almost pure $\alpha\underline{d}_4$, the broad \underline{ac} -polarized absorption indicates complete mixing of the $\alpha\underline{d}_4$ $\underline{k} = 0$ state with the \underline{h}_8 impurity states. The mixing is so complete that it is no longer legitimate to speak of the excitation of $\alpha\underline{d}_4$ or \underline{h}_8 alone. The same interpretation can be made for the last graph. The sharp \underline{ac} component is almost pure \underline{h}_8 and the \underline{b} component now becomes a mixture of the \underline{h}_8 $\underline{k} = 0$ state and the $\alpha\underline{d}_4$ states. In between these extremes, both the \underline{ac} and \underline{b} components show the effect of mixing and broadening. A gradual transition from the excitation of one molecule to the other occurs over the whole concentration range. The widths of the individual components clearly bear out this fact.

Further reduction in the strength of the perturbation results in a situation not very different from that of the pure crystal. In Fig. 11, we see that for naphthalene- \underline{h}_8 and $\beta\underline{d}_1$ ($\Delta = 21 \text{ cm}^{-1}$), both the density-of-states function and the optical spectrum approach those of the pure

crystal. Two sharp lines are predicted. These lines shift gradually from the Davydov components of the pure \underline{h}_g to those of pure $\beta\underline{d}_1$. In the limit of the dilute crystal, no bound state or virtual state will be observed.

The various types of behavior of the self-energy $\Sigma(E)$ are illustrated in Figs. 13a to d. It can be seen that the imaginary part of $\Sigma(E)$ is larger in the impurity region and smaller in the main band (Figs. 13a and c). Since we are effectively calculating the response of the crystal to wave-type excitation, it is not surprising that the damping of the excitation is larger in the impurity band, which is formed by localized excitations, as compared with the damping in the main band. In Fig. 13d, we notice that when $\text{Re } \Sigma(E) = 0$, $\text{Im } \Sigma(E)$ has its maximum. This behavior is somewhat common. The same type of resonance peaking was also observed in the similar studies involving lattice vibrations. In fact, Taylor³⁹ observed the same behavior (see Fig. 3 of his paper) in his calculation of the lattice dynamics of mixed crystals of gold and copper.

The behavior of the real part of the Green's function, which is by definition the principal value of the following integral,

$$F(E) = p \int \frac{D(E')dE'}{E - E'} \quad (50)$$

is illustrated in Figs. 14 and 15. A useful analogy¹⁹ can be used in the discussion of the general behavior of this function. If $D(E')$ is understood as the charge distribution function and $E - E'$ the distance

between the point of observation and the charge, the function $F(E)$ then, by analogy, is the potential function. For a density-of-states function that consists of only one band (Fig. 14), there is only one source. At distances much larger than the dimension of the source, the source can be regarded as a point charge and the potential is inversely proportional to the distance. As the distance is reduced, the potential increases and reaches its maximum near the band edge. On approaching the center of gravity of the distributed charges, the potential decreases due to the mutual compensation of the charges in the outer region and finally equals zero at the center of gravity. Thus the shape of the F -function can be understood in the region $E >$ the center of gravity. By changing the repulsive potential to the attractive potential we can use the same argument to explain the behavior of the F -function in the region $E <$ the center of gravity, where the F -function is inverted.

When two bands exist, the behavior of the F -function resembles that of the potential due to two sources. By superimposing two F -functions similar to Fig. 14, we have the situation shown in Fig. 15. The F -function is seen to possess two maxima and two minima due to the presence of two bands.

Notice that the F -functions were not calculated from Eq. (50), but rather obtained directly as solutions of Eqs. (48). The agreement between the results obtained from Eqs. (50) and (48) is evidence of the self-consistency of Eqs. (48).

B. Calculations Based on the Octopole Model

Calculations were also performed using the density-of-states derived from the octopole model of Craig and Walmsley.²⁶ This was done (1) to study the effect of the density-of-states function of the pure crystal on the density-of-states function and optical spectrum of mixed crystals and (2) to compare the results obtained by solving Eqs. (48) with those of the incomplete machine calculations by Craig and Philpott.¹⁴ The octopole model of exciton interactions in naphthalene predicts a density-of-states function that is rather asymmetric. As shown in Fig. 16, this asymmetry is carried over to the mixed crystal density-of-states function. It can be seen that in Fig. 16 the density-of-states functions for 10% \underline{h}_s / 90% \underline{d}_s and 10% \underline{d}_s / 90% \underline{h}_s are quite different. In the former case, the density-of-states function attributable to the guest (\underline{h}_s) is much broader and extends closer to the main band edge, while in the latter case the density-of-states attributable to \underline{d}_s is farther from the main band. This is believed to be due to the larger density of states on the higher energy side of the band center and, consequently, larger repulsive interaction felt by the guests when they are above the band. The same effect was also predicted in the theory of impurity levels in dilute crystals. Generalization of this effect to the heavily-doped mixed crystals will predict a narrower impurity band for guests above the main band.

To compare with calculations based on the experimental density-of-states function,²⁷ we have shifted the position of the band center from the octopole model to higher energy so that the two Davydov

components coincide with those of Section 3. A. It should be pointed out that theoretical calculations of the band structure deal only with the intermolecular interactions that lead to the exciton band without any reference to the absolute position of the band center. In principle, the merits of different models for exciton interactions should be weighed by using the band center as the common energy reference. From this point of view, if we accept the absolute position of the band center obtained from hot-band spectroscopy of Colson *et al.*,²⁷ the octopole model is already erroneous (by 26 cm^{-1}) in predicting the absolute positions of the Davydov components, although their relative positions given by the Davydov splitting are in good agreement with experiments. However, since the position of the band center is not directly observable physically, another approach would be to use the position of the lowest Davydov component as common energy reference. In doing this, we are effectively comparing the shape of the density-of-states function in the region spanned by the Davydov components. This approach was adopted by Sommer and Jortner¹⁶ and by Hanson *et al.*⁸ and will also be used here.

In Fig. 17, we have plotted the relative positions of the Davydov components of $\underline{h}_g / \underline{d}_g$ mixed crystals as a function of concentration for the two different models. It can be seen that the Davydov components are rather symmetric for the experimental density-of-states function in the sense that the plot has roughly a center of inversion. On the other hand, the octopole model gives a highly asymmetric plot. In the idealized situation where the density-

of-states function is symmetric and the Davydov components are located symmetrically with respect to the band center, the plot will have an exact center of inversion. Knowing the Davydov components, we can use this method to gain some information about the shape of the density-of-states function. In this respect, it is an extension of the method of the variation of energy denominators used by Sommer and Jortner¹⁶ and by Hanson *et al.*⁸ Both methods were based on the same principle that the optical spectrum is completely determined by the density-of-states function and the energy gap.

The intensity distributions can be discussed by using the "rule of the lever" contained in Eqs. (49). Compared with the calculations based on the experimental density-of-states function, the \underline{ac} -polarized absorption is stronger in the \underline{h}_g region and weaker in the \underline{d}_g region. The \underline{b} -polarized absorption behaves oppositely. This provides another criterion for comparing the experimental results with different types of density-of-states functions.

Unlike the corresponding lattice problem,⁴¹ complete machine calculations of the electronic levels of heavily-doped mixed crystals based on some kind of dispersion relations have been lacking. The only data available for comparison are those of Craig and Philpott.¹⁴ Since their calculations were made for super cells with relatively small dimensions ($2 \times 2 \times 2$), their results can only be regarded as suggestive. In Fig. 18, we compare our calculations with those of Craig and Philpott.¹⁴ The agreement is actually better than expected considering the fact that only a few of all the possible guest

distributions were included in their calculation. Notice that we did not compare our results with the "average" energies obtained by Craig and Philpott. Such an averaging process, although intuitively appealing, is not justifiable. What we observe experimentally is not a single level corresponding to the average energy but rather a broad absorption due to all the levels of all the different guest distributions.

As shown in earlier sections, the cluster states that are important when the energy gaps are large and the concentration of one of the components is small are only treated approximately in Eqs. (48). To study the detailed features of the guest band, several approaches are available:

- (1) The present formulation may be improved by including higher-order self-energies. This calculation will become much more involved and may not be feasible for practical purposes.
- (2) Refined machine calculations must be done especially at low guest concentrations. As mentioned by Craig and Philpott,¹⁴ their calculations were very confusing in this region. Some of the features in the guest band cannot be followed with certainty. A more complete calculation would certainly improve the situation.
- (3) Koster and Slater's equations for isolated cluster states or its asymptotic form involving larger gaps⁴² may be used and extended to higher concentrations by assuming that only broadening occurs. As was pointed out by YM²⁹ and by Lifschitz,¹⁸ these isolated cluster states formed the low concentration limits of the true cluster states. In the regions where the present

calculations fail to show the detailed structure of the guest band, qualitative discussions can be made in terms of these isolated cluster states. This will be discussed more thoroughly in conjunction with our discussions of the experimental results.

C. Some Comments on Broude and Rashba's

Model Sheka's Experiments

According to Broude and Rashba's²³ simple model, the positions of the optically active levels in a heavily-doped mixed crystal are given by the following equation:

$$\frac{1}{\epsilon_{\rho}} = \sum_i \frac{C_i}{E - \epsilon_i} \quad , \quad (51)$$

where ϵ_i is the "ideal mixed crystal" level (or the exciton band center) of component i with concentration C_i , and ϵ_{ρ} is the energy difference between the Davydov component ρ and ϵ_i . Using the present notation, we have $\epsilon_{A_u} = I_{\alpha\alpha}(0) + I_{\alpha\beta}(0)$ and $\epsilon_{B_u} = I_{\alpha\alpha}(0) - I_{\alpha\beta}(0)$ for naphthalene crystals. Since two Davydov components exist, two equations can be written. For a binary system, each equation is a second-order equation of E . Two solutions, $E_{A_{\rho}}$, $E_{B_{\rho}}$, will give the excitation energies of A and B respectively. Thus the theory always predicts four sharp lines in the optical spectrum without taking into account any broadening due to disordering.

Furthermore, the theory also fails to account for the exciton interactions that cause the quasiresonance shift in the limit of dilute

mixed crystals. According to Eq. (51), when C_A approaches unity ($C_B \rightarrow 0$) $E_{A\rho} = \epsilon_A + \epsilon_\rho$, while $E_{B\rho} = \epsilon_B$. The single-impurity level is predicted to be the same as the "ideal mixed crystal" level!

Conceptually, what Broude and Rashba's model really amounts to is a model in which the mixed crystal is considered as a virtual crystal consisting of two non-interacting but interpenetrating crystals of A and B, each possessing perfect lattice symmetry (including both the translation symmetry and the factor-group symmetry). Davydov's formulation for pure crystals is then extended to this type of idealized mixed crystal. The results, thus obtained, are quite expected: a "scaled-down" Davydov splitting due to the increased "lattice" parameter and eventually, at zero concentration, the ideal mixed crystal level without quiresonance shift. In this connection, Craig and Philpott's¹⁴ method is an improvement over Broude and Rashba's in that it takes into account some disordering by allowing random impurity distributions within the supercell. However, the translational symmetry among the supercells is, obviously, an artifact. This "residual" symmetry is removed in the present formulation.

Sheka's experiments^{24, 25} are difficult to assess at this moment because of the uncertainty involved in the determination of the compositions of his samples. We will defer detailed discussion until a later publication of additional experimental results from this Laboratory. It is sufficient to mention two of the problems inherent in Sheka's analysis:

1. The ϵ_i 's were determined from Broude's⁴³ method of vibronic analysis. This method has been criticized by Nieman and Robinson.⁵ In this particular case, ϵ_i was determined for naphthalene- \underline{h}_8 to be $\sim 31,530 \text{ cm}^{-1}$, which is even lower than the isolated impurity level of naphthalene- \underline{h}_8 at $31,542 \text{ cm}^{-1}$. According to Hanson *et al.*⁸ and also Sommer and Jortner,¹⁷ it should be around $31,556 \text{ cm}^{-1}$.
2. To circumvent the difficulties in Broude and Rashba's formula at both $C_{h_8} \rightarrow 0$ and $C_{d_8} \rightarrow 0$, Sheka assumed that ϵ_{h_8} and ϵ_{d_8} had a linear dependence on the concentrations. Although this modification allowed some superficial consistencies between theory and experiments involving the naphthalene- \underline{h}_8 absorption bands, it also added to the inconsistencies involving the naphthalene- \underline{d}_8 bands.

ACKNOWLEDGMENTS

I would like to express my sincere thanks to Dr. David M. Hanson for providing me with the numerical tabulations of the density-of-states functions and for many helpful discussions.

REFERENCES

1. (a) J. Frenkel, *Phys. Rev.* 37, 17, 1276 (1931); (b) A. S. Davydov, *Theory of Molecular Excitons* (McGraw-Hill Book Co., New York, 1962); (c) A. S. Davydov, *Sov. Phys. -Usp.* 7, 145 (1964).
2. (a) D. P. Craig and S. H. Walmsley, *Physics and Chemistry of the Organic Solid State*, D. Fox, M. M. Labes, and A. Weissberger, Eds. (Interscience Publishers, Inc., New York, 1963), Vol. 1, Chap. 10; (b) S. A. Rice and J. Jortner, *Physics and Chemistry of the Organic Solid State*, D. Fox, M. M. Labes, and A. Weissberger, Eds. (Interscience Publishers, Inc., New York, 1967), Vol. III, Chap. 4.
3. C. Kittel, *Quantum Theory of Solids* (John Wiley & Sons, Inc., New York, 1963).
4. *Excitons, Magnons and Phonons*, A. B. Zahlan, Ed. (Cambridge University Press, London, 1968).
5. G. C. Nieman and G. W. Robinson, *J. Chem. Phys.* 39, 1298 (1963).
6. M. A. El-Sayed, M. T. Wauk, and G. W. Robinson, *Mol. Phys.* 5, 205 (1962).
7. S. D. Colson and G. W. Robinson, *J. Chem. Phys.* 48, 2550 (1968).
8. D. M. Hanson, R. Kopelman, and G. W. Robinson, *J. Chem. Phys.* 51, 212 (1969), "Information on the Exciton Band Structure of the $^1B_{2U}$ State of Crystalline Naphthalene from the Variation of Energy Denominators Method."

9. E. I. Rashba, *Opt. Spektrosk.* 2, 568 (1957).
10. E. I. Rashba, *Fiz. Tverd. Tela* 4, 3301 (1962) [*Sov. Phys. — Solid State* 4, 2417 (1963)].
11. R. G. Body and I. G. Ross, *Australian J. Chem.* 19, 1 (1966).
12. S. Takeno, *J. Chem. Phys.* 44, 853 (1966).
13. D. P. Craig and M. R. Philpott, *Proc. Roy. Soc. (London)* A290, 583 (1966).
14. D. P. Craig and M. R. Philpott, *Proc. Roy. Soc. (London)* A290, 602 (1966).
15. D. P. Craig and M. R. Philpott, *Proc. Roy. Soc. (London)* A293, 213 (1966).
16. B. S. Sommer and J. Jortner, *J. Chem. Phys.* 50, 187 (1969).
17. B. S. Sommer and J. Jortner, *J. Chem. Phys.* 50, 822 (1969).
18. I. M. Lifschitz, *Advan. Phys.* 13, 483 (1964).
19. Y. A. Izyumov, *Advan. Phys.* 14, 569 (1965).
20. G. F. Koster and J. C. Slater, *Phys. Rev.* 95, 1167 (1954).
21. G. F. Koster and J. C. Slater, *Phys. Rev.* 96, 1208 (1954).
22. G. F. Koster, *Phys. Rev.* 95, 1436 (1954).
23. V. L. Broude and E. I. Rashba, *Sov. Phys. — Solid State* 3, 1415 (1962).
24. E. F. Sheka, *Opt. Spectrosc.* 10, 360 (1961) [*Opt. Spektrosk.* 10, 684 (1961)].
25. E. F. Sheka, *Bull. Acad. Sci. USSR Phys. Series* 27, 501 (1963).
26. D. P. Craig and S. H. Walmsley, *Mol. Phys.* 4, 113 (1961). The density-of-states function used in the present calculation was taken from Refs. 8 and 27.

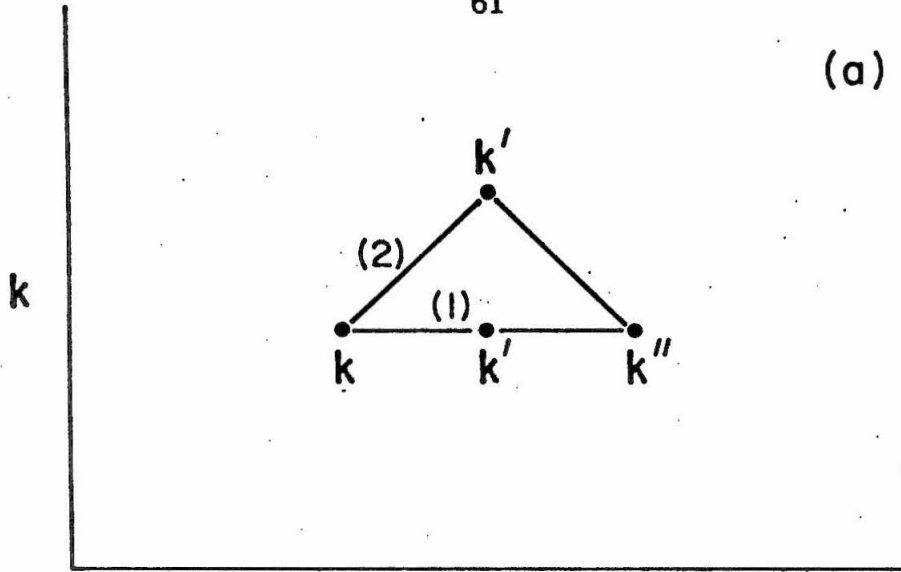
27. S. D. Colson, D. M. Hanson, R. Kopelman, and G. W. Robinson, *J. Chem. Phys.* 48, 2215 (1968).
28. M. Lax, *Rev. Mod. Phys.* 23, 287 (1951); *Phys. Rev.* 85, 621 (1952).
29. (a) F. Yonezawa and T. Matsubara, *Progr. Theoret. Phys.* (Kyoto) 35, 357 (1966); (b) *ibid.* 35, 759 (1966); (c) *ibid.* 37, 1346 (1967).
30. S. D. Colson, R. Kopelman, and G. W. Robinson, *J. Chem. Phys.* 47, 27 (1967).
31. The molecular axes are signed according to the same convention as in Ref. 27. The C_2 interchange operation was used rather than the reflection operation (ca. Ref. 26).
32. S. D. Colson, *J. Chem. Phys.* 48, 3324 (1968).
33. D. A. Goodings and B. Mozer, *Phys. Rev.* A136, 1093 (1964).
34. P. L. Leath and B. Goodman, *Phys. Rev.* 148, 968 (1966).
35. R. Kubo, *J. Phys. Soc. Japan* 17, 1100 (1962).
36. S. F. Edwards, *Phil. Mag.* 3, 1020 (1958).
37. R. Klauder, *Ann. Phys. (U.S.)* 14, 43 (1961).
38. See, for example, R. D. Mattuck, *A Guide to Feynman Diagrams in Many-Body Problems* (McGraw-Hill Book Co., Inc., New York, 1967).
39. D. W. Taylor, *Phys. Rev.* 156, 1017 (1967).
40. Y. Onodera and Y. Toyozawa, *J. Phys. Soc. Japan* 24, 341 (1968).

41. A fairly complete machine calculation on the lattice vibration of disordered solids has been done by D. N. Payton and W. M. Visscher, Phys. Rev. 154, 802 (1967). Similar calculations on the exciton properties of disordered crystals would be very desirable.
42. At low guest concentrations, these isolated cluster states can be observed in a long crystal. See D. M. Hanson, Ph. D. Thesis, California Institute of Technology, 1969. Hanson treated the isolated cluster state as a two-body problem, neglecting the interactions with the host band, which is much higher in energy.
43. V. L. Broude, Usp. Fiz. Nauk 74, 577 (1961) [Sov. Phys. —Usp. 4, 584 (1962)].

FIG. 1. Possible scattering routes contained in M_2 for (a) single-branched exciton band and (b) double-branched exciton band. Route (1) corresponds to $\delta(p_1)\delta(p_2) = 1$, and route (2) corresponds to $\delta(p_1 + p_2) = 1$. The definition of the delta function used here is given in the text.

61

(a)



(b)

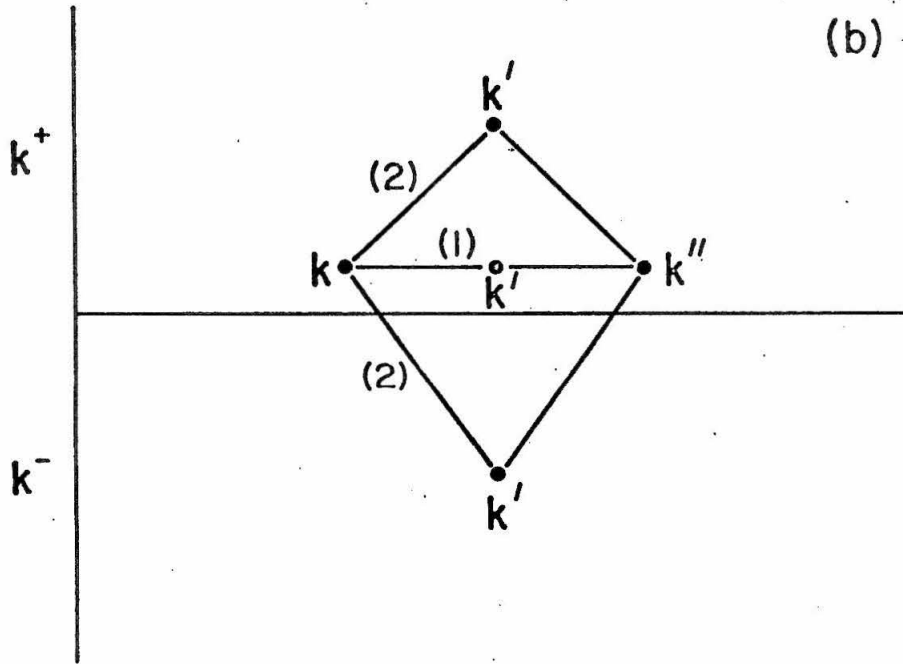
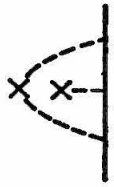


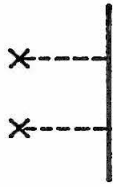
FIG. 2. Diagrams representing the expansion of the true propagator in terms of the free propagator.



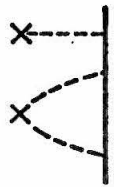
+



+



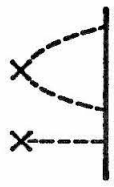
+



+



+



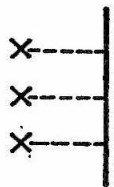
+



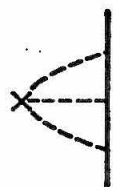
+



||



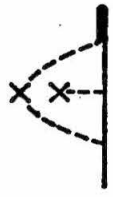
+



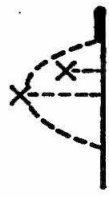
+



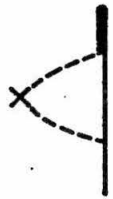
FIG. 3. Diagrams representing the expansion terms to be summed if the last propagator G_0 in Fig. 2 is replaced by the true propagator $\langle G \rangle$.



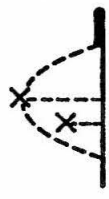
+



+



+



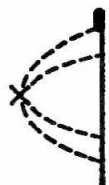
+



+



+

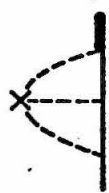


+

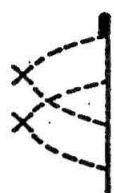


+

||



+



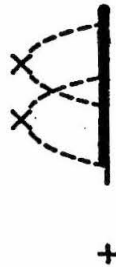
+



FIG. 4. Diagrams representing the expansion terms to be summed if all but the first propagator in Fig. 2 are replaced by the true propagator $\langle G \rangle$.



+



+



+



+



||



+



+



FIG. 5. Possible scattering routes given by $\delta(k - k_1 + k_2 - k_3)$
 $\times \delta(k_1 - k_2 + k_3 - k)$ according to our definition of the delta
functions. Terms to be summed are those in (a) and terms
not to be summed are those in (b).

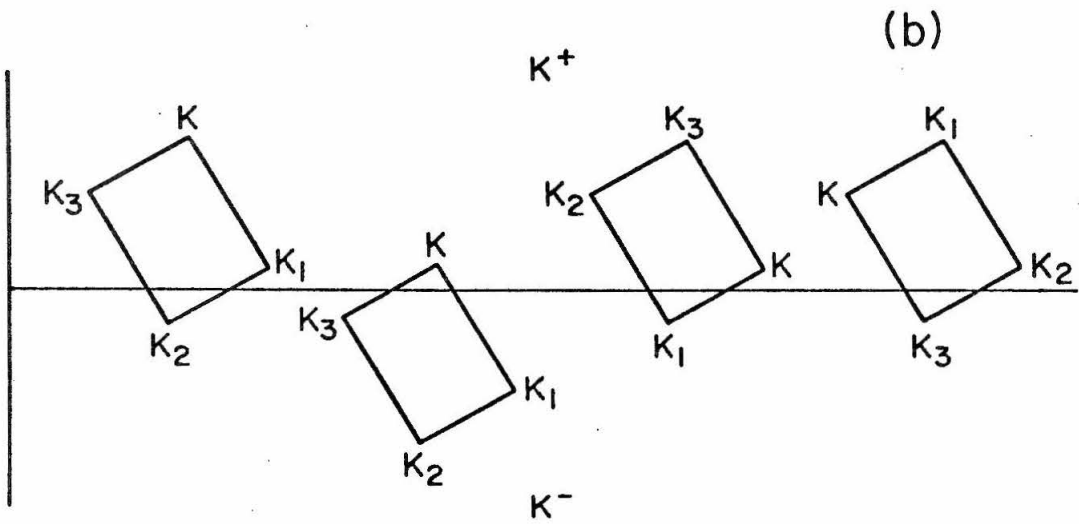
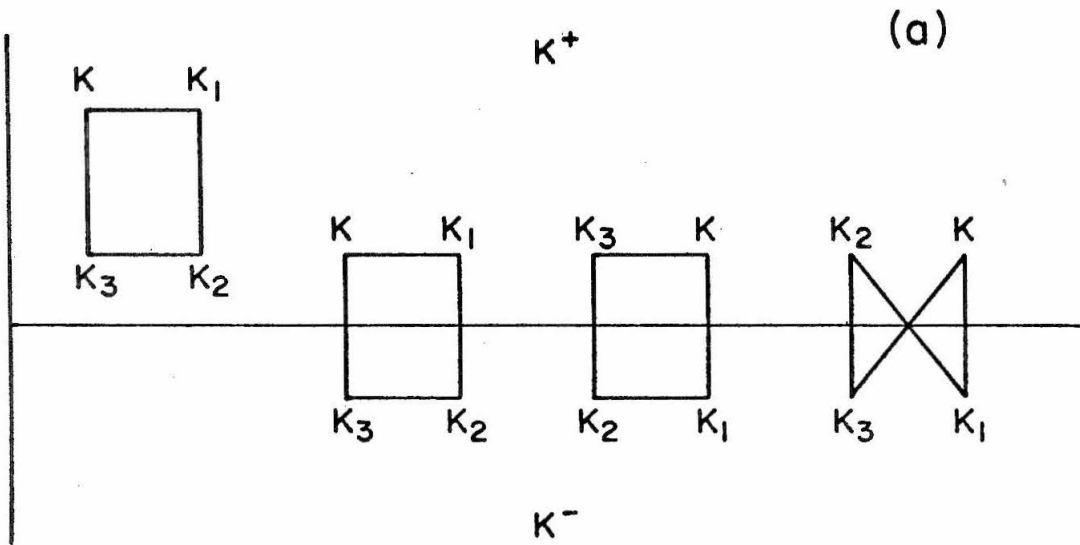


FIG. 6. Density-of-states function obtained experimentally by Colson et al.²⁷ The two Davydov components are represented by two heavy vertical bars.

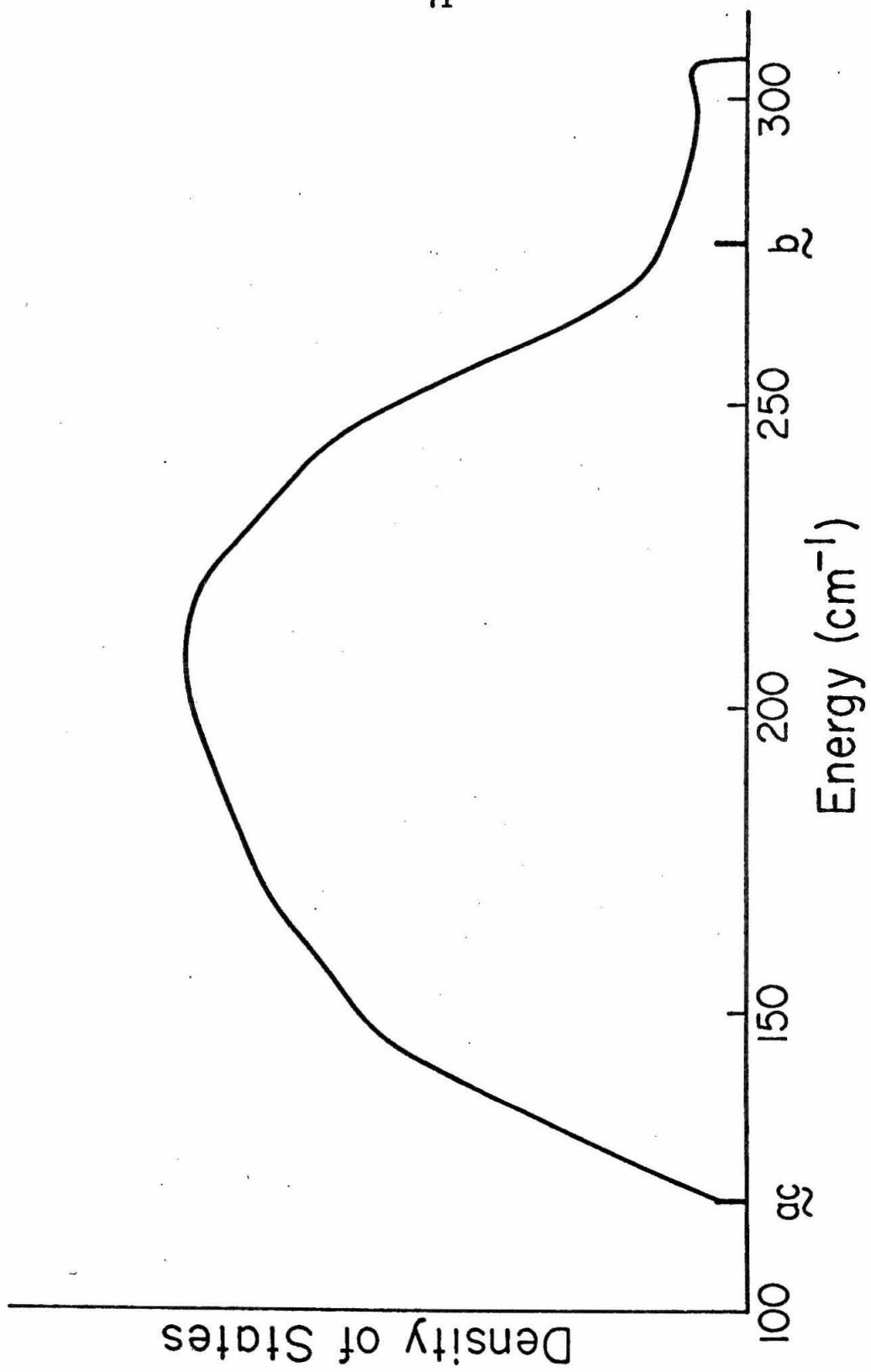


FIG. 7. Density-of-states function according to the octopole model of Craig and Walmsley.²⁶ The dots indicate the actual values. A smooth curve has been drawn to show the approximate shape of the function.

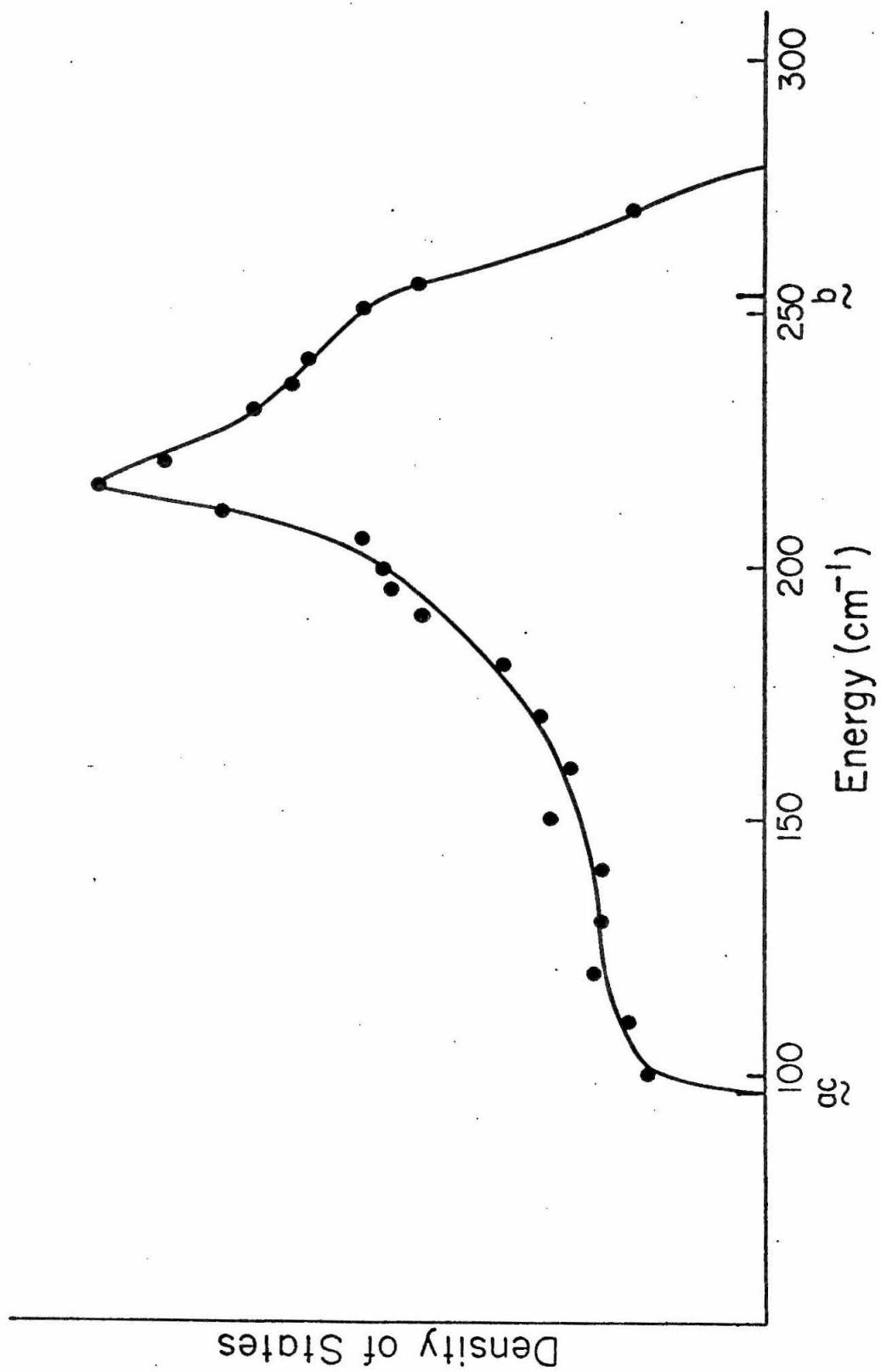


FIG. 8. Calculated density-of-states function (dotted line) and optical spectrum (solid line) for naphthalene- \underline{h}_8 and \underline{d}_8 , using the experimental density-of-states function of Colson *et al.*²⁷ ϵ_A and ϵ_B are band centers for naphthalene- \underline{h}_8 and \underline{d}_8 , respectively. The concentration ratios given correspond to naphthalene- \underline{h}_8 : naphthalene- \underline{d}_8 .

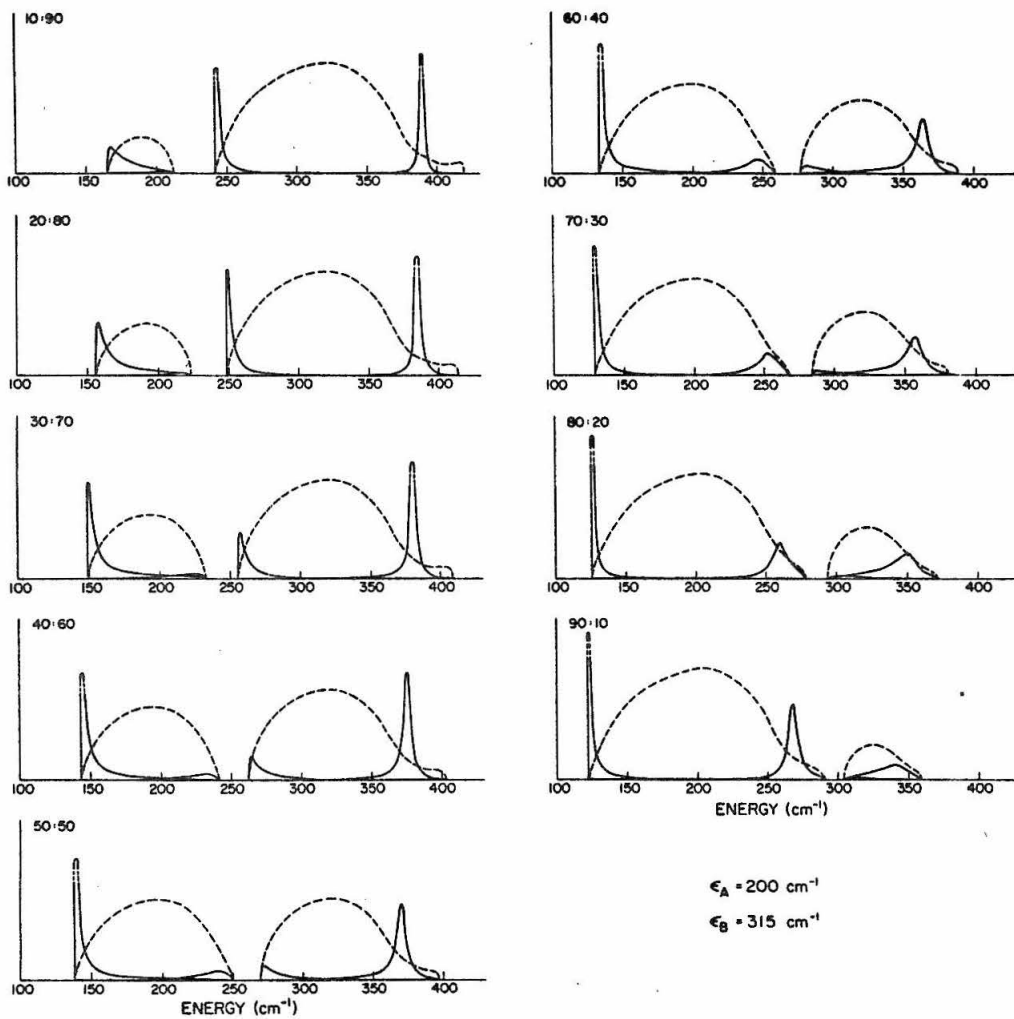


FIG. 9. Calculated density-of-states function and optical spectrum for naphthalene- \underline{h}_8 and naphthalene- $\underline{\beta d}_4$ using the experimental density-of-states function of Colson et al.²⁷ The conventions are the same as those in Fig. 8.

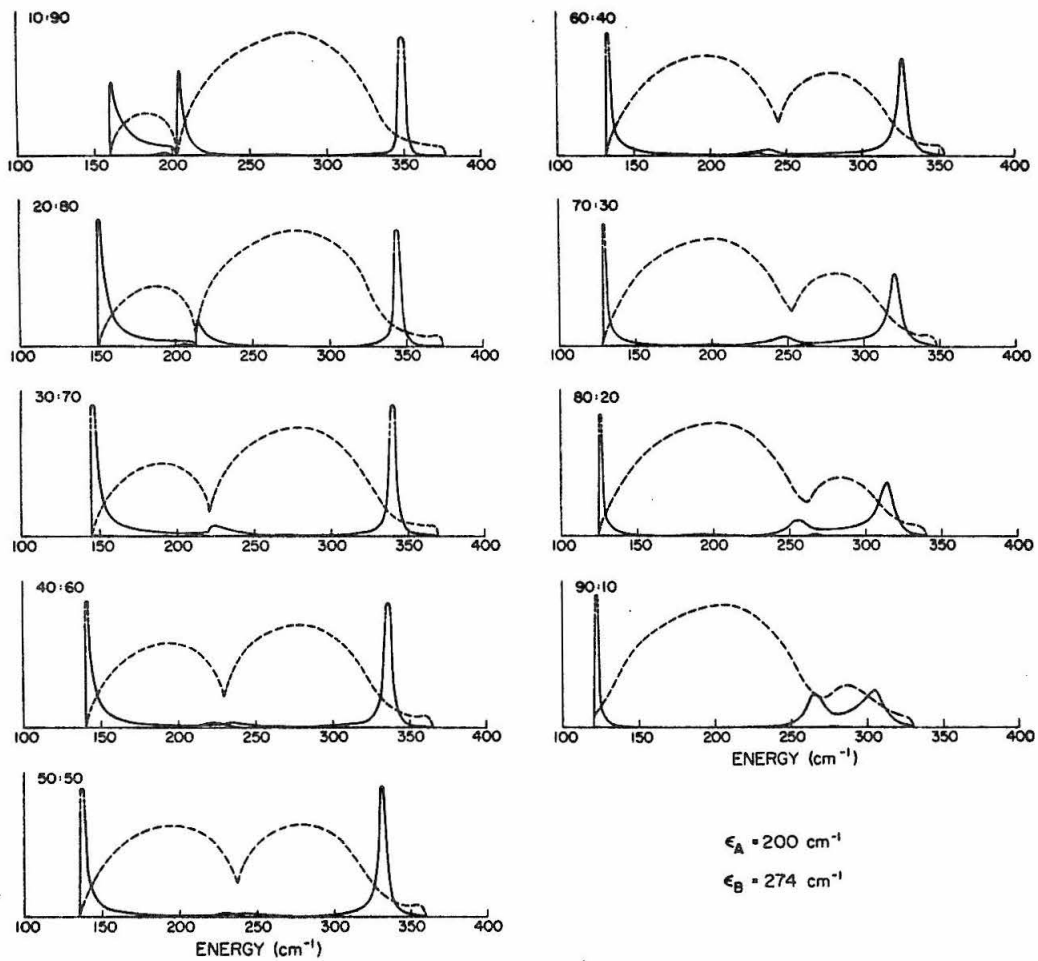
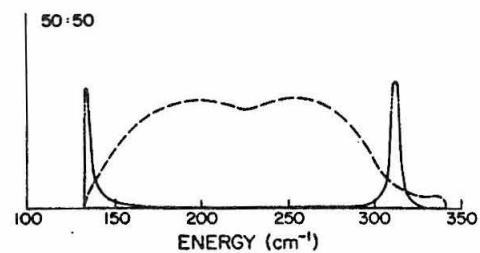
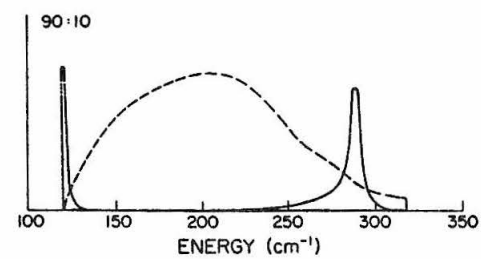
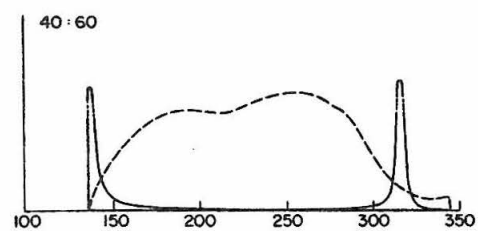
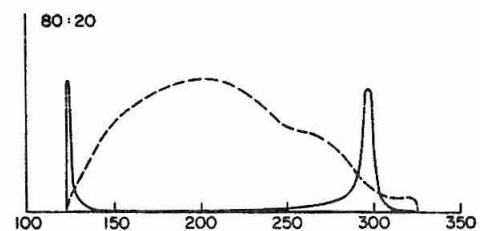
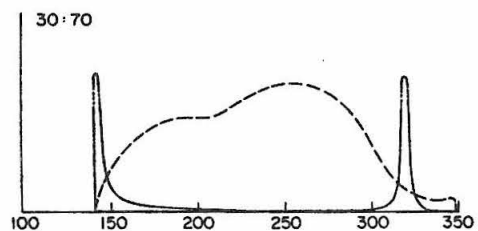
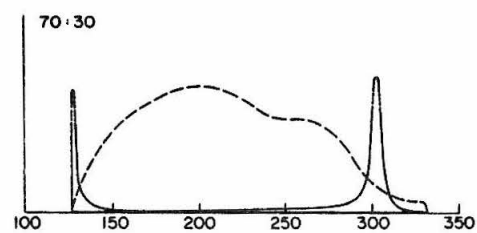
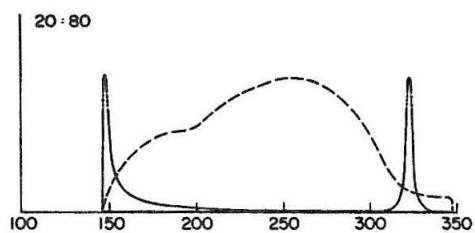
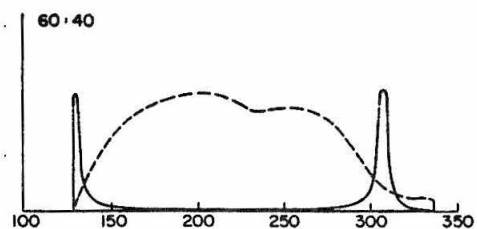
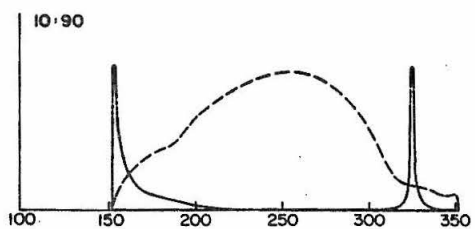


FIG. 10. Calculated density of-states function and optical spectrum for naphthalene- \underline{h}_8 and naphthalene- $\underline{\alpha d}_4$ using the experimental density-of-states function of Colson et al.²⁷ The conventions are the same as those in Fig. 8.



$$\epsilon_A = 200 \text{ cm}^{-1}$$

$$\epsilon_B = 251 \text{ cm}^{-1}$$

FIG. 11. Calculated density-of-states function and optical spectrum for naphthalene- \underline{h}_8 and naphthalene- $\underline{\beta d}_1$ using the experimental density-of-states function of Colson et al.²⁷ The conventions are the same as those in Fig. 8.

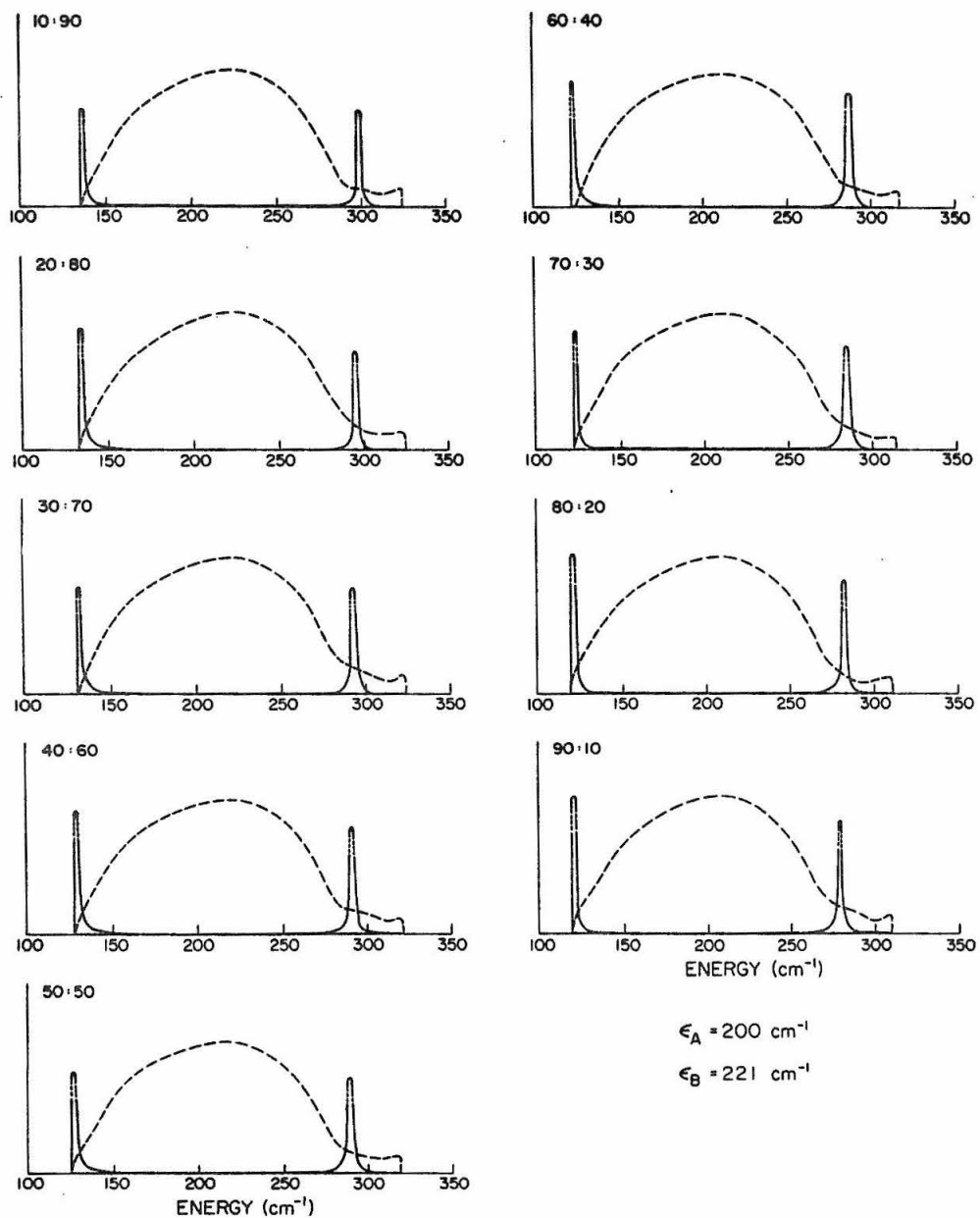


FIG. 12. Intensity distributions of Davydov components for mixed crystals of naphthalene- \underline{h}_8 and \underline{d}_8 as a function of concentration. Data used here were extracted from Fig. 8 by integrating the optical spectrum.

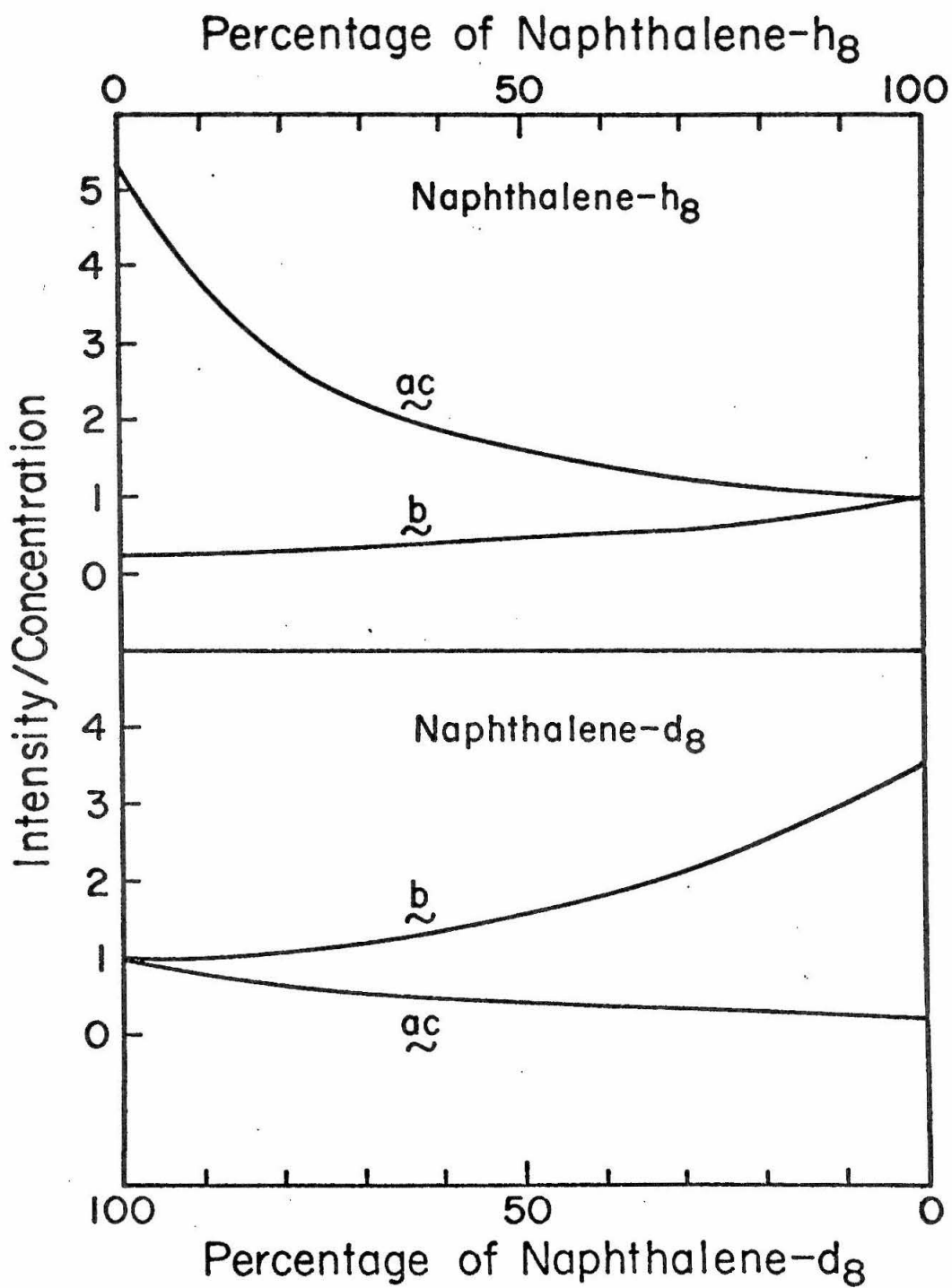


FIG. 13. The behavior of the self-energy $\Sigma(E)$ calculated from the experimental density-of-states function of Colson *et al.*²⁷ for (a) 10% naphthalene- \underline{h}_8 and 90% naphthalene- \underline{d}_8 ; (b) 50% naphthalene- \underline{h}_8 and 50% naphthalene- \underline{d}_8 ; (c) 90% naphthalene- \underline{h}_8 and 10% naphthalene- \underline{d}_8 ; and (d) 80% naphthalene- \underline{h}_8 and 20% naphthalene- $\beta\underline{d}_4$.

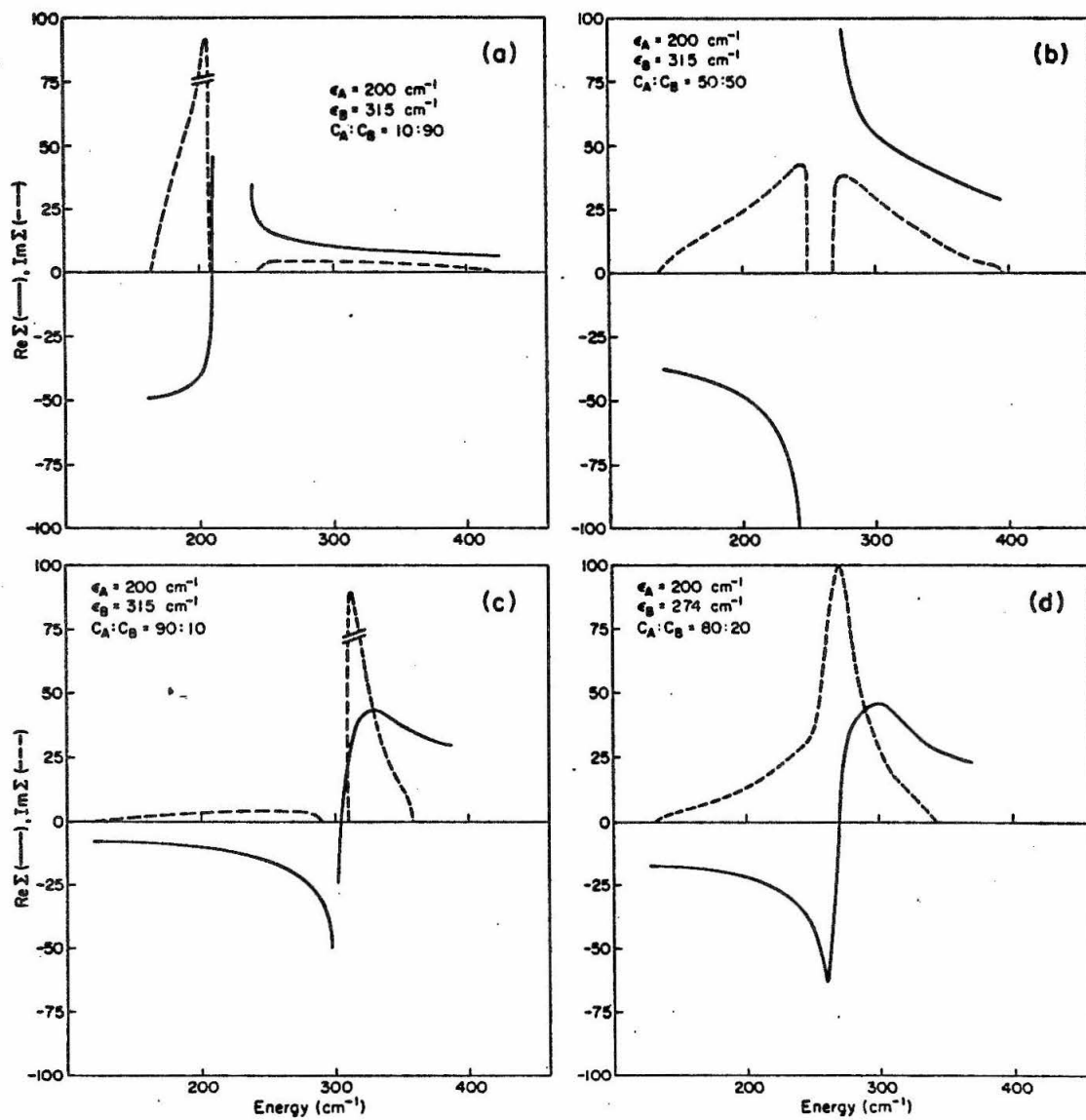


FIG. 14. Calculated F-function (the real part of the Green's function) for mixed crystals of naphthalene- \underline{h}_8 and $\beta\underline{d}_1$ using the experimental density-of-states function of Colson et al.²⁷

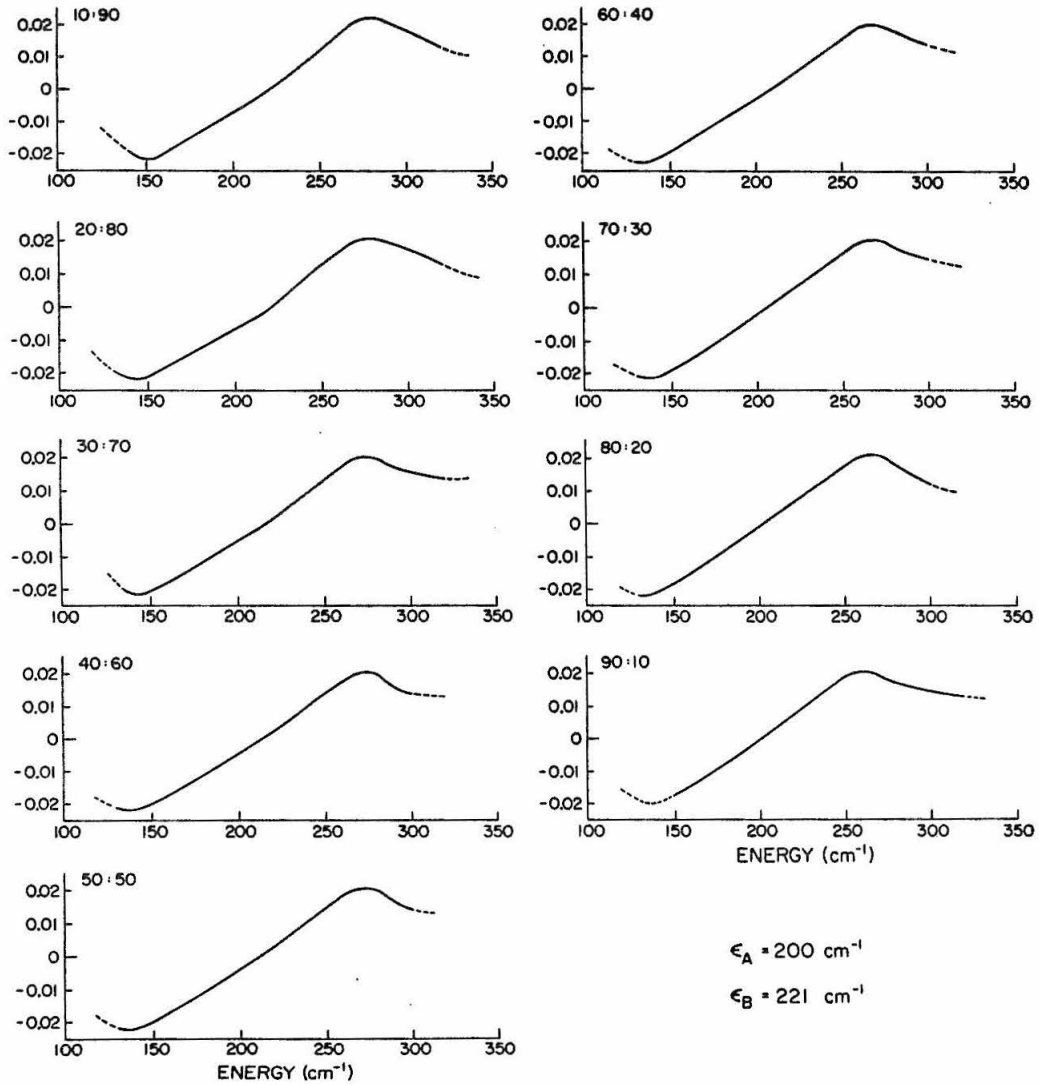


FIG. 15. Calculated F-function (the real part of the Green's function) for mixed crystals of naphthalene- \underline{h}_8 and \underline{d}_8 using the experimental density-of-states function of Colson et al.²⁷

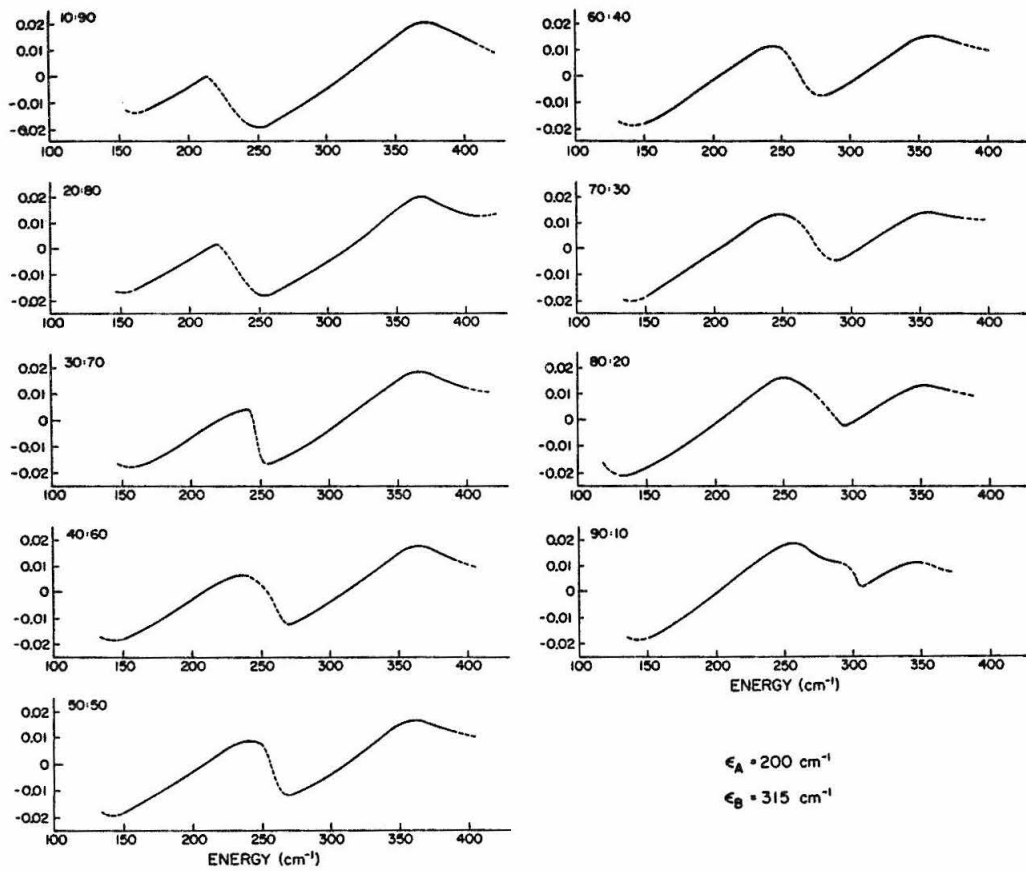


FIG. 16. Calculated density-of-states function (dotted line) and optical spectrum (solid line) for naphthalene- \underline{h}_8 and \underline{d}_8 using the octopole model. The conventions are the same as those in Fig. 8.

FIG. 17. The calculated absorption maxima of the Davydov components for mixed crystals of naphthalene- \underline{h}_8 and \underline{d}_8 . Dotted line corresponds to results obtained by using the octopole model, and solid line corresponds to results obtained by using the experimental density-of-states functions. We assumed that the octopole model predicted the correct energies of the Davydov components in the pure crystal; see text. (They are at 119 cm^{-1} and 227 cm^{-1} in this diagram, while the actual experimental values are $31,475 \text{ cm}^{-1}$ and $31,633 \text{ cm}^{-1}$.)

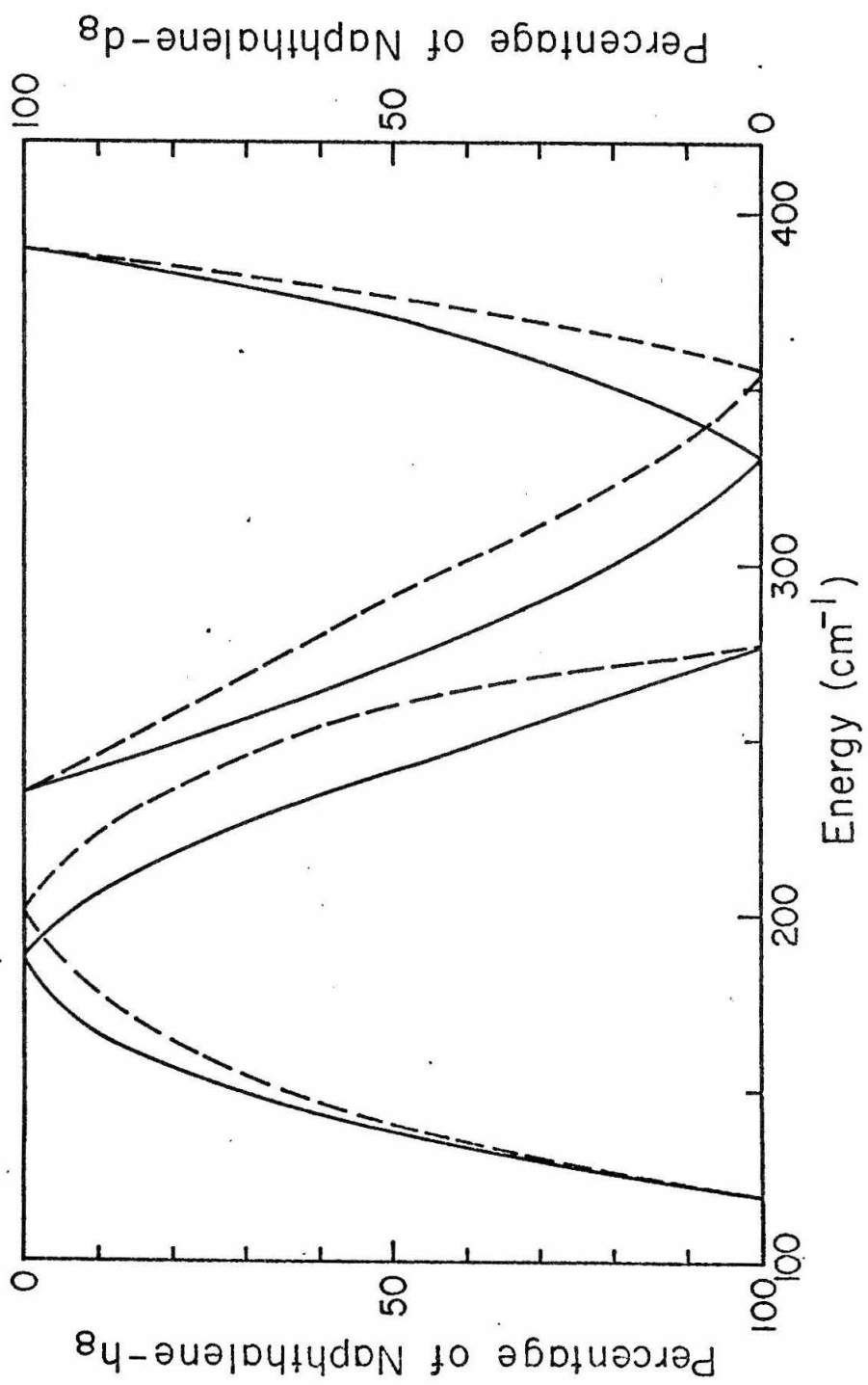
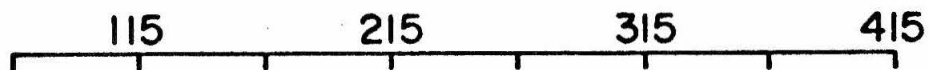
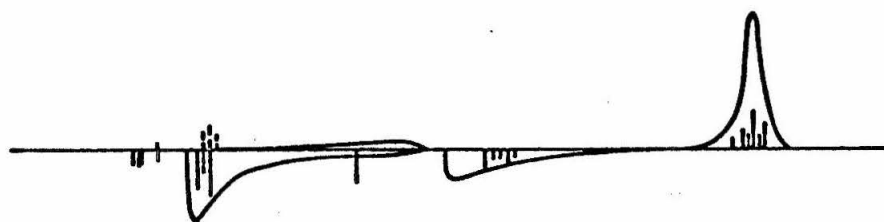


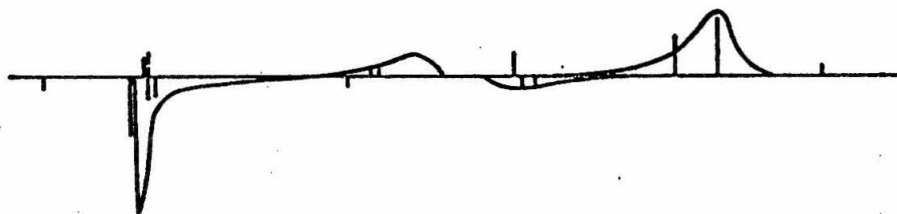
FIG. 18. Comparison between this work (the smooth curves) and the machine calculations by Craig and Philpott¹⁴ (the vertical bars) on the spectra of $C_{10}H_8$ - $C_{10}D_8$ mixed crystals. The curves (or bars) above the horizontal line represent the \underline{b} -polarized spectra and those below represent the \underline{ac} -polarized spectra. The ratios given correspond to naphthalene- \underline{h}_8 : naphthalene- \underline{d}_8 . Intensities are given in arbitrary units.

Energy (cm⁻¹)

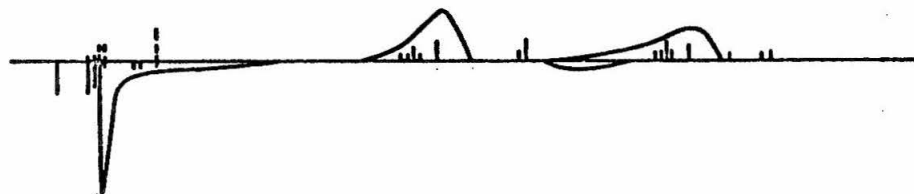
25:75



50:50



75:25



PART II
ELECTRONIC STATES OF HEAVILY-DOPED
MOLECULAR CRYSTALS--NAPHTHALENE
II. EXPERIMENTAL

1. INTRODUCTION

Isotopically-mixed crystals are widely used as convenient systems for the study of intermolecular interactions in molecular aggregates. The chief advantages of studying such systems are: (1) the intermolecular interactions can be assumed, to a large extent, to be invariant upon isotopic substitutions; (2) the guest molecules introduced go substitutionally into the host lattice without disturbing the crystal structure. Thus, a study of the mixed crystal problem not only provides information about the mixed crystal itself but it also provides information concerning the pure crystal.

In the discussion of mixed crystals, two cases can be distinguished: (1) the dilute mixed crystal and (2) the heavily-doped mixed crystal. In the former case, the energy level of the guest is governed predominantly by the quasisonance interactions¹ with the host (the host levels are essentially unchanged). In the latter case, the energy spectrum of the entire system is now determined by both the resonance interactions between like molecules and the quasisonance interactions between unlike molecules. Further complications due to the random distributions of the two components also add to the complexity of the latter problem.

In the first paper (I) of this series,² we presented a Green's function formulation for the electronic states of heavily-doped molecular crystals with multiple-branched exciton bands. By assuming that the factor-group operations can be applied to all the \underline{k} -states,³

we have been able to do the statistical averaging exactly. It was also shown that, in the first approximation, the density-of-states function and optical spectrum of a mixed crystal are completely determined by the density-of-states function of the pure crystal and the energy gaps between the two components. Model calculations on the electronic states of the naphthalene mixed crystals, based on both the experimental density-of-states function of Colson *et al.*⁴ and that of the octopole model of Craig and Walmsley⁵ were also presented. The present experimental investigations are aimed at a critical evaluation of the theory. And, furthermore, wherever discrepancies are observed, we hope to present some experimental facts that might suggest directions for the future improvement in the theory of disordered solids.

Although the optical spectra of some naphthalene mixed crystals have been investigated by Sheka⁶ at 20° K, he did not use weighed samples. Rather, the approximate formula of Broude and Rashba⁷ was used to fit the spectra and to determine the compositions. When additional experimental data at lower temperatures with weighed samples were gathered in the present study, some disagreements with Sheka's results were noted and some new features observed. These will be discussed in the text. In addition, the present study was carried out to include systems with smaller energy gaps and to undertake a more thorough study of the band-to-band (vibronic) transitions at different temperatures.

2. EXPERIMENTAL

The absorption spectra of naphthalene mixed crystals were taken at 4.2° K using an 800-W Hanovia high pressure Xenon lamp and a 2-m Czerny-Turner spectrograph in third order. The dispersion on the plate is about 2.4 Å/mm. An aqueous solution filter of cobalt chloride in a 5-cm quartz cell and a Corning 9863 glass filter were used to eliminate overlapping orders. The fluorescence spectra at 4.2° K were taken photographically with the same spectrograph. Front surface excitation was employed using a P. E. K. 200 W mercury lamp with air cooling. A small 0.25-m Bausch and Lomb high intensity monochromator was used in addition to a CoCl_2 solution filter to provide a narrow band at 3100 Å for excitation. A Corning 9863 filter (and/or 5840 filter) was placed in front of the slit to eliminate the phosphorescence. With a typical slit setting of 30 μ , the exposure times ranged from 30 min to 1 hr. At nitrogen temperature, the fluorescence was found to be considerably weakened. For the fluorescence experiments, the same optical arrangement as above was employed, except that a large Osram XBO-6500 lamp and a 1.8-m Jarrell-Ash photoelectric spectrometer were used for excitation and dispersion. An EMI 6256S photomultiplier selected for low dark current and installed in a light-tight housing suitable for dry-ice cooling was used as a detection probe.

The spectral line positions on a photographic plate were measured relative to the standard emission of an iron-neon hollow

cathode on a Jarrell-Ash high precision recording microphotometer (Model No. 23-500). When the photoelectric method was used, the wavelengths were measured by calibrating the spectrometer readings with known mercury emission lines. The measured wavelengths were then converted to wavenumbers and corrected for vacuum using Keyer's Tabelle der Schwingungszahlen.

Eastman Kodak recrystallized naphthalene was purified with zone-refining and potassium fusion.⁸ Deuterium-substituted naphthalenes (naphthalene- d_8 , naphthalene α - d_4 , naphthalene β - d_4) were all obtained from Merck, Sharp and Dohme of Canada Ltd. and subjected to the same purification processes. The purified substances were removed from the vacuum sealed tube and exposed to air temporarily while being weighed and mixed. To minimize air contamination, the following procedures were followed to introduce the weighed samples into the vacuum line: (1) The vacuum system was evacuated to a pressure of $10^{-6} \sim 10^{-7}$ Torr. (2) The system was filled with helium gas and maintained at a pressure slightly above the atmospheric. (3) The system was opened with a torch and the sample was introduced. Since the system had a positive pressure, no air was admitted into the system during this operation. (4) The helium pressure was reduced to nearly atmospheric and the system was sealed again. (5) The sample inside the vacuum line was cooled to 77° K while helium gas was pumped away. (6) The mixture was then transferred to a crystal-growing quartz cell that was subsequently pulled from the vacuum line at a pressure of $10^{-6} \sim 10^{-7}$ Torr. To assure good mixing, the sample

cell was placed in an oven maintained at a temperature slightly above the melting point of naphthalene (80.2°C) for 1 hr, then crystals were grown inside the quartz cell. Since the crystal obtained was apparently not single, no polarization measurements were attempted.

The thickness of the sample cells ranged from $10\ \mu$ to $100\ \mu$. Normally, thicker cells were used for preparations composed predominantly of one component in order to observe weaker absorptions due to the minor component, and thinner cells were used for equimolecular mixtures. Some crystals did not have uniform thickness over the whole window area, and it was necessary to take absorption spectra at different locations to select an optimum thickness.

3. RESULTS AND DISCUSSION

A. Absorption

Naphthalene- h_8 and Naphthalene- d_8

This system was investigated by Sheka⁶ at 20°K using tiny single crystals ($\sim 1\ \text{mg}$) with thicknesses ranging from 10 to $0.3\ \mu$. From the experimental results, Sheka concluded that: (a) At low concentrations ($< 10\%$), the guest level appeared as an unsplit level with mixed polarization. At slightly higher concentrations ($\gtrsim 10\%$), two levels with unique polarizations were observed. The splitting between the two was found to gradually increase with increasing concentration until it reached the full Davydov splitting characteristic of the pure crystal. (b) Due to the exciton interactions (coupling between the

oscillators) Beer's law is violated. The absorption attributable to each component is no longer proportional to its concentration. Furthermore, the outer bands (i. e., the $\underline{a_c}$ component of naphthalene- \underline{h}_8 absorption and the \underline{b} component of the naphthalene- \underline{d}_8 absorption) are enhanced while the inner bands are weakened. The behavior of these features is qualitatively in agreement with the approximate model of Broude and Rashba.⁷ In Fig. 1 the experimental results of Sheka and the theoretical curve of Broude and Rashba are reproduced. Although the agreement appears to be satisfactory, it is for the most part superficial as can be concluded from the following points:

1. The ideal mixed crystal level (or the center of the exciton band), which is the quantity required in applying the formulas of Broude and Rashba, was determined from Broude's⁹ method of vibronic analysis. This method has been criticized by Nieman and Robinson¹⁰ in the past and its limitations were recently reexamined by Colson.¹¹ Unless it is critically used, this method is likely to yield incorrect values. In this particular instance, the ideal mixed crystal level was determined by Broude's method to be $31,530 \text{ cm}^{-1}$ for the naphthalene- \underline{h}_8 pure crystal. This is even lower than the isolated impurity level of naphthalene- \underline{h}_8 in \underline{d}_8 at $31,542 \text{ cm}^{-1}$. On the other hand, reliable data obtained from hot band spectroscopy place the ideal mixed crystal level at $31,556 \text{ cm}^{-1}$.^{1a,3}
2. To circumvent the difficulties in the method of Broude and Rashba at both $C_{\underline{h}_8} \rightarrow 0$ and $C_{\underline{d}_8} \rightarrow 0$, Sheka apparently assumed that

$\epsilon_{\underline{h}_8}$ and $\epsilon_{\underline{d}_8}$ had a linear dependence on the concentration. That is,

$$\epsilon_{\underline{h}_8} = \epsilon_{\underline{h}_8}^i - C_{\underline{h}_8} (\epsilon_{\underline{h}_8}^i - \epsilon_{\underline{h}_8}^0) \quad (1)$$

and

$$\epsilon_{\underline{d}_8} = \epsilon_{\underline{d}_8}^0 - C_{\underline{h}_8} (\epsilon_{\underline{h}_8}^i - \epsilon_{\underline{h}_8}^0) , \quad (2)$$

where $\epsilon_{\underline{h}_8}^0$ and $\epsilon_{\underline{d}_8}^0$ are the band centers of pure crystalline naphthalene- \underline{h}_8 and \underline{d}_8 , respectively. $\epsilon_{\underline{h}_8}^i$ corresponds to the experimental value of the isolated impurity level of naphthalene- \underline{h}_8 in \underline{d}_8 . Equation (1) was designed such that at $C_{\underline{h}_8} = 0$, $\epsilon_{\underline{h}_8} = \epsilon_{\underline{h}_8}^i$. Since the model of Broude and Rashba did not take into account the quasiresonance interactions, Sheka must have inferred from his erroneous value of $\epsilon_{\underline{h}_8}^0$ that the shift from $\epsilon_{\underline{h}_8}^0$ to $\epsilon_{\underline{h}_8}^i$ was due to the change in the static environmental perturbations (i. e., a change in the D-term in the conventional Davydov exciton theory). In order to be self-consistent, Eq. (2) was devised. Although this procedure enabled Sheka to obtain better agreement between theory and experiment for the naphthalene- \underline{h}_8 bands, it inevitably added to the discrepancies involving the naphthalene- \underline{d}_8 bands. There appears to be ample experimental evidence to support the assumption that the D-term for the naphthalenes is invariant with respect to isotopic substitution. In fact, using the correct values of the ideal mixed crystal levels, both Hanson *et al.*^{1a} and Sommer and Jortner^{1b} have satisfactorily interpreted the isolated impurity levels of various naphthalene mixed crystals in terms of

the quairesonance shift, assuming that no change in the D-term was involved.

3. Sheka did not use weighed samples because of difficulties involved in weighing small quantities of his preparations. Rather he determined the compositions of mixed crystals by fitting the experimental values of the long wavelength absorptions ($\underline{a_c}$ component of naphthalene- \underline{h}_8 absorption) with the theoretical curve obtained from the above procedures. This introduced more uncertainties into his experimental results. In addition, the $\underline{a_c}$ component of the naphthalene- \underline{d}_8 absorption was not observed by Sheka, probably because he used very thin samples. Several features associated with cluster states (vide infra) were also missing in Sheka's spectra.

The spectra obtained in the present work are shown in Fig. 2. The $\underline{a_c}$ component of naphthalene- \underline{d}_8 is easily identifiable. Unfortunately due to the relative broadness of the \underline{b} -component of the naphthalene- \underline{h}_8 absorption (and probably because of additional broadening due to the disorder), the two inner bands are barely separated at higher naphthalene- \underline{h}_8 concentrations. Furthermore, fine structure that is indeed very pronounced in the guest band involving mixed crystals of lower naphthalene- \underline{h}_8 concentration can be noted. These are absorption lines attributable to cluster states (dimers, trimers, etc.). Although these cluster states were expected within the theoretical framework presented in Part I, the exact treatment has been hampered by both the lack of reliable dispersion relations and

cumbersome mathematical manipulations.¹² In our numerical calculations, we have neglected the \underline{k} -dependence in the self-energy expression. This enables us to calculate the spectra using only the density-of-states functions. The same approximation also leads to the loss of fine structure in the calculated guest band. It is conceivable that a trial and error scheme involving an assumed dispersion relation to fit the spectra can be employed. In practice this might not be feasible. Here we choose to make some semi-quantitative statements about the cluster state within a physically reasonable limit and draw some conclusion concerning the magnitude of the intermolecular interaction matrix elements that are responsible for the entire exciton band.

Cluster states in dilute mixed crystals have been investigated by Hanson¹³ using crystals of larger thickness (~ 1 mm). Both the translationally inequivalent and translationally equivalent dimers were identified. Under the conditions Hanson used (impurity concentration smaller or equal to 1.4%), the host band was essentially undisturbed and isolated cluster states were the subject of study. The present problem is quite different in nature. Since appreciable amounts of impurities are introduced, interactions among these islands of clusters must be taken into account. It is only when the intermolecular interactions are really short-range that some degree of simplification can be achieved. Under such conditions, the true cluster states can be correlated with isolated cluster states present in dilute systems. Fortunately this seems to be the case for naphthalene. The spectrum at 10% naphthalene- \underline{h}_8 resembles markedly that of the more dilute

mixed crystals and the broadening is only slight. The following conclusions are drawn mainly from a study of naphthalene- \underline{h}_8 cluster states. The corresponding naphthalene- \underline{d}_8 states are obscure and less informative.

1. It is noted that the $31,542 \text{ cm}^{-1}$ peak reported by Hanson *et al.*^{1a} to be the isolated impurity state of naphthalene- \underline{h}_8 persists up to a concentration of almost 50% naphthalene- \underline{h}_8 . The same thing is true for the isolated impurity state of naphthalene- \underline{d}_8 , although it is obscured by the broad \underline{b} -component of naphthalene- \underline{h}_8 absorption and hence is only recognizable up to about 30% naphthalene- \underline{d}_8 . This is a strong indication that the intermolecular interactions are indeed short-range. An isolated impurity state is essentially formed if the sites in the direct vicinity of the guest are occupied by host molecules. If the interactions are long-range, such an aggregate could hardly be described as "isolated."
2. Two peaks to the lower energy side of the isolated impurity state are observed at $31,526 \text{ cm}^{-1}$ and $31,519 \text{ cm}^{-1}$. These peaks appear weakly at 10% naphthalene- \underline{h}_8 (lost in the microphotometer tracing in Fig. 2) and become apparent at 30% naphthalene- \underline{h}_8 . Another weak line at $31,558 \text{ cm}^{-1}$ was observed for 10% and 20% naphthalene- \underline{h}_8 . The lines at $31,526 \text{ cm}^{-1}$ and $31,519 \text{ cm}^{-1}$ must be the \underline{ac} polarized absorption due to the translationally inequivalent dimer and trimer, respectively, judging from the intensity changes with respect to concentration. A simple calculation for

isolated dimer and trimer places the corresponding energies at M_{12} and $\sqrt{2} M_{12}$ from the monomer line. Thus if we take $M_{12} = 16 \text{ cm}^{-1}$, $\sqrt{2} M_{12} = 22.5 \text{ cm}^{-1}$, then these two lines fall within the expected energy range. The $31,558 \text{ cm}^{-1}$ line, which is 16 cm^{-1} to the blue of the monomer line, is assigned as the \hat{b} -component of the dimer absorption. Hanson¹³ assigned the $31,519 \text{ cm}^{-1}$ line as a lattice defect and the $31,558 \text{ cm}^{-1}$ line as the naphthalene- $\beta\hat{d}_1$ absorption. These do not necessarily contradict the present assignment since minute amounts of isotopic impurities and defects are not important for heavily-doped mixed crystals of short path length.

3. Broadening of the naphthalene- \hat{h}_8 isolated impurity line was observed. The broadening is for the most part toward the red. This is consistent with Hanson's¹³ finding that translationally equivalent dimer lines appear to the red of the monomer line. It could only be concluded that translationally equivalent interactions are all negative and smaller in magnitude than the translationally inequivalent interaction. No further information can be obtained concerning different translationally equivalent pairs due to the broadness of the line at this relatively high impurity concentration.

From the above discussion, it is concluded that the translationally inequivalent interaction between nearest neighbors is the largest intermolecular interaction in crystalline naphthalene. This interaction also contributes the major portion of the pure crystal Davydov splitting (144 cm^{-1} out of a total of 158 cm^{-1}). It is worth

noting that the density-of-states function calculated from these pairwise interactions has been shown by Hanson¹³ to be in general agreement with the experimental results from the hot-band study. Our calculations are thus self-consistent.

Examining carefully the published spectra of Sheka,⁶ it is noted that the B_1^1 band (or the \underline{b} -polarized Davydov component of naphthalene- \underline{h}_8) at low naphthalene- \underline{h}_8 concentrations is probably the largely \underline{b} -polarized isolated impurity state near 31,542 cm^{-1} . Since Sheka assumed a concentration-dependent $\epsilon_{\underline{h}_8}$, this assignment appeared to be self-consistent. However, Sheka's own spectra also show that this band actually has a small amount of \underline{ac} polarization. Our spectra show that the 31,542 cm^{-1} band persists up to 50% naphthalene- \underline{h}_8 . This is probably why the B_1^1 band of Sheka appears to be nearly concentration-independent over a wide range of low naphthalene- \underline{h}_8 concentrations. This band then undergoes an abrupt change when $C_{\underline{h}_8}$ is near unity. This misinterpretation of the isolated impurity absorption plus the fact that Sheka's spectra were taken at 20° K and hence are structureless might have led Sheka to overlook the possibility of cluster states. Consequently he and probably also Broude and Rashba⁷ inferred that heavily-doped mixed crystals behave like pure crystals with Davydov splittings associated with each component throughout the entire concentration range. From the present study, it would appear to us that it is only legitimate to speak of "quasi-Davydov splitting" where the concentration of the component in question reaches 50% or more. At low concentrations the terms Davydov components and Davydov

splittings are only meaningful in an average sense. This is exactly why our calculations that treat the cluster states in an average manner do show a broad \underline{ac} component and a broad \underline{b} component separated from each other reminiscent of the Davydov splitting in pure crystals.

In Fig. 3, we compare our experimental results with calculations presented in Part I, using the experimental density-of-states function of Colson *et al.*⁴ It is noted that the agreement is fairly good except for the guest band at low concentrations. Calculations based on the density-of-states function of the octopole model because of its large asymmetry do not coincide with the observed spectra. On the other hand, using the correct values of $\epsilon_{\underline{h}_8}$ and $\epsilon_{\underline{d}_8}$, the formula of Broude and Rashba will yield incorrect isolated impurity levels. Furthermore, this formula predicts that the \underline{ac} -polarized band of naphthalene- \underline{d}_8 will be concave down and the \underline{b} -polarized band of naphthalene- \underline{h}_8 will be concave up. The effect of the guest on the host band is thus much overestimated. The experimental density-of-states function leads to larger discrepancies when an impurity is placed above the host band. This is reflected in a slightly larger deviation for the naphthalene- \underline{d}_8 bands.

The comparison of intensity distributions and line shapes between theory and experiment cannot be made easily. Both the Green's function method and the model of Broude and Rashba predict the enhancement of outer bands and the weakening of the inner band. Sheka found this to be true but offered no quantitative discussion. In the present investigation, thicker samples are used and much of the

absorption appears to be almost complete. Intensity measurements are therefore not very reliable. The overlapping of inner bands also complicates the situation. As to the line shapes, it can be noted that the \underline{a}_c -polarized naphthalene- \underline{h}_8 absorption does behave as predicted. The \underline{b} -polarized absorptions are intrinsically broad and appear to be somewhat dependent upon crystal preparations. Further broadening due to disorder cannot be assessed from the spectra.

From the above discussion, the theory presented in Part I provides a good description of the basic physics concerning the energy states of heavily-doped mixed crystals. Agreement between the theoretical results was found to be good for the host band. In the guest band, fine structure due to cluster states was not accounted for by the approximate calculations. These features are discussed here semi-quantitatively. Future improvement on the theory will have to consider contributions from higher-order self-energies and derive workable expressions to account for these cluster states from such considerations.

Naphthalene- \underline{h}_8 and Naphthalene- $\underline{\alpha d}_4$

With an energy gap of 51 cm^{-1} , this system represents a case in between the very strong perturbation in one limit and the very weak perturbation in the other. The perturbation is neither strong enough to separate the guest band from the host band nor weak enough to retain the \underline{k} -symmetry. Two absorption bands were predicted by the numerical calculations in Part I. These two bands are broadened by the

\underline{k} -mixing and their energies are predicted to vary nonlinearly with concentration.

In the limit of infinite dilution, a bound naphthalene- \underline{h}_8 level 1 cm^{-1} below the $\alpha\underline{d}_4$ band edge is predicted by the theory¹ (using the experimental density-of-states function by Colson *et al.*⁴). In addition, the theory of Koster and Slater¹ yields a virtual state of naphthalene- $\alpha\underline{d}_4$ 10 cm^{-1} below the \underline{b} -component of naphthalene- \underline{h}_8 . On the experimental side, the naphthalene- \underline{h}_8 isolated impurity state was observed by Broude *et al.*¹⁴ at $31,519 \pm 2 \text{ cm}^{-1}$ ($7 \pm 4 \text{ cm}^{-1}$ below the $\alpha\underline{d}_4$ band edge). No evidence has yet been found for the virtual state of dilute naphthalene- $\alpha\underline{d}_4$ in the naphthalene- \underline{h}_8 mixed crystal.

For the heavily-doped (10-90%) mixed crystal, theory² predicts that at 10% naphthalene- \underline{h}_8 the \underline{b} -component remains sharp whereas the \underline{ac} -component is somewhat broadened due to the interaction between the $\alpha\underline{d}_4$ $\underline{k} = \underline{0}$ state and the naphthalene- \underline{h}_8 impurity state. The perturbation comes from below the band. As the naphthalene- \underline{h}_8 concentration increases, the \underline{ac} -component becomes sharper and the \underline{b} -component becomes broader. At 10% naphthalene- $\alpha\underline{d}_4$, the virtual state of $\alpha\underline{d}_4$ appears as shoulder background below the \underline{b} -component absorption of naphthalene- \underline{h}_8 . The perturbation now affects mostly the states near the top edge.

The spectra of naphthalene- \underline{h}_8 plus naphthalene- $\alpha\underline{d}_4$ are shown in Fig. 4. The main features are consistent with the theoretical predictions. Broude *et al.*¹⁴ reported that at low concentrations ($\ll 10\%$) the naphthalene- \underline{h}_8 impurity absorption is almost as intense as the

\underline{ac} -component of $\alpha\underline{d}_4$ due to the strong intensity borrowing from the host (known as Rashba's effect¹⁵). As the concentration of naphthalene- \underline{h}_8 increases the intensity of the naphthalene- \underline{h}_8 band should increase while that of naphthalene- $\alpha\underline{d}_4$ diminishes. This explains why at 10% naphthalene- \underline{h}_8 a single band showing broadening toward the blue was observed. The virtual states in dilute mixed crystals have never been observed experimentally. Granted that the experimental density-of-states is essentially correct, the virtual states are only expected when impurities are placed above the band. The broad \underline{b} -component makes such observations extremely difficult. In the 20% $\alpha\underline{d}_4$ spectrum, broadening of the \underline{b} -component absorption of naphthalene- \underline{h}_8 can be noted. This broadening might loosely be designated as due to the virtual states of naphthalene- $\alpha\underline{d}_4$. If the naphthalene- $\alpha\underline{d}_4$ concentration were reduced, theory predicts that a single level separated from the \underline{b} -component of naphthalene- \underline{h}_8 exists; however, it will certainly be obscured by the broad \underline{b} -component of naphthalene- \underline{h}_8 . Similar difficulties also prohibit the observation of $\beta\underline{d}_4$ virtual state.⁶ It would appear that virtual states are only evident in the spectra of heavily-doped mixed crystals.

The nonlinearity is apparent in Fig. 5 where the positions of the \underline{ac} - and \underline{b} -components are plotted against concentration. The slightly large discrepancies involving the \underline{b} -component absorption reflect largely the uncertainties in measuring broad lines. Although the formula of Broude and Rashba⁷ predicts similar concentration dependence for the outer bands, it fails to account for the broadening.

The four-level scheme of Broude and Rashba also gives two inner bands shown by dotted lines in Fig. 5. According to their analysis, the intensity of an absorption line is proportional to the quantity $F(E_{\lambda\rho})$ given by

$$F(E_{\lambda\rho}) = \frac{[(C_1/\epsilon_1 - E_{\lambda\rho}) + (C_2/\epsilon_2 - E_{\lambda\rho})]^2}{[C_1/(\epsilon_1 - E_{\lambda\rho})^2] + [C_2/(\epsilon_2 - E_{\lambda\rho})^2]}, \quad (3)$$

where $E_{\lambda\rho}$ is the λ^{th} root of the energy secular equation and corresponds to the excitation of the λ^{th} component. The factor-group classification is designated by ρ , the concentrations by C , and the ideal mixed crystals levels by ϵ . The intensity distributions calculated from Eq. (3) show that the outer bands carry as much as 90% or more of the oscillator strength with the remaining 10% or less being carried by the inner bands. The prediction concerning the existence of these inner bands not only disagrees with the experiments but also presents some conceptual difficulties that must be regarded as inherent in the four-level scheme (vide infra). In our model calculation, the inner bands show both broadening and weakening at large perturbation strength. They disappear smoothly going from strong to weak perturbation. In this particular case, the outer bands show a long tailing and no inner bands are apparent. As pointed out in Part I, this difference in the descriptions of the energy states is basically a result of different starting points. Our formulation allows random distribution of impurities while only one configuration is considered in the model of Broude and Rashba.

Finally, according to the model of Broude and Rashba, the two long-wavelength bands are portrayed as the \underline{ac} - and \underline{b} -components of naphthalene- \underline{h}_8 absorptions and the other two short-wavelength bands as the corresponding naphthalene- $\alpha\underline{d}_4$ absorptions (in Sheka's notations they are A_1^1 , B_1^1 , A_1^2 , and B_1^2 , respectively, in the order of increasing energy). The energy difference between A_1^1 and B_1^1 (between A_1^2 and B_1^2) is regarded as the "Davydov splitting" of naphthalene- \underline{h}_8 (of naphthalene- $\alpha\underline{d}_4$). It is built into the theory that the sum of the two Davydov splittings is always equal to the Davydov splitting in pure crystals. (This can be seen from Fig. 5.) This picture is quite misleading in many ways. For example, the A_1^1 band, which is presumably designated as such to mean the \underline{ac} -polarized excitation of naphthalene- \underline{h}_8 , actually involves the excitation of both naphthalene- \underline{h}_8 and $\alpha\underline{d}_4$, as does the B_1^2 band. The B_1^1 band, which is designated to mean the \underline{b} -polarized absorption due to naphthalene- \underline{h}_8 , actually does not converge to the \underline{b} -component of pure naphthalene- \underline{h}_8 absorption. The same thing can be said about the A_1^2 band. Our interpretation of the energy system presented in earlier sections is void of such contradictions. The two bands observed in the spectra can certainly be regarded as the Davydov splitting in mixed crystals. This splitting is noted to have its direct parentage in but different in magnitude from the Davydov splitting in the pure crystal.

Naphthalene- \underline{h}_8 and Naphthalene- $\beta\underline{d}_1$

In our formulation presented in Part I, the average Green's

function is expressed as an infinite perturbation expansion involving different powers of (Δ/T) , where Δ is the perturbation strength and T is the bandwidth. For naphthalene- \underline{h}_8 and $\beta\underline{d}_1$ system, the energy gap is 21 cm^{-1} (compared with a total width of $\sim 160 \text{ cm}^{-1}$). The expansion is expected to converge rapidly and $\Sigma(\underline{k}, E)$ is very small. In this weak perturbation limit,

$$\langle G(\underline{k}, E) \rangle \cong \frac{1}{E - C_A \epsilon_A - C_B \epsilon_B - \epsilon(\underline{k})} ,$$

hence the \underline{k} -mixing is negligible and the whole band is shifted from the band center of ϵ_A to $C_A \epsilon_A + C_B \epsilon_B$. Each $\underline{k} = \underline{0}$ level will be a linear function of concentration and practically no broadening is expected. In the limit of infinite dilution, no solution to the equation of Koster and Slater¹ for isolated impurity can be obtained.

The spectra are shown in Fig. 6. They resemble the spectra of pure crystals and no appreciable amount of broadening can be observed. Similar plots of line positions vs concentration are shown in Fig. 7 and yield a straight line. It should be noted that the model of Broude and Rashba again predicts two inner bands plotted as a dotted line in Fig. 7. Although the intensities of the inner bands calculated from Eq. (3) are only about 1% of the total intensity, the same inherent difficulties of this model can be noted.

B. Band-to-Band Transitions

General Discussion

The usefulness of studying band-to-band transitions in molecular crystals has long been recognized. Rashba¹⁶ first proposed the method in connection with the study of exciton density of states. Its recent utilization to crystalline benzene and naphthalene was carried out by Colson *et al.*⁴ Due to the familiar $\Delta\mathbf{k} = \mathbf{0}$ selection rule, the standard spectroscopic data involve only the optical transitions from the vibrationless ground state to some specific points (i. e., $\mathbf{k} = \mathbf{0}$) in the exciton Brillion zone. In band-to-band transitions, however, the initial states consist of all the \mathbf{k} -states in the vibrational (or electronic) exciton band and hence optical transitions to all the \mathbf{k} -states of the electronic (or vibrational) exciton band are accessible to spectroscopic investigation. Further simplification can be achieved if the vibrational exciton bandwidth is much smaller than the electronic exciton bandwidth. In this case, band-to-band transitions will directly yield information concerning the density-of-states of the electronic exciton band.

In the formulation presented in Part I,² calculations were done only for the upper states. Similar calculations can also be done for the vibrational exciton band. This type of calculation would involve two different vibrational excitations of the two different components. However, it is now known that vibrational exciton bandwidths in molecular crystals are likely to be of the order of a few wavenumbers. If the perturbation is strong, the weak intermolecular interactions are

too small to induce coupling between the two bands. On the other hand, if the perturbation is weak, the resulting bandwidth would be very small compared to the electronic exciton bandwidth. In both cases, detailed calculations concerning the vibrational band structure would be unnecessary in interpreting the band-to-band spectra. Therefore, in the following analysis the exciton behavior of the ground state vibrational band will be neglected. Vibrational levels will simply be treated as a degenerate set of levels rather than as a band.

When the coupling between vibrational levels is neglected, it is logical to use the localized representations $\Psi_{\text{vib}}(\underline{R}_i)$, which is defined as¹⁷

$$\Psi_{\text{vib}}(\underline{R}_i) = \phi_{\text{vib}}^*(\underline{R}_i) \prod_{j \neq i} \phi_{\text{vib}}(\underline{R}_j) \quad , \quad (4)$$

where $\phi_{\text{vib}}^*(\underline{R}_i)$ denotes the vibrational excitation at site \underline{R}_i , and $\phi_{\text{vib}}(\underline{R}_j)$ corresponds to the vibrationless wavefunction at site \underline{R}_j . Using this representation, all the $\Psi_{\text{vib}}(\underline{R}_n^A)$'s corresponding to the excitation of A molecules will be degenerate and independent of site index n , as are the $\Psi_{\text{vib}}(\underline{R}_m^B)$'s. Thus we have two sets of degenerate levels, one with energy ϵ_A^{vib} and the other ϵ_B^{vib} , the degree of degeneracy being equal to the number of molecules of the component in question, namely N_A or N_B .

Now consider a particular distribution of hosts and guests. The electronic wavefunction of a particular level \underline{k} with energy $E_{\underline{k}}$ can be written as

$$\Phi_{\text{elec}}^k = \sum_i a_i^k \Psi_{\text{elec}}(\underline{R}_i) \quad , \quad (5)$$

where $\Psi_{\text{elec}}(\underline{R}_i)$, similar to $\Psi_{\text{vib}}(\underline{R}_i)$ in Eq. (4), denotes the electronic excitation at site \underline{i} . Linear combination of one-site excitation functions is necessary because of the larger mobility of the electronic excitons. The transition moment between the \underline{k} -level and, say, one of the levels having energy ϵ_A^{vib} and corresponding to the excitation of A-molecule at site \underline{R}_{n_A} will be

$$\sum_i a_i^k \langle \Psi_{\text{elec}}(\underline{R}_i) | \underline{M} | \Psi_{\text{vib}}(\underline{R}_{n_A}) \rangle = a_{n_A}^k \underline{M}_A \quad , \quad (6)$$

where \underline{M}_A is the transition moment of the same transition of the free molecule A. Since all the vibrational excitations of A in different sites are degenerate, the total intensity of the transition $E_k - \epsilon_A^{\text{vib}}$ will be

$$|\underline{M}_A|^2 \sum_{n_A} |a_{n_A}^k|^2 \quad . \quad (7)$$

Similarly the transition $E_k - \epsilon_B^{\text{vib}}$ will carry the intensity

$$|\underline{M}_B|^2 \sum_{m_B} |a_{m_B}^k|^2 \quad (8)$$

with

$$\sum_{n_A} |a_{n_A}^k|^2 + \sum_{m_B} |a_{m_B}^k|^2 = 1 \quad ,$$

because the wavefunction is normalized.

Normally, if we consider closely related vibrational levels of A and B, \underline{M}_A and \underline{M}_B are essentially the same. Under this condition a comparison of intensities of the transition $E_k - \epsilon_A^{\text{vib}}$ and $E_k - \epsilon_B^{\text{vib}}$ will reveal the true nature of the excitation involved in level \underline{k} , i. e., whether it is pure A excitation, pure B excitation, or a mixture of the two. This is the technique Broude et al.¹⁸ used in determining the excitation amplitude of impurity centers in dilute mixed crystals of naphthalenes. However, the assumption that $\underline{M}_A \cong \underline{M}_B$ were neither clearly stated nor carefully examined.

Notice that in applying to the case of a pure crystal the approximation used here is more restricted than the "restricted Frenkel limit" of Colson et al.⁴ Delocalized sets were used by Colson et al. although the finite vibrational exciton bandwidth was neglected. In our limit, the band-to-band transition in pure crystals can still be interpreted in terms of the density-of-states function. Instead of using the $\Delta \underline{k} = \underline{0}$ selection rule for the $\underline{k} \neq \underline{0}$ state to prove that intensity is conserved, the normalization condition here guarantees the same results.

When configuration averaging of random lattices was carried out, a state nearly degenerate with the \underline{k} -level discussed above might have different characteristics from the \underline{k} -level itself. In this case the band-to-band transition is rather difficult to discuss. It is only under two conditions that the band-to-band spectra can be interpreted simply as the density-of-states function:

$$1. \quad \sum_{n_A} |a_{n_A}^k|^2 \cong 1, \quad \sum_{m_B} |a_{m_B}^k| \cong 0, \quad \text{or vice versa;}$$

$$2. \quad \epsilon_A^{\text{vib}} \cong \epsilon_B^{\text{vib}} .$$

In Toyozawa's language,¹⁹ case 1 would be strong persistent type \leftrightarrow strong persistent type transitions, and case 2 would be persistent or amalgamated type (electronic band) \leftrightarrow amalgamated type (vibrational band) transitions. In Fig. 8 we illustrate different situations diagrammatically. It can be seen that only in cases (a), (c), and (e) can the band-to-band transitions be directly related to the density-of-states function.

Finally, it should be pointed out that the excitation amplitude a_i^k can not be calculated from the average Green's function obtained in Part I. It is necessary to calculate the excitation amplitude for each individual Green's function by solving the equation,

$$\underline{G}^{-1} \underline{a} = 0$$

and then average over all impurity distributions, rather than solving a similar equation involving the average Green's function. In order to determine the nature of excitation we will have to resort to experimental observations.

Naphthalene- \underline{h}_8 and \underline{d}_8

The fluorescence spectra of naphthalene- \underline{h}_8 and \underline{d}_8 mixed crystals were taken at 4° K to determine (1) whether the low energy absorption edge is actually the edge of the density-of-states function as predicted by the theoretical calculations, (2) whether it is justified

to neglect the exciton behavior of the vibrational exciton band in the ground electronic state, and (3) whether any cooperative electronic excitation¹⁸ involving both the host and the guest actually occurs in this particular system.

The spectra are shown in Fig. 9 and their assignments are given in Table I. The 0-0 transitions are very weak in each case due to strong reabsorption; however, they can be located by adding a constant quantum of 510 cm^{-1} corresponding to ν_{17} (or ν_1 , vide infra) to the first strong vibronic bands. The positions of the band edges in the upper state can thus be determined. From a comparison of Table I and Figs. 2 and 3, it can be seen that the band edges coincide with the absorption edges in agreement with our theoretical predictions. Furthermore, constancy of the vibrational intervals is observed. As shown in the $\Delta\nu$ columns of Table I, the spectra have similar vibronic structures built on varying origins. The widths of the vibronic bands, which are roughly 10 cm^{-1} , are about the same as those of the pure crystal fluorescence. If the interactions between the vibrational levels were strong, the resonance interactions would cause the spreading of the vibrational states and the quasisonance interactions would induce the coupling between the vibrational levels of the host and the guest. None of these effects are observed, indicating that vibrational excitations are essentially localized. The $\sim 10\text{ cm}^{-1}$ widths of the vibronic bands are believed to be due to either the thermal population of the upper states or the intrinsic linewidth or both. It follows from a comparison between the linewidths of mixed crystals and those of pure

crystals that the vibrational interactions can not be larger than a few wavenumbers. In fact, the only factor-group splitting observed in the pure crystal Raman spectra measures only 0.7 cm^{-1} .²⁰

The spectra of 10% naphthalene- \underline{h}_8 have two origins: one coincides with the dimer state discussed in Section 3. A, and the other coincides with the trimer state (within the experimental uncertainty caused by the width of the vibronic bands). This fact not only supports the idea of a localized vibrational excitation but also indicates that the density-of-states function is probably not continuous at this concentration. Due to the breakdown of the $\Delta \underline{k} = \underline{0}$ selection rule in mixed crystals, any state no matter whether it is optically active in ordinary absorption can be observed in a band-to-band transition.²¹ The fact that two relatively sharp lines are observed instead of a broad band must mean that there are few or no states in between the dimer and the trimer states.

The analysis of the vibronic structure given in Table I is essentially the same as those of Broude et al.²² and Pröpstl and Wolf²³ for the pure crystal fluorescence. It also correlates well with McClure's²⁴ fluorescence results of naphthalene in durene and the gas phase hot band data of Craig et al.²⁵ The 510 cm^{-1} vibration has been shown by Broude et al. to be an unresolved band involving both a b_{3g} vibration (ν_{17}) and an a_{1g} vibration (ν_1). The 1023 cm^{-1} band, which is nearly degenerate with ν_3 (a_{1g}), is assigned here as $\nu_{17} + \nu_1$ (b_{3g}) in accordance with Craig's polarization results. The 937 cm^{-1} band was also assigned by Broude et al. to be an unresolved band of 935 cm^{-1}

(b_{3g}) and 940 cm^{-1} (a_{1g}). It is assigned here as b_{3g} (ν_{18}) alone since no a_{1g} vibration of 940 cm^{-1} was observed in the pure crystal Raman spectra.²⁰ The 1459 cm^{-1} line was reported by Broude *et al.* but left unassigned. It is tentatively assigned as ν_6 corresponding to the Raman value of 1464 cm^{-1} .²⁰

In the search for naphthalene- \underline{d}_8 vibrations we concentrate on the four bands at 510 , 764 , 937 , and 1380 cm^{-1} . It was reported by Broude *et al.*¹⁸ that at low concentrations of naphthalene- \underline{h}_8 cooperative excitation does occur, based on the finding that a naphthalene- \underline{d}_8 vibration of 496 cm^{-1} was observed. From the intensity ratio, the excitation amplitude at the impurity center was set to be 0.9 . As we pointed out in the previous section, a cooperative excitation can only be positively identified if the entire host vibronic bands are observed in a supposed guest emission. The naphthalene- \underline{d}_8 emission has been studied by McClure²⁶ in a durene host. The ground state fundamental was also determined from hot bands by Craig and Hollas.²⁷ These two sources are in general agreement, although McClure's spectra seemed to be more complicated possibly due to the presence of isotopic impurities. The corresponding vibrations of ν_{17} , ν_2 , ν_{18} and ν_5 are found to be 491 , 694 , 880 , and 1380 cm^{-1} , respectively. Of all the four vibrations only the first one was identified by Broude *et al.*¹⁸ and none are apparent in our spectra. It is thus concluded that although some degree of cooperative excitation might be operating at low naphthalene- \underline{h}_8 concentration, for heavily-doped mixed crystals the low energy band edges are mainly comprised of naphthalene- \underline{h}_8 states,

or equivalently the excitation is mainly trapped in naphthalene- \underline{h}_8 centers.

To investigate the entire naphthalene- \underline{h}_8 band, we resort to band-to-band transitions at elevated temperatures. The fluorescence spectra at 77° K are shown in Fig. 10. Two features can be noted; firstly, the peaks show a gradual shift to higher energy as the concentration of naphthalene- \underline{h}_8 is reduced, and secondly, the bandwidth decreases in the same direction, especially the 510 and 1893 cm^{-1} bands, which are relatively isolated. The corresponding transitions at 4° K are also given at the bottom of the figure for comparison. The large overlapping of bands makes the identification of an individual band more difficult; however, in each case the positions of the strong peaks do correlate well with the strong bands at 4° K.

It is apparent that only the well-separated bands at 510 and 1893 cm^{-1} can be utilized in evaluating the density of states in mixed crystals. Since these two peaks are broad at 77° K and the difference in vibrational energies is small ($\sim 10 \text{ cm}^{-1}$), the question of whether cooperative excitation exists cannot be answered with certainty. However, the density-of-states functions can still be calculated from the fluorescence band shape. This is concluded from the following considerations:

1. Cooperative excitation as observed in fluorescence is equivalent to splitting the density-of-states function into two parts and shifting one part from the other by the amount equal to the difference in energies of vibrational quanta ($\sim 10 \text{ cm}^{-1}$ in this case). Since the

naphthalene- \underline{h}_8 bandwidth is large compared to this shift, the effect of cooperative excitation on the fluorescence band shape is insignificant. Considering the much larger experimental uncertainties in measuring the band shape and intensity, this effect can be safely neglected. This would put the naphthalene- \underline{h}_8 and \underline{d}_8 systems into the category of case (c) in Fig. 8.

2. On the other hand, the 4° K spectra that are well resolved give no indications of cooperative excitation. The 77° K spectra, although less uncertain, do not seem to involve large cooperative excitation either. From this point of view, this system would belong to case (a) in Fig. 8.

In both cases, the density-of-states function is directly related to the fluorescence band shape.

The 510 cm^{-1} band is singled out and carefully rescanned to obtain the best band shape. The same method used by Colson *et al.*⁴ in determining the pure crystal density-of-states function was used. The fluorescence data at 4° K serve to locate the band edge and the intensity of emission to the blue of the band edge is corrected with proper Boltzmann factors at 77° K. The results are shown in Fig. 11. Also included in the figures are the density-of-states functions theoretically calculated in Part I.² These density-of-states functions were drawn such that the heights roughly match the experimentally determined height. In the 10% naphthalene- \underline{h}_8 fluorescence spectrum, the shoulder to the blue of the band edge was taken as the host emission. Both the host and the guest density-of-states functions were

taken from the theoretical calculations properly proportionated and further separated by 10 cm^{-1} to account for the difference in vibrational excitation energies. Similar to the pure crystal case, large phonon contributions to the red of the band edge can be noted. A band-to-band absorption (hot band) would probably be clear of such complications; however, since they are so similar to the pure crystal emissions, which have been thoroughly investigated in the past, no further attempt was made to show that they are indeed due to phonons.

The agreement between theory and experiment is generally good. The emission intensity in between the host and guest density-of-states functions in the 10% sample could be due to the phonon associated with the host emission or due to the cooperative excitations discussed above or both. As pointed out above, the density-of-states function in the guest band is probably not continuous for the 10% sample. The continuous curve obtained here must be due to the effect of phonon broadening.

Naphthalene- \underline{h}_8 and Naphthalene- $\alpha\underline{d}_4$

As shown in Fig. 4, the absorption spectra of this system show only one \underline{ac} component consistent with the theoretical model. This \underline{ac} -polarized absorption can only be interpreted as a cooperative excitation of both naphthalene- \underline{h}_8 and $\alpha\underline{d}_4$. This interpretation is substantiated by the vibrational analysis of the emission spectra at 4° K shown in Fig. 12. For comparison, the bands that are attributable to naphthalene- \underline{h}_8 are also given. Additional bands assigned as

$\alpha\bar{d}_4$ vibrations are found at 708, 860, 958, 1005, and 1395 cm^{-1} , respectively. It can be seen that the positions of these bands vary with concentration whereas their relative positions with respect to naphthalene- \bar{h}_8 bands remain unchanged. Furthermore, their intensities diminish as the concentration of naphthalene- \bar{h}_8 increases. This evidence shows that they are indeed originating from the same upper state and hence cannot be assigned as impurity emissions. The prominent lines at 510 cm^{-1} and 1893 cm^{-1} are much broader ($\sim 20 \text{ cm}^{-1}$) than the rest of the bands. They must be the unresolved naphthalene- \bar{h}_8 bands plus the $\alpha\bar{d}_4$ bands. At higher naphthalene- \bar{h}_8 concentrations, these two bands become sharper while the other naphthalene- $\alpha\bar{d}_4$ bands reduce in intensity, indicating the gradual decrease of the degree of cooperative excitation.

The emission spectra of naphthalene- $\alpha\bar{d}_4$ are not available in the literature; however, both the normal mode calculations²⁸ and the Raman spectra²⁹ in the liquid state have been done. It must be pointed out that due to the change in the normal coordinates and, probably to a lesser extent, the change in the geometry of the excited state upon isotopic substitution, the correlations between naphthalene- \bar{h}_8 and $\alpha\bar{d}_4$ vibronic structures are only approximate. Thus the 708 and 1005 cm^{-1} bands are undoubtedly the $\alpha\bar{d}_4$ analogies of 764 and 1023 cm^{-1} bands in \bar{h}_8 emission. ν_5 for $\alpha\bar{d}_4$ has been calculated to be 1340 cm^{-1} ; however, the next higher frequency a_{1g} vibration, namely the 1395 cm^{-1} vibration, seems to play the same role as the 1383 cm^{-1} band in \bar{h}_8 . Both bands were identified from the Raman spectra of $\alpha\bar{d}_4$ at 1355 and

1397 cm^{-1} . The 860 and 958 cm^{-1} bands were assigned by Mitra and Bernstein²⁹ as a_{1g} and b_{3g} , respectively, and an 844 cm^{-1} band was assigned as the $\alpha d_4 \nu_{18}$ (937 cm^{-1} in \underline{h}_8). Our results would classify both bands as b_{3g} , playing roughly the same role as the 937 cm^{-1} in \underline{h}_8 with 860 cm^{-1} carrying most of the fluorescence intensity. Another alternative assignment more consistent with the results of Mitra and Bernstein would be to correlate the 958 cm^{-1} band with the 937 cm^{-1} band in \underline{h}_8 and both the 860 and 1395 cm^{-1} bands with the 1383 cm^{-1} band in \underline{h}_8 . However, the intensity distribution seems to rule out this possibility.

The degree of cooperative excitation can be estimated from the intensity ratio of fluorescence bands (of \underline{h}_8 and αd_4). Assuming that $\underline{M}_A \cong \underline{M}_B$, we estimate that for 3.5%, 11%, 21%, 28%, and 38% of naphthalene- \underline{h}_8 , the sums of the squares of the excitation amplitudes at naphthalene- \underline{h}_8 centers are 0.5, 0.6, 0.8, 0.9, and 1.0, respectively.³⁰ It is interesting to note that, using the experimental density-of-states function, Sommer and Jortner^{1b} calculated the same quantity for dilute mixed crystals of naphthalene- \underline{h}_8 in αd_4 to be ~ 0.4 . Thus our estimations are bracketed by this value and unity (in the pure crystal). A theoretical treatment would have to involve, firstly, the identification of the particular configuration that gives the lowest excitation energy and, subsequently, the evaluation of excitation amplitudes (i. e., calculating the crystal wavefunction). At the present stage, this has not been possible to do. However, the energy vs concentration plot shows an upward bending (Fig. 5). The experimental observation that

the parameter discussed above increases faster than linearly with naphthalene- \underline{h}_8 concentration appears to be reasonable.

Similar to the system discussed in the last section, the emission spectra at 77° K are characterized by large bandwidths and large overlapping of bands. All except the 510 and 1893 cm^{-1} bands are actually composite bands. Nothing can be said about the degree of cooperative excitation. The shapes of the 510 and 1893 cm^{-1} bands are quite similar to that of the naphthalene- \underline{h}_8 and $\beta\underline{d}_1$ system (vide infra) except, of course, they shift more drastically with concentration. The theoretical calculations show that the electronic exciton bandwidth of this system is slightly larger than that of the pure crystal and also that there is a small dip separating the naphthalene- \underline{h}_8 band from the $\alpha\underline{d}_4$ band. These features cannot be verified experimentally due to uncertainties in measuring the fluorescence intensities. As a consequence, the density-of-states functions are found to be very similar in shape to that of the naphthalene- \underline{h}_8 and $\beta\underline{d}_1$ system to be discussed in the next section.

Naphthalene- \underline{h}_8 and Naphthalene- $\beta\underline{d}_1$

This system is a good example of case (e) in Fig. 8. As far as all the prominent lines assigned in Fig. 9 are concerned, the vibrational frequencies are practically the same for both naphthalene- \underline{h}_8 and $\beta\underline{d}_1$. This is supported by the vibrational analysis of naphthalene- $\beta\underline{d}_1$ pure crystal fluorescence. Within the experimental vibronic bandwidth at 4° K ($\sim 10 \text{ cm}^{-1}$), the vibronic spacings in the emission spectra

of \underline{h}_8 and $\beta\underline{d}_1$ are found to be the same. Thus at 4° K the mixed crystal spectra show origins that vary with concentration and coincide with the low energy absorption edge. Furthermore, the vibronic structures show no change in going from pure naphthalene- \underline{h}_8 to pure naphthalene- $\beta\underline{d}_1$. Notice that these features are also observed in spectra of naphthalene- \underline{h}_8 and \underline{d}_8 (Fig. 9). However, the interpretations are quite different. In the case of \underline{h}_8 and \underline{d}_8 no cooperative excitations are observed while here cooperative excitations are expected but cannot be observed because $\epsilon_A^{\text{vib}} \cong \epsilon_B^{\text{vib}}$. It is worth noting that if no \underline{k} -mixing occurs, the sum of the squares of excitation amplitudes of a component should be proportional to its concentration. Investigations of other systems³¹ with a small energy gap but a large vibrational energy difference would be of great interest in this respect.

The emission spectra at 77° K are shown in Fig. 13. They resemble pure crystal fluorescence in every respect. The origin shifts slightly with concentration with no change in the band shape. Without further elaboration, it should be evident that the density-of-states functions also resemble that of the pure crystal. This not only agrees with the theoretical calculations in Part I but also indicates that all the deuterated naphthalenes have indeed the same band structure (see also the top band in Fig. 10). Thus the assumption that intermolecular interactions are invariant to isotopic substitutions is well justified.

4. CONCLUSIONS

In this series of investigations, we attempt to answer the following questions: (1) What parameters govern the energy states and optical spectra of heavily-doped mixed crystals? (2) How well do we know about these parameters? In the theoretical treatment, we illustrate that in the first approximation these parameters are: density-of-states function of the pure crystal, energy gap, and the location of the $\underline{k} = \underline{0}$ levels. Calculations based on these parameters are found to be in general agreement with experiments except for cluster states important at low guest concentrations and large energy gap. Therefore in the general theory of disordered solids, workable solutions that account for the pair effects are yet to be sought. As to the second question, the experimental density-of-states function is found to be basically sound. However, more accurate dispersion relations³² are still needed as well as a better understanding of the quantum mechanical origin of exciton interactions. In the latter aspect, the inadequacy of the octopole model has been demonstrated by several workers.^{1, 4} Since the present formulation, which is based on a neutral Frenkel exciton model is generally supported by experimental results, the role of the charge-transfer³³ interaction cannot be a predominant one. The same conclusion was also reached by Hanson *et al.*^{1a} and by Sommer and Jortner^{1b} in connection with their studies of isolated impurity states. In short, none of the present theories on the exciton interactions seem to be completely satisfactory. A refined treatment involving higher-order multipole interactions might be the subject of future explorations.

REFERENCES

1. (a) D. M. Hanson, R. Kopelman, and G. W. Robinson, J. Chem. Phys. 51, 212 (1969); (b) B. S. Sommer and J. Jortner, ibid. 50, 187, 822 (1969).
2. H. K. Hong and G. W. Robinson, J. Chem. Phys. 51, 0000 (1969), "The Electronic States of Heavily-Doped Molecular Crystals--Naphthalene. I. Theoretical," (hereinafter referred to as Part I).
3. S. D. Colson, R. Kopelman, and G. W. Robinson, J. Chem. Phys. 47, 27 (1967).
4. S. D. Colson, D. M. Hanson, R. Kopelman, and G. W. Robinson, J. Chem. Phys. 48, 2215 (1968).
5. D. P. Craig and S. H. Walmsley, Mol. Phys. 4, 113 (1961).
6. E. F. Sheka, Opt. Spektrosk. 10, 684 (1961) [Opt. Spectrosc. 10, 360 (1961)] and also Bull. Acad. Sci. USSR Phys. Series 27, 501 (1963).
7. V. L. Broude and E. I. Rashba, Sov. Phys. --Solid State 3, 1415 (1962).
8. D. M. Hanson and G. W. Robinson, J. Chem. Phys. 43, 4174 (1965).
9. V. L. Broude, Usp. Fiz. Nauk 74, 577 (1961) [Sov. Phys. --Usp. 4, 584 (1962)].
10. G. C. Nieman and G. W. Robinson, J. Chem. Phys. 39, 1298 (1963).
11. S. D. Colson, J. Chem. Phys. 48, 3324 (1968).

12. In a recent paper by R. N. Aiyer, R. E. Elliott, J. A. Krumhansl, and P. L. Leath, *Phys. Rev.* 181, 1006 (1969), attempts were made to study the pair effects in disordered alloys. However, according to these authors, "The final analytic expressions derived are rather complex and calculations have so far only been made in approximations which are not entirely satisfactory." In a disordered molecular crystal, pair effects are even more complicated due to the additional factor group symmetry. See discussions in Part I.
13. D. M. Hanson, "Energy States and Intermolecular Interactions in Molecular Aggregates: Resonance Pair Spectra of Crystalline Naphthalene," unpublished manuscript.
14. V. L. Broude, E. I. Rashba, and E. F. Sheka, *Sov. Phys. -- Dokl.* 6, 718 (1962) [*Dokl. Akad. Nauk SSSR* 139, 1085 (1961)].
15. E. I. Rashba, *Opt. Spektrosk.* 2, 568 (1957) and *Fiz. Tverd. Tela* 4, 3301 (1962) [*Sov. Phys. --Solid State* 4, 2417 (1963)].
16. E. I. Rashba, *Fiz. Tverd. Tela* 5, 1040 (1963) [*Sov. Phys. -- Solid State* 5, 757 (1963)].
17. (a) D. P. Craig and S. H. Walmsley, Physics and Chemistry of the Organic Solid State, D. Fox, M. M. Labes, and A. Weissberger, Eds. (Interscience Publishers, Inc., New York, 1963), Vol. I, Chap. 10; (b) S. A. Rice and J. Jortner, Physics and Chemistry of the Organic Solid State, D. Fox, M. M. Labes, and A. Weissberger, Eds. (Interscience Publishers, Inc., New York, 1967), Vol. III, Chap. 4.

18. V. L. Broude, A. I. Vlacenko, E. I. Rashba, and E. F. Sheka, Fiz. Tverd. Tela 7, 2094 (1965) [Sov. Phys. --Solid State 7, 1686 (1966)].
19. Y. Onodera and Y. Toyozawa, J. Phys. Soc. Japan 24, 341 (1968).
20. D. M. Hanson and A. R. Gee, J. Chem. Phys. 51, 0000 (1969), "Raman Scattering Tensors for Single Crystals of Naphthalene."
21. In an ordinary absorption experiment the intensity of the transition is proportional to $|\sum_i a_i^k|^2$, whereas in a band-to-band transition the intensity is proportional to $\sum_i |a_i^k|^2$. States that are not observable in absorption spectra should be observable in the band-to-band spectra.
22. V. L. Broude, E. F. Sheka, and M. T. Shpak, Bull. Acad. Sci. USSR Phys. Series 27, 597 (1963) [Izv. Akad. Nauk SSSR Ser. Fiz. 27 596 (1963)].
23. A. Pröpstl and H. C. Wolf, Z. Naturforsch. 18a, 724, 822 (1963).
24. D. S. McClure, J. Chem. Phys. 22, 1668 (1954).
25. D. P. Craig, J. M. Hollas, M. F. Redies, and S. C. Wait, Jr., Phil. Trans. Roy. Soc. London 253A, 543 (1961).
26. D. S. McClure, J. Chem. Phys. 24, 1 (1956).
27. D. P. Craig and J. M. Hollas, Phil. Trans. Roy. Soc. London 253A, 569 (1961).
28. D. E. Freeman and I. G. Ross. Spectrochim. Acta 16, 1393 (1960).
29. S. S. Mitra and H. J. Bernstein, Can. J. Chem. 37, 553 (1959).

30. At higher naphthalene- \underline{h}_8 concentrations, the emission spectra contain only naphthalene- \underline{h}_8 vibrations.
31. The system of C_6H_6 and $^{13}CC_5H_6$, which also corresponds to the very shallow trap limit, was investigated by D. M. Hanson, [J. Chem. Phys. 51, 0000 (1969), "Optical Transitions in $^{13}CC_5H_6-C_6H_6$ Mixed Crystals in the Region of the Factor Group Components of Crystalline Benzene"]. However, no emission study was reported.
32. Attempts were made in this direction by D. M. Hanson; see Ref. 13.
33. R. Silbey, J. Jortner, M. T. Vala, and S. A. Rice, J. Chem. Phys. 42, 2948 (1965).

TABLE I. Fluorescence spectra of naphthalene- h_8 and d_8 mixed crystals (in cm^{-1}).

90:10 ^a			70:30 ^a		30:70 ^a		10:90 ^a	
$\bar{\nu}$	$\bar{\nu}-\nu_{0-0}$ ^b	Assignment	ν	$\Delta\nu^c$	ν	$\Delta\nu^c$	ν	$\Delta\nu^c$
30,967	510	$\nu_{17}(b_{3g}), \nu_1(a_g)^d$	30,975	8	30,991	24	31,014 31,006	47 39
30,713	764	$\nu_2(a_g)$	30,720	7	30,735	22	---	--
30,540	937	$\nu_{18}(b_{3g})$	30,545	5	30,560	20	30,587 30,579	47 39
30,454	1023	509 + 514	30,461	7	30,478	24	30,500 30,494	46 40
30,201	1276	510 + 764	30,208	7	30,222	21	---	--
30,094	1383	$\nu_5(a_g)$	30,100	6	30,115	21	30,141 30,133	47 39
30,032	1445	510 + 937	30,038	6	30,052	20	---	--
30,018	1459	$\nu_6(a_g)$	30,025	7	30,040	22	---	--
29,943	1534	2×764	29,948	5	29,966	23	---	--
29,849	1628	$\nu_{22}(b_{3g})$	29,855	6	29,871	22	---	--
29,584	1893	510 + 1383	29,590	6	29,605	21	29,631 29,624	47 40
29,165	2312	impurity?	---	-	---	--	---	--
29,155	2322	937 + 1383	29,160	5	29,177	22	---	--

TABLE I. (continued)

^aThe ratio given refers to naphthalene-h₈ : naphthalene-d₈.

^b0-0 is missing due to reabsorption. The value used here, 31,477 cm⁻¹, is measured from the absorption.

^c $\Delta\nu$ refers to $\nu - \bar{\nu}$, where $\bar{\nu}$ is the value given in the first column.

^d ν_1 and ν_{17} are nearly degenerate. Broude *et al.*²² reported them to be 514 and 509 cm⁻¹ in the crystalline state. They are unresolved here.

FIG. 1. The positions of Davydov components vs concentration for naphthalene- \underline{h}_8 and \underline{d}_8 mixed crystals as reported by Sheka.⁶ The solid curves are calculated by Sheka based on the model of Broude and Rashba.⁷

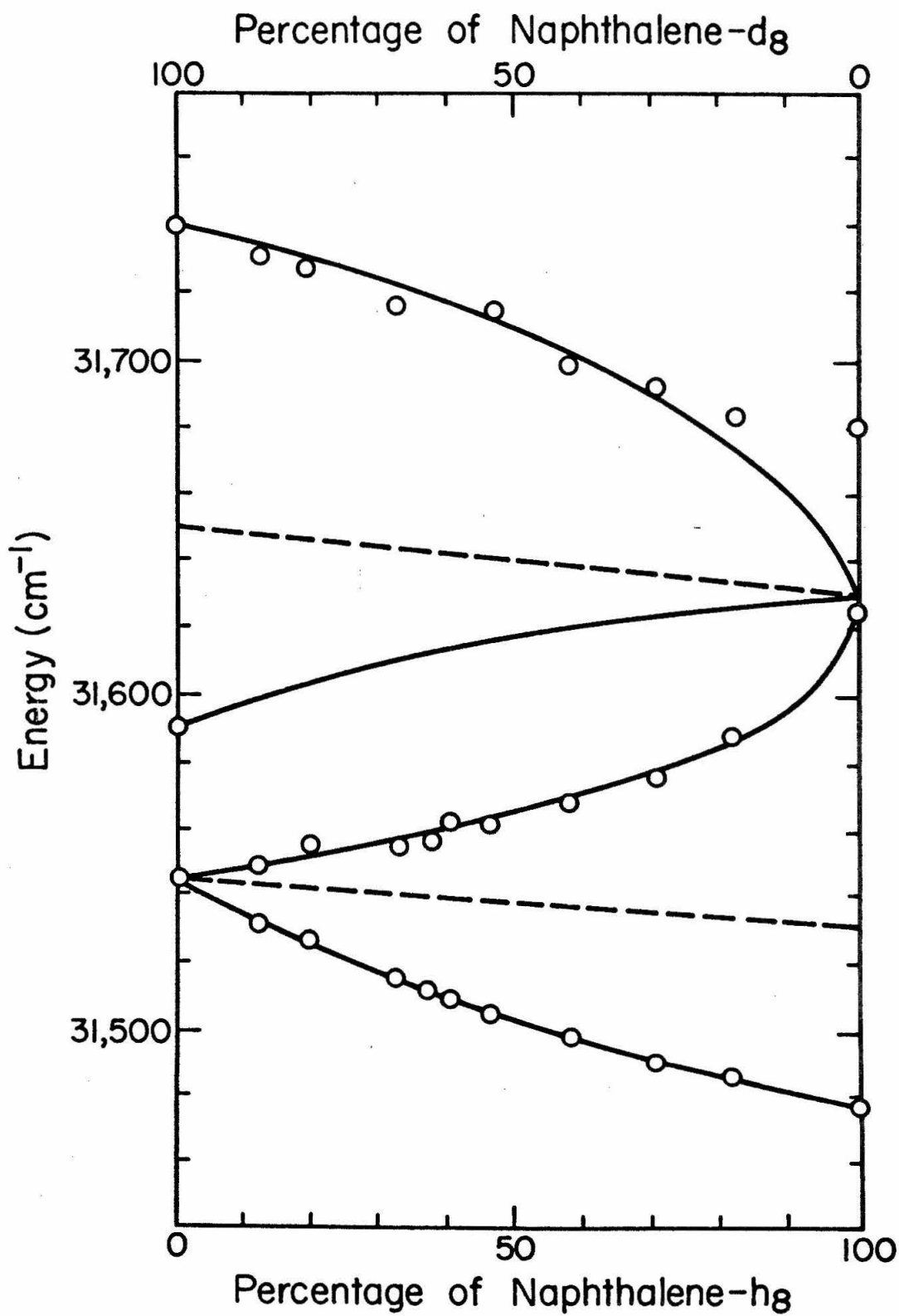


FIG. 2. The absorption spectra of naphthalene- \underline{h}_8 and \underline{d}_8 mixed crystals obtained in this work. The calculated positions of the Davydov components are shown by daggers. The ratios correspond to naphthalene- \underline{h}_8 : naphthalene- \underline{d}_8 given to the closest 10% ($\pm 2\%$). Some of the weak absorptions due to cluster states are lost in the microphotometer tracing. See text.

141

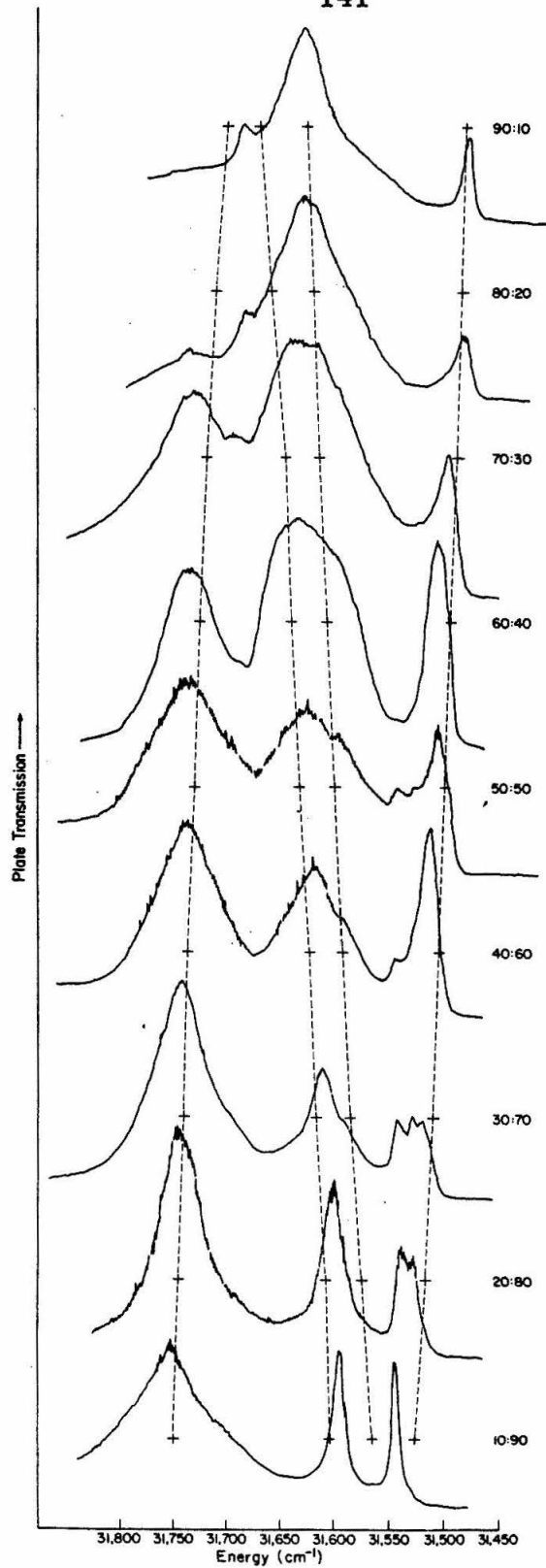


FIG. 3. The positions of the absorption peaks vs concentration for naphthalene- \underline{h}_8 and \underline{d}_8 mixed crystals as observed in this work. The solid circles represent strong lines easily identified from Fig. 2. The open circles represent absorptions that are either weak or not evident in Fig. 2. The triangles represent peaks whose positions are only estimated from Fig. 2 due to large overlapping. The solid curves are the calculated results.

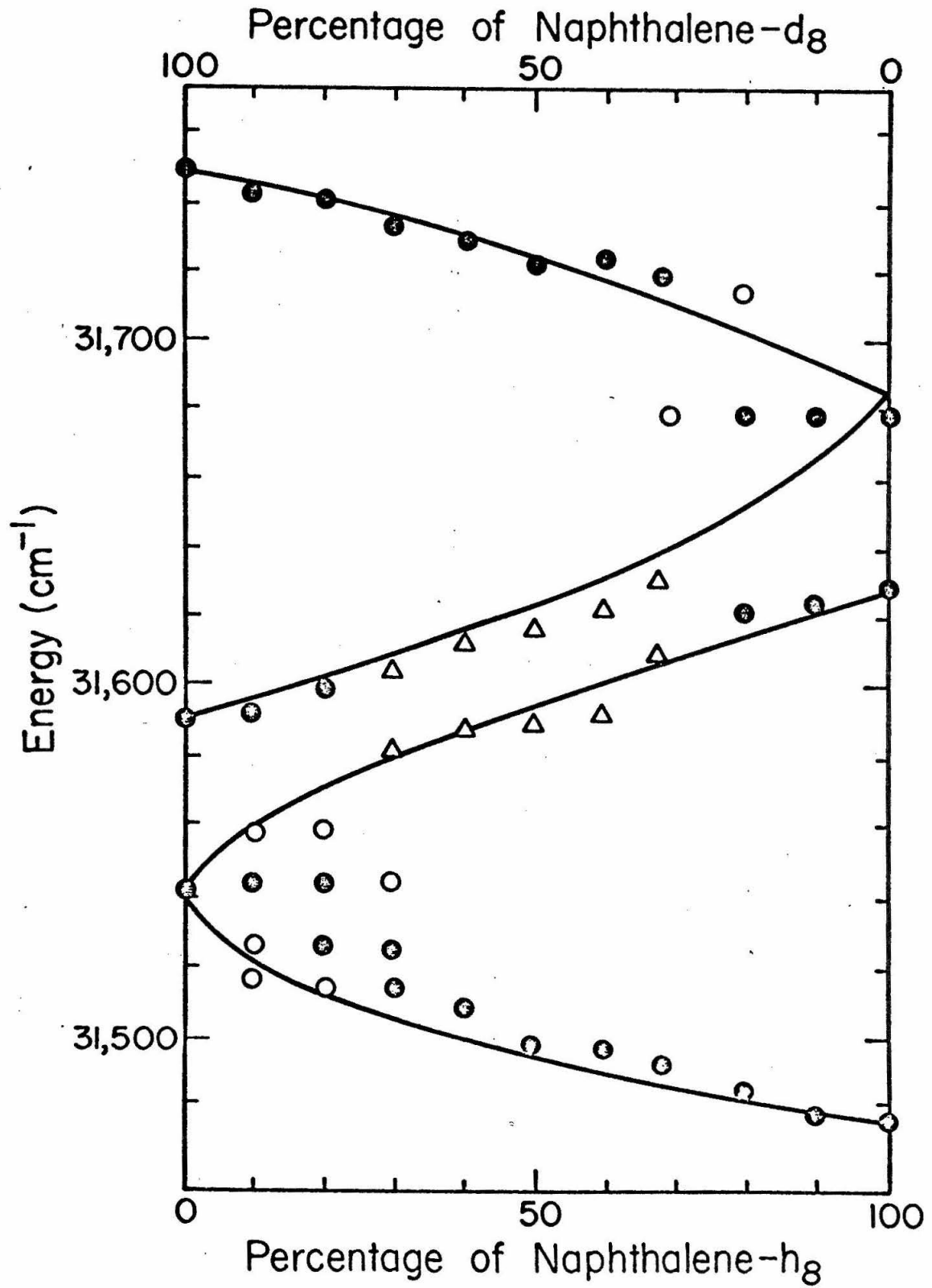


FIG. 4. The absorption spectra of naphthalene- \underline{h}_8 and $\alpha\underline{d}_4$ mixed crystals. The ratios correspond to naphthalene- \underline{h}_8 : naphthalene- $\alpha\underline{d}_4$ given to the closest 10% ($\pm 2\%$).

145

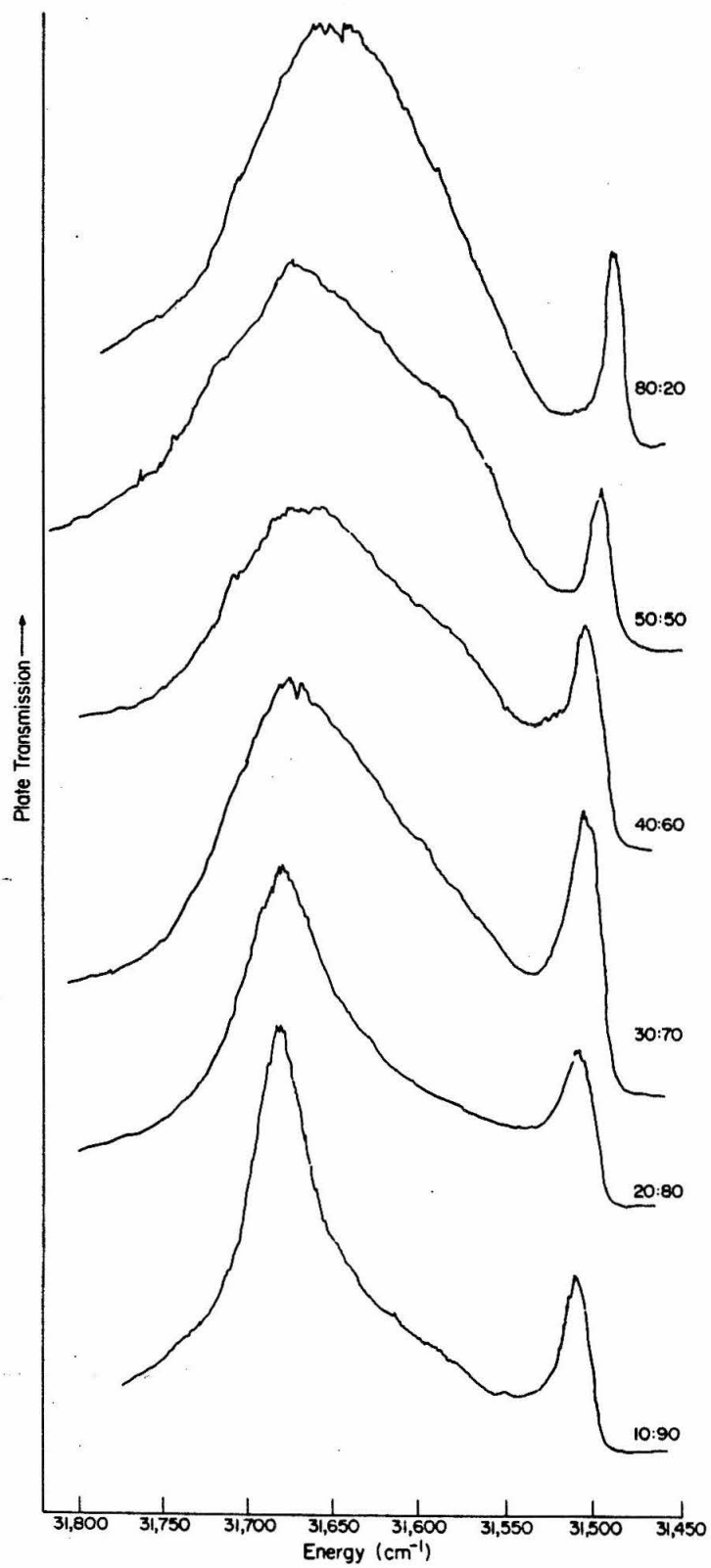


FIG. 5. The positions of the Davydov components vs concentration for naphthalene- \underline{h}_8 and $\alpha\underline{d}_4$ mixed crystals. The solid curves are calculated results in Part I.² The dotted lines indicate extra bands obtained from the formula of Broude and Rashba. See text.

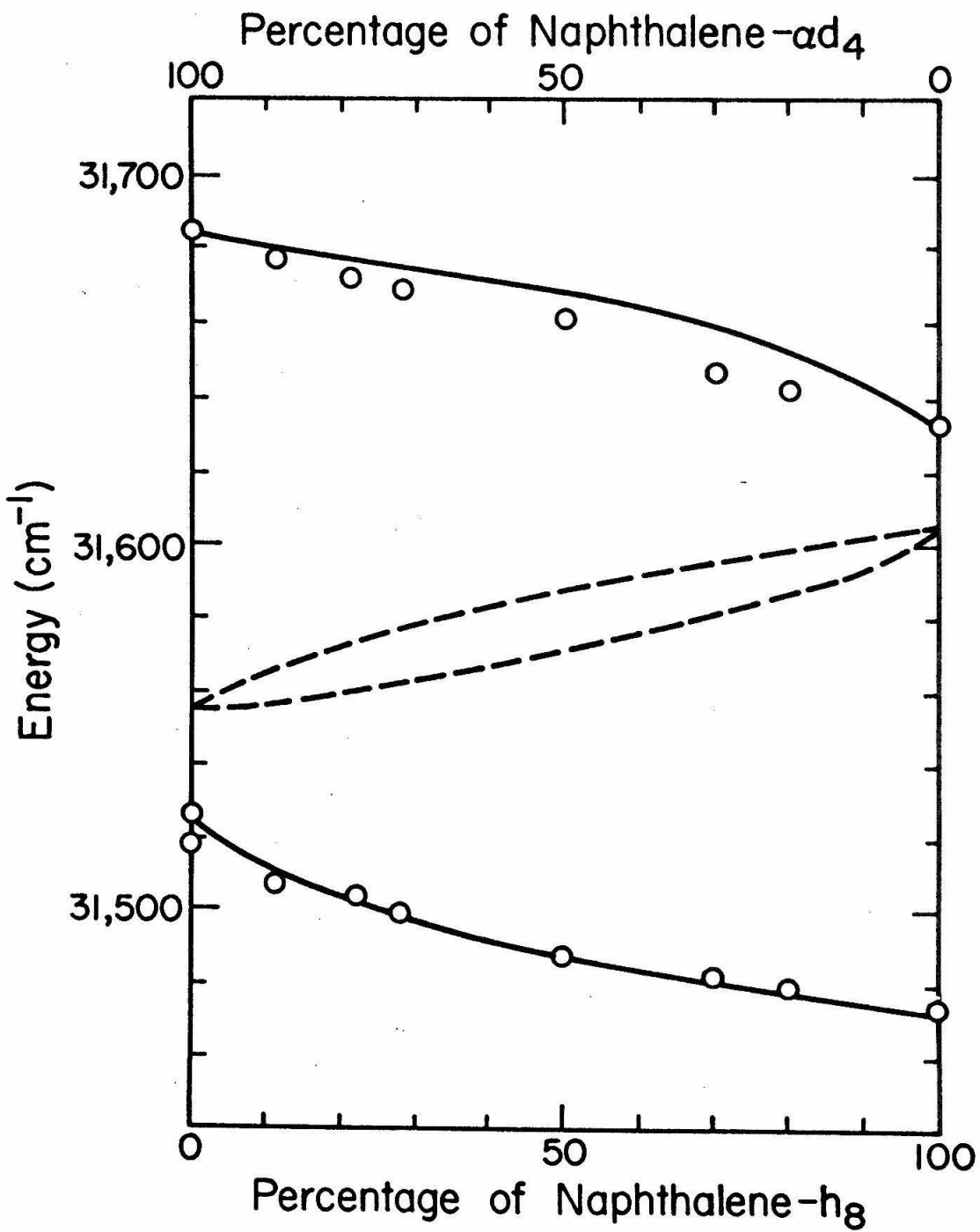


FIG. 6. The absorption spectra of naphthalene- \underline{h}_8 and $\beta\underline{d}_1$ mixed crystals. The ratio corresponds to naphthalene- \underline{h}_8 : naphthalene- $\beta\underline{d}_1$ given to the closest 10% ($\pm 2\%$).

149

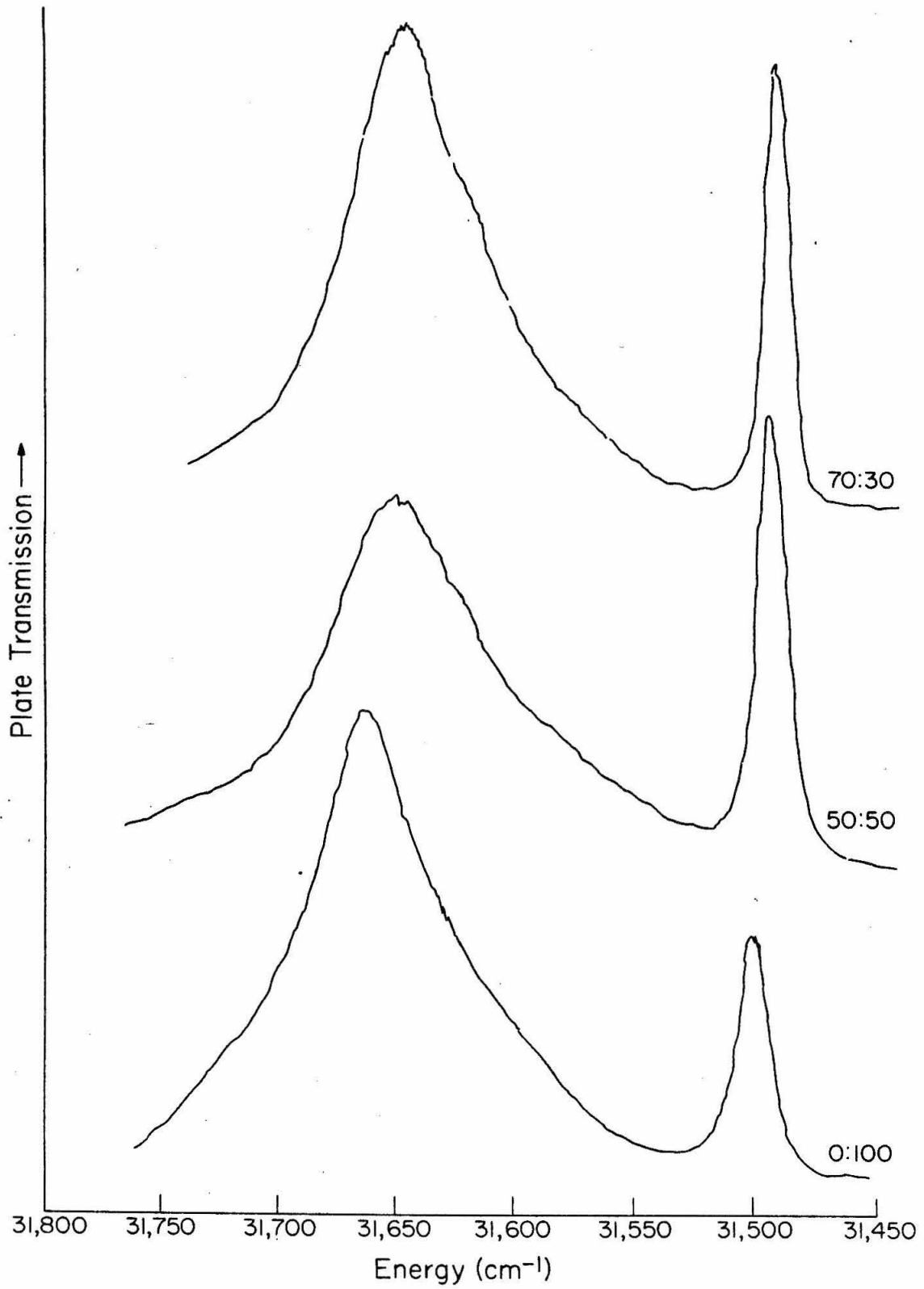


FIG. 7. The positions of the Davydov components vs concentration for naphthalene- \underline{h}_8 and $\beta\underline{d}_1$ mixed crystals. The solid curves are calculated results in Part I.² The dotted lines indicate extra bands obtained from the formula of Broude and Rashba. See text.

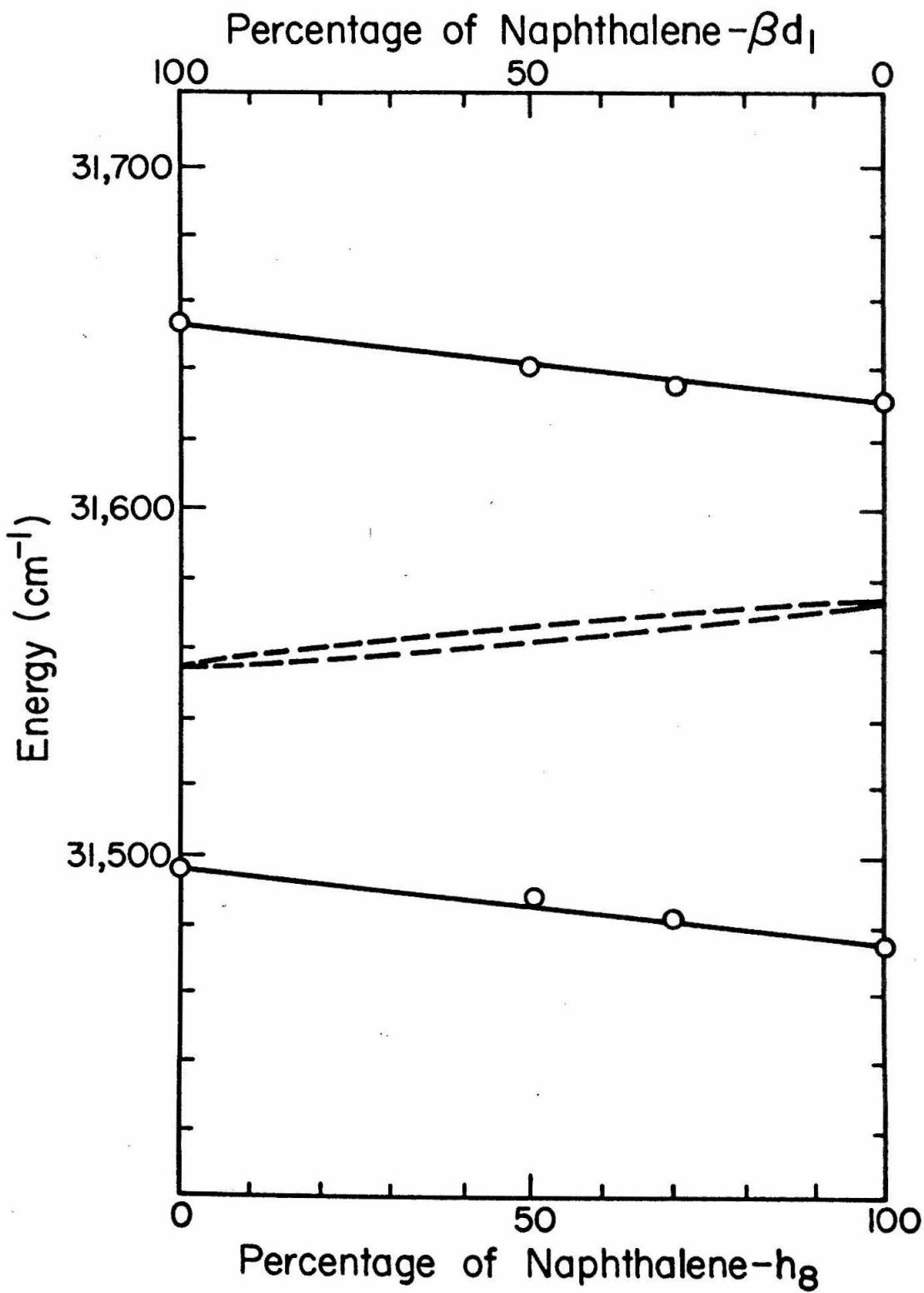


FIG. 8. Schematic diagrams of band-to-band transitions in mixed crystals. The electronic exciton bands are shown with finite bandwidth while the vibrational exciton bands are assumed to be of delta-function type. Possible transitions are indicated by arrows. ϵ_A^{vib} and ϵ_B^{vib} are vibrational quanta of the A-molecule and the B-molecule, respectively.

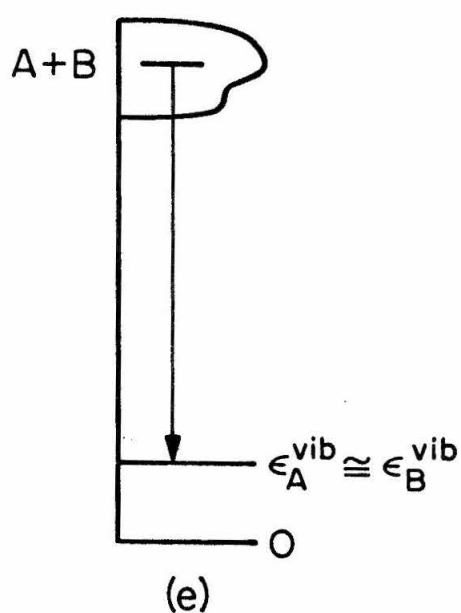
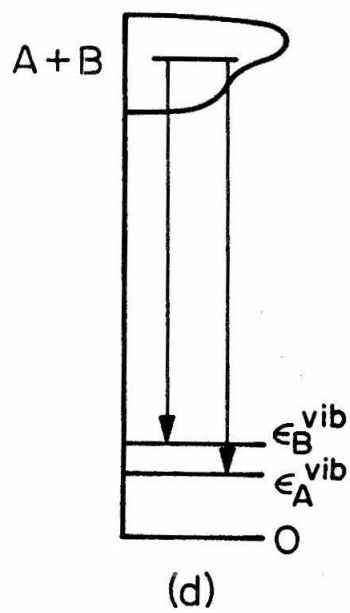
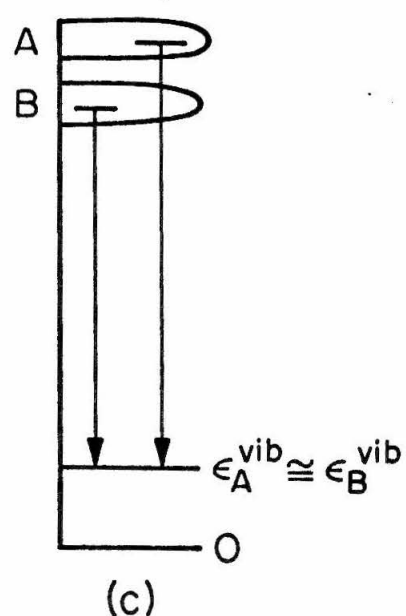
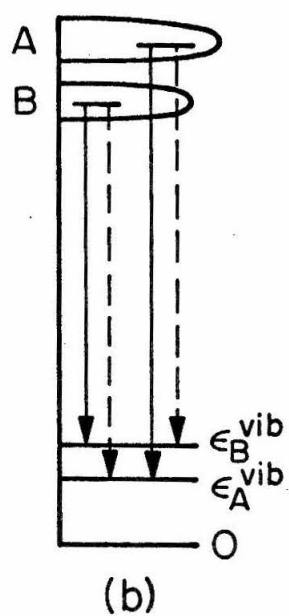
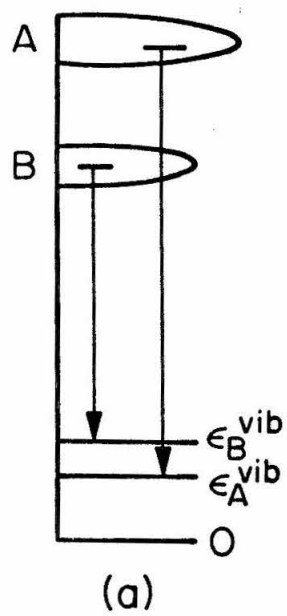


FIG. 9. The fluorescence spectra of naphthalene- \underline{h}_8 and \underline{d}_8 mixed crystals at 4° K. The ratios correspond to naphthalene- \underline{h}_8 : naphthalene- \underline{d}_8 given to the closest 10% ($\pm 2\%$). Vibrational analysis is given at the bottom of the figure and in Table I.

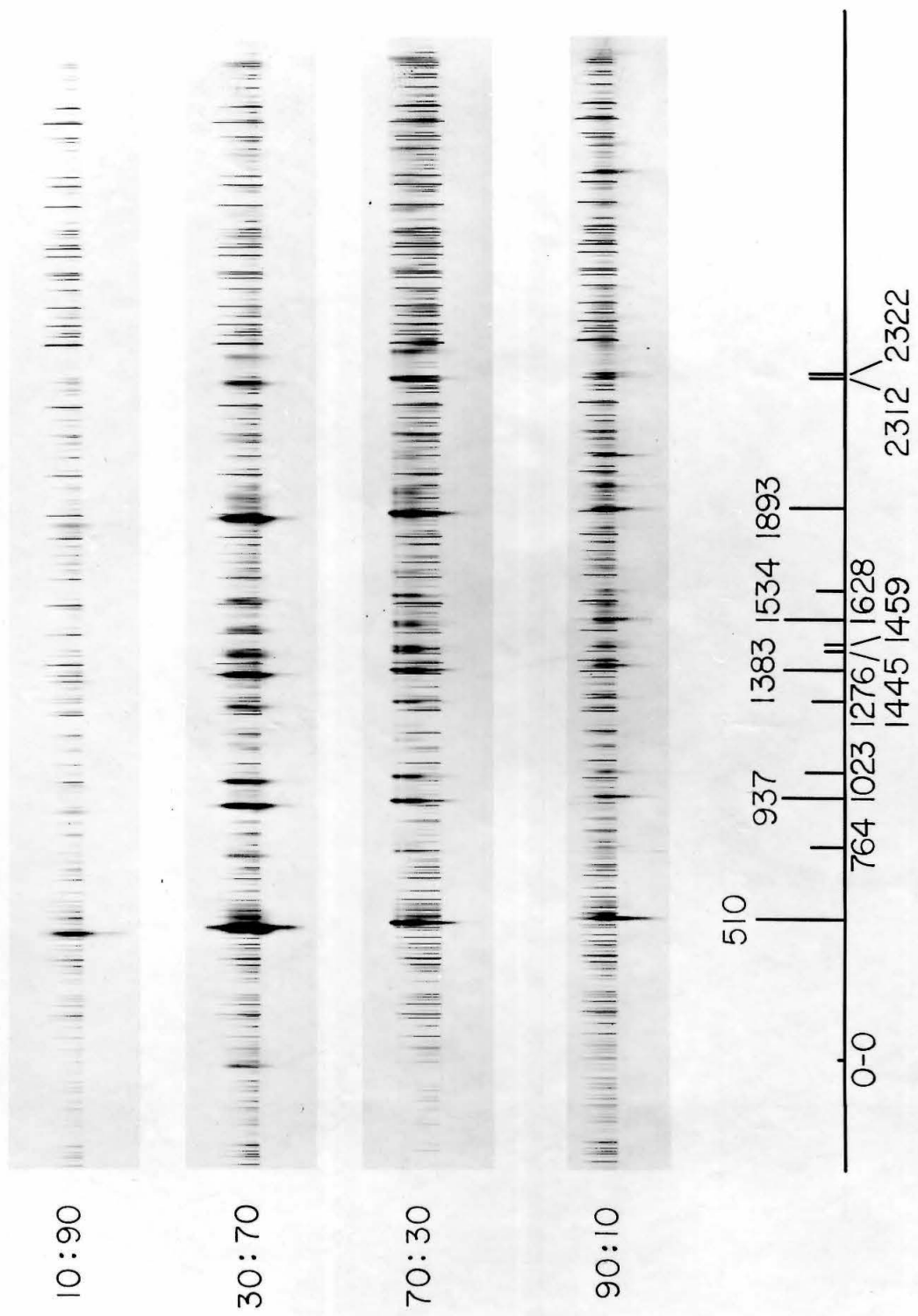


FIG. 10. The fluorescence spectra of naphthalene- \underline{h}_8 and \underline{d}_8 mixed crystals at 77° K. The ratios correspond to naphthalene- \underline{h}_8 : naphthalene- \underline{d}_8 given to the closest 10% ($\pm 2\%$). Vibrational analysis is given at the bottom of the figure.

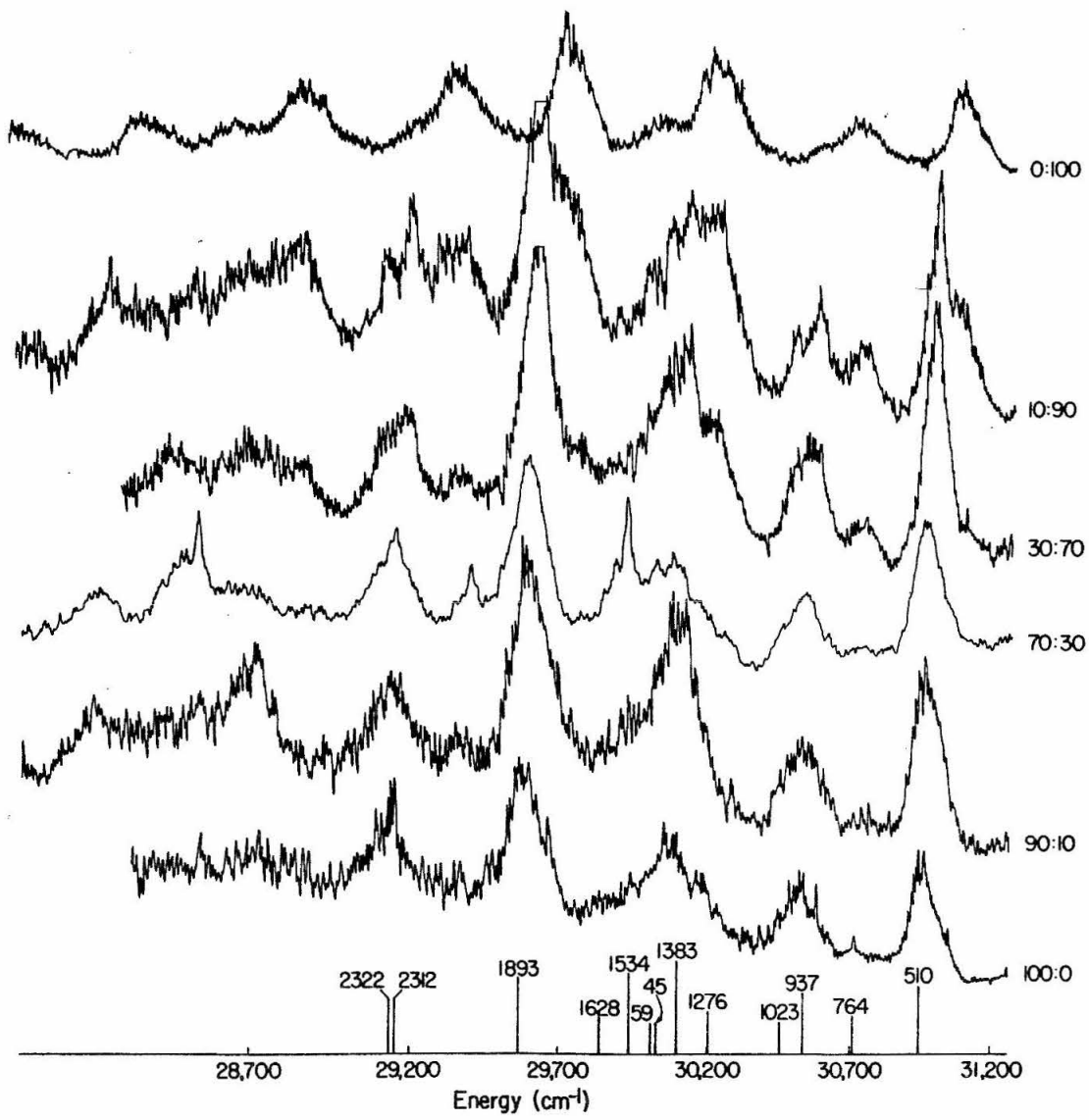


FIG. 11. The density-of-states functions of naphthalene- \underline{h}_8 and \underline{d}_8 mixed crystals calculated from the fluorescence band shapes. The vertical bars are error bars. The fluorescence intensity to the red of the band edge is attributable to phonons and not corrected with Boltzmann factors. Each of the curves under the vertical bars is a calculated density-of-states function. The ratios correspond to naphthalene- \underline{h}_8 :naphthalene- \underline{d}_8 given to the closest 10% ($\pm 2\%$).

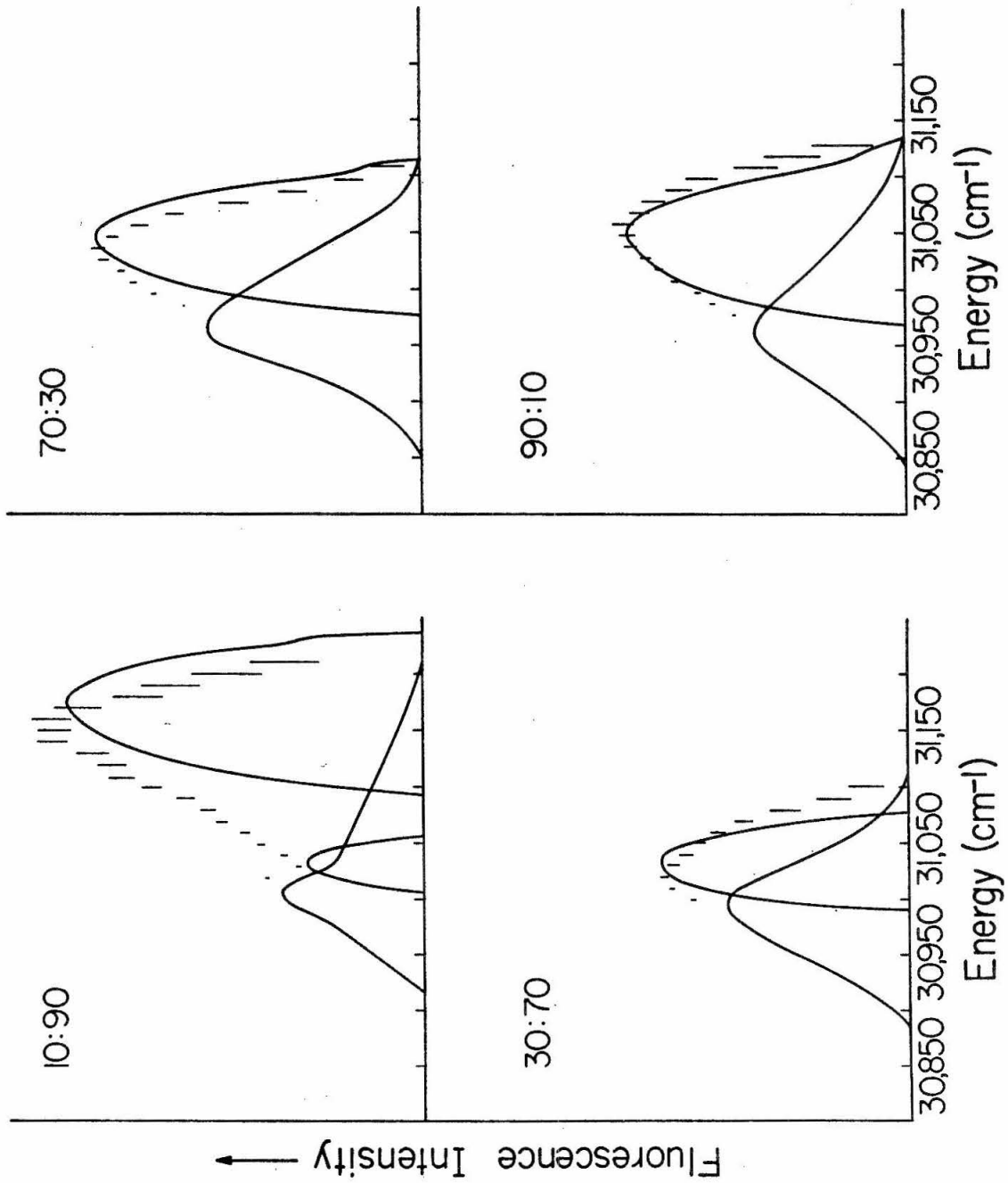


FIG. 12. The fluorescence spectra of naphthalene- \underline{h}_8 and $\alpha\underline{d}_4$ at 4° K. Vibrational analysis is given at the bottom of the figure.

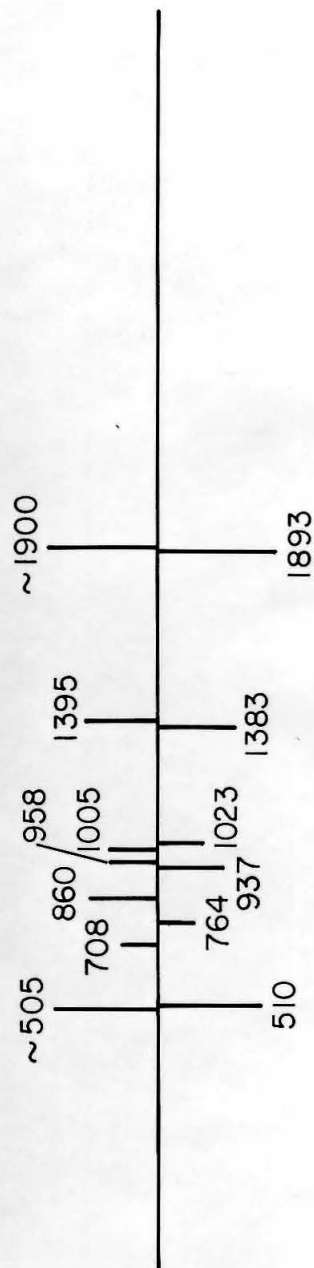
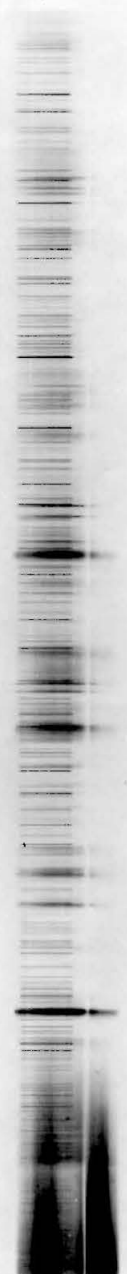
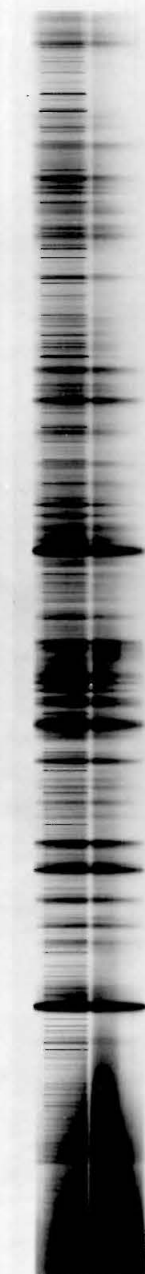
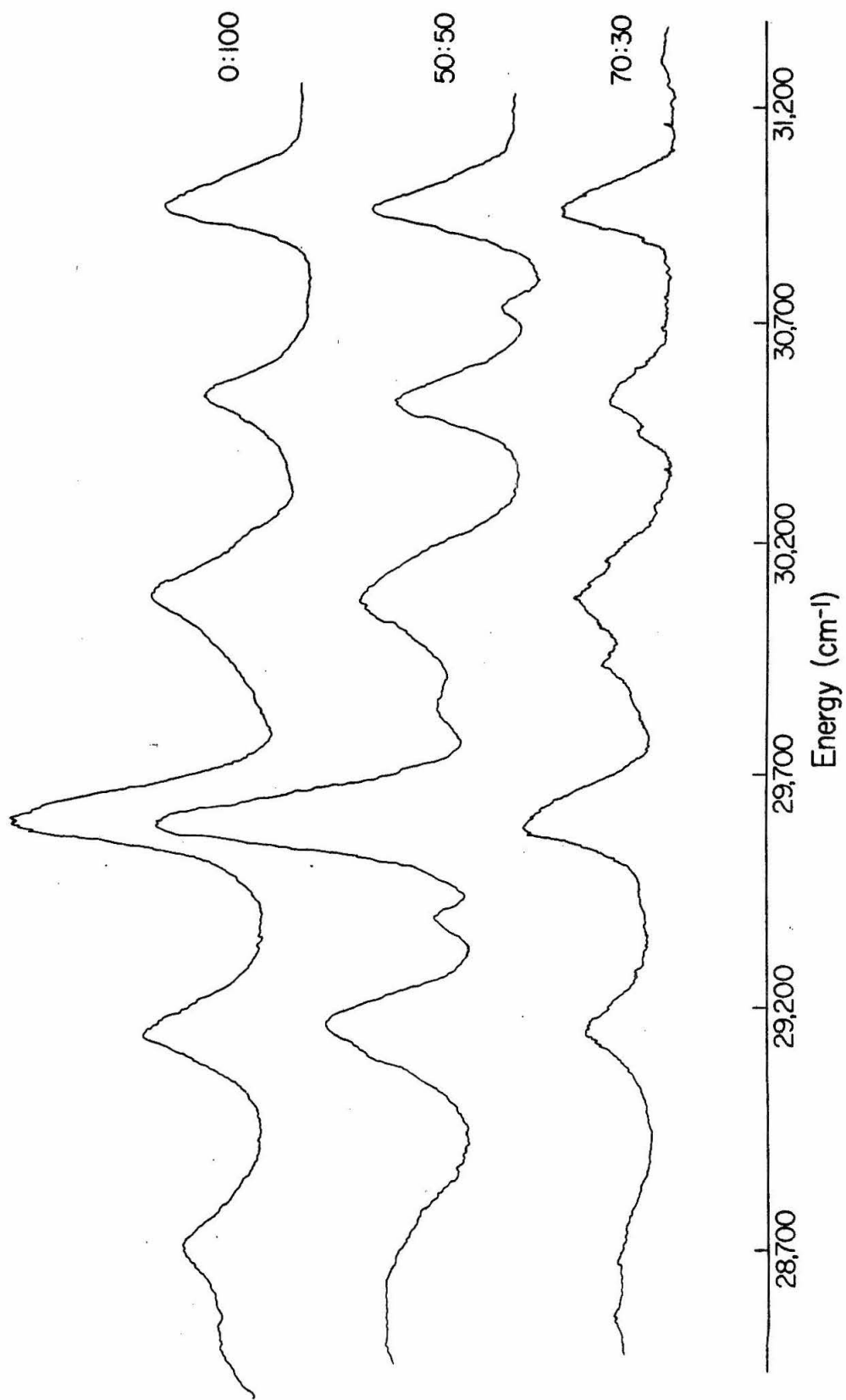


FIG. 13. The fluorescence spectra of naphthalene- \underline{h}_8 and $\beta\underline{d}_1$ at 77° K. The ratios correspond to naphthalene- \underline{h}_8 : naphthalene- $\beta\underline{d}_1$ given to the closest 10% ($\pm 2\%$).



PART III
LOWEST SINGLET AND TRIPLET EXCITED
STATES OF PYRAZINE

1. INTRODUCTION

The near-ultraviolet absorption spectrum of pyrazine vapor was first subjected to a detailed vibronic analysis by Ito et al.¹ These authors observed that the spectrum consisted of a sharp system and a broad system. They concluded that the spectrum is a superposition of two $n-\pi^*$ transitions, one allowed and one forbidden, belonging respectively to the ${}^1B_{3u}$ and ${}^1B_{2g}$ representations of the D_{2h} ² symmetry group.

Similar conclusions were reached by El-Sayed and Robinson.³ They studied the absorption and emission spectra of pyrazine in rare-gas matrices at helium temperature and claimed to have identified the ${}^1B_{2g}$ state. They placed the ${}^1B_{3u}$ state above the ${}^1B_{2g}$ state on the belief that the diffuse system observed by Ito et al., and assigned to the ${}^1B_{2g} \leftarrow {}^1A_{1g}$ transition had its origin below the 0-0 band of the ${}^1B_{3u}$ state.

On the other hand, Innes and his co-workers⁴ investigated the rotational structure of the vibronic transition in the gas phase and found that it was possible to account for all the spectral features observed by Ito et al. on the assumption of a single electronic transition. They argued that the strongest bands in the diffuse system were really a forbidden part of the ${}^1B_{3u} \leftarrow {}^1A_{1g}$ transition, stealing intensity from an allowed ${}^1B_{1u}$ transition through vibronic coupling. The isotopic effect, the band type, and the corresponding polarization were all consistent with this assignment.

The phosphorescence spectrum of pyrazine was first observed

by Goodman and Kasha⁵ in EPA at 77° K. They assigned it as an n- π^* spin-forbidden transition on the grounds that methyl substitutions at 2,5 positions caused a blue shift. El-Sayed and Robinson³ carried out a further study of the gas-phase singlet-triplet absorption spectrum and the low temperature phosphorescence spectrum and presented strong evidence that emission and absorption involved the same upper state. Thus, the transition has been assigned as $^3B_{3u} \leftarrow ^1A_{1g}$ and of n- π^* type.

In this paper, a further study of the electronic spectrum is carried out using benzene as a host. To compare crystal perturbations, isotopically mixed crystals are also investigated. The results obtained definitely place the $^1B_{3u}$ state as the lowest singlet. Some of the vibronic structure that has never been observed is discussed in detail. A similar study of the phosphorescence and T \leftarrow S absorption also leads to the conclusion that the lowest triplet state is $^3B_{3u}$.

2. EXPERIMENTAL

Pyrazine-h₄, obtained from the Aldrich Chemical Company, was purified by several vacuum sublimations. Pyrazine-d₄ was made by Merck, Sharp and Dohme of Canada, Ltd. and was treated in the same way. Benzene of high purity from the Phillips' Petroleum Company was used without further purification.

Solutions of pyrazine in benzene with a concentration ranging from 1% to 0.04% were first outgassed carefully in a vacuum manifold, then transferred to quartz cells with windows of 2-cm i. d. and

of 20 μ pathlength. The solutions in the sample cells were immersed into the helium Dewar directly. A more elaborate crystal-growing technique gave better mixed crystals. However, no difference was found in the spectral properties of the two types of crystals. Samples of pyrazine- h_4 in d_4 with concentrations around 1% were also prepared in the same manner.

All the spectra reported here were taken in the third order of a 2-m grating spectrograph with a resolving power of about 35,000. Appropriate Corning filters were used to cut off light coming from other orders. The excitation phosphorescence spectra were obtained in a manner described elsewhere.⁶

Different excitation sources have been used. These included a P. E. K. X151 Xenon lamp and a G. E. H100 A4/T medium pressure mercury lamp. No effects on the emission spectra were observed. In the case of the absorption spectrum, the xenon lamp was used. A Kasha filter⁷ placed between the light source and the sample cut off most of the infrared radiation from the source. The iron spectrum from an iron-neon hollow cathod served as the wavelength standard.

Because of the high phosphorescence yield, typical exposure times were around 5 min with a slit width of 50 μ . In the case of fluorescence, the exposure time was increased to an hour and the slit width to 150 μ . The wavelengths were measured on a comparator and corrected for vacuum.

3. DISCUSSION

Benzene has its lowest singlet and triplet states at 38,086 and 29,658 cm^{-1} above the ground state, respectively, as determined from isotopic mixed crystal emissions.⁸ For pyrazine-h₄, the 0-0 band of $^1\text{B}_{3\text{u}} \leftarrow ^1\text{A}_{1\text{g}}$ transition in the gas phase lies at 30,875 cm^{-1} ⁴ and the corresponding triplet transition $^3\text{B}_{3\text{u}} \leftarrow ^1\text{A}_{1\text{g}}$ occurs at 26,818 cm^{-1} .³ For pyrazine-d₄, no data have been reported. Because of the rapid excitation transfer and triplet-triplet annihilation in the benzene host crystals, the fluorescence and phosphorescence from the host are virtually impossible.⁹ In the pyrazine-benzene mixed crystal, the singlet and triplet states of pyrazine behave as traps for excitation. Enhancement of emission intensity over that obtained for a nonabsorbing host would be expected. In the case of absorption, the $^3\text{B}_{2\text{u}} \leftarrow ^1\text{A}_{1\text{g}}$ transition of benzene does not interfere due to its low oscillator strength. Using benzene as a host, therefore, a wide spectral region free from host absorption and emission is possible.

The similarity between the molecular structures of benzene and pyrazine proves to be another advantage of this system. The guest molecules apparently reside at substitutional sites of the benzene crystal without disturbing the crystal structure (vide infra). All the lines observed in absorption and emission spectra are extremely sharp, comparable to those obtained in isotopically mixed benzene crystals.⁸

To distinguish extrinsic crystal perturbations from intrinsic spectral features, isotopically mixed crystals of pyrazine-h₄ in d₄

were also investigated. These spectra, together with those of pyrazine-benzene mixed crystals, will be discussed in the following sections.

A. Singlet-Triplet System

Position of the 0-0 Band

Figures 1-3 show the phosphorescence spectra of pyrazine- \underline{h}_4 and \underline{d}_4 in a benzene matrix (hereafter referred to as \underline{h}_4 in \underline{h}_6 and \underline{d}_4 in \underline{h}_6 , respectively) and pyrazine- \underline{h}_4 in pyrazine- \underline{d}_4 mixed crystals (hereafter referred to as \underline{h}_4 in \underline{d}_4).

Previous work on pyrazine in rare-gas matrices by El-Sayed and Robinson³ has shown that the absorption and emission probably involve the same upper state. This conclusion was based on the comparison of the location of the gas phase T \leftarrow S absorption with that of emission in rare-gas matrices. To eliminate the uncertainty involved in comparing the absorption and emission under different experimental conditions, we have taken both the phosphorescence spectrum and the excitation phosphorescence spectrum under the same condition.

It can be seen that the phosphorescence spectrum of pyrazine in benzene has two origins. For \underline{h}_4 in \underline{h}_6 , a strong 0-0 band is observed at 25,996.0 cm^{-1} and another weak origin at 26,080.5 cm^{-1} , 84.5 cm^{-1} to the blue of the strong one. In fact, the spectrum is found to be a superposition of two nearly identical spectra originating from these two origins. The same feature was observed in the spectrum of \underline{d}_4 in \underline{h}_6 , where the strong origin is observed at 26,144.1 cm^{-1} ,

and the weak origin lying 87.2 cm^{-1} higher. This same kind of effect was also reported by Shimada;¹⁰ however, he listed 25,986 and $25,923 \text{ cm}^{-1}$ as two origins. The $25,986 \text{ cm}^{-1}$ component is undoubtedly our $25,996.0 \text{ cm}^{-1}$ (\underline{h}_4 in \underline{h}_6), and Shimada's $25,923 \text{ cm}^{-1}$ component is probably a broad phonon band. Apparently the weaker origin reported here was not observed by Shimada.

In addition, weak satellite lines associated with these two origins were also observed. The lines at 5.2 and 9.0 cm^{-1} to the blue of the strong origin can be attributed to N^{15} and C^{13} isotopes, respectively. Lines were also found at approximately 20 cm^{-1} to the blue of each origin. It is apparent that the interaction potential in which the pyrazine molecule finds itself has several minima. The $\sim 85 \text{ cm}^{-1}$ splitting is probably associated with the tilting of the pyrazine molecular plane and the $\sim 20 \text{ cm}^{-1}$ splitting with the rotation normal to the plane. It is interesting to note that Bernstein *et al.*¹¹ observed the same effect in benzene- Pd_2 in \underline{d}_6 mixed crystals. It was found that of all the three possible orientations of benzene- Pd_2 , two are nearly degenerate and lie $\sim 10 \text{ cm}^{-1}$ higher than the third. The situations here are more complicated because we don't know *a priori* that the pyrazine molecular plane actually coincides with the benzene molecular planes. Only good polarization data can resolve this problem. The same effect was also observed in the ${}^1\text{B}_{3u} \leftarrow {}^1\text{A}_{1g}$ absorption spectrum to be discussed in another section.

Despite the fact that two origins are observed, one is led to believe that most of the pyrazine molecules go into the host crystal

substitutional site with preferential orientation because of the sharpness of the lines and much stronger intensity of one origin compared with the other.

Four bands were observed in the excitation phosphorescence spectrum. The longest wavelength band, lying at $25,995.7 \text{ cm}^{-1}$, coincides with the 0-0 of the emission within the experimental error, clearly showing that the triplet state was symmetry allowed. In addition, three bands having vibrational frequencies of 588.2, 716.1, and 1180.1 cm^{-1} were also observed.

Another piece of evidence comes from the spectrum of \underline{h}_4 in \underline{d}_4 . The 0-0 is observed at $26,258.6 \text{ cm}^{-1}$.¹² This lies extremely close to the two exciton components observed at $26,247.5$ and $26,254.4 \text{ cm}^{-1}$ in a 1.5-mm pure crystal. It is therefore quite certain that the lowest triplet state of pyrazine is ${}^3B_{3u}$ as previously assigned by Goodman and Kasha.⁵

The exact coincidence of the 0-0 transition in absorption and emission has another significance. In a recent paper by Moomaw and El-Sayed,¹³ a 102 cm^{-1} gap between absorption and emission was observed in a pure crystal. These authors interpret this effect to result from molecular reorientation that occurs during the time the molecule is excited and the time it emits. Our results rule out the possibility of relaxation of the excited molecule to a more stable configuration prior to emission at least in our crystals. If the possibility of molecular reorientation before emission is ruled out in the case of mixed crystals, it seems reasonable that the possibility of reorientation

in the case of the pure crystal will also be ruled out.¹⁴

The complicated vibrational analysis of Moomaw and El-Sayed is also different from our analysis. This will be discussed in the following section.

Vibrational Analysis

The main vibrational progression in the phosphorescence spectrum was previously believed to involve only the angular distortion frequency of pyrazine.⁵ Based on this argument, it was impossible to explain the alternation in frequency of adjacent band spacings observed by El-Sayed and Robinson.³ The same difficulties arose in the analysis of the phosphorescence spectrum of pure crystals reported recently by Moomaw and El-Sayed. To remove these difficulties, Shimada¹⁰ proposed that the third member of the progression should be assigned as a C-H bending mode ν_{9a} . This suggestion has been substantiated by the phosphorescence spectrum of \underline{d}_4 in \underline{h}_6 obtained there. The presence of an 881.1 cm^{-1} C-D bending mode together with its combinational band with ν_{6a} gives compelling evidence that the 1227 cm^{-1} band of \underline{h}_4 in \underline{h}_6 and the 1249.4 cm^{-1} band of \underline{h}_4 in \underline{d}_4 should be assigned as a C-H bending mode instead of the first overtone of the ring mode. The actual overtone of ν_{6a} , by the way, was also observed in both cases and occurs at 1191.9 and 1211.5 cm^{-1} , respectively.

Another peculiar feature of the high resolution phosphorescence spectrum is the presence of a strong band at 1207.0 (\underline{h}_4 in \underline{h}_6) and 1231.2 cm^{-1} (\underline{h}_4 in \underline{d}_4). This band is so close to the overtone of ν_{6a}

and the fundamental of ν_9 that they merge together under low resolution. This is the reason why all previous workers assigned them to a single band $2\nu_{6a}$. The same triplet structure was observed at successive 600 cm^{-1} intervals beyond the $\sim 1200 \text{ cm}^{-1}$ group. In \underline{h}_4 in \underline{h}_6 these components are: (1) 1804.4, 1825.4, and 1857.6 cm^{-1} ; (2) 2422.3, 2436.9, and 2459.9 cm^{-1} ; (3) 3034.5, 3056.9, and 3084.3 cm^{-1} . In \underline{h}_4 in \underline{d}_4 they are: (1) 1837.9, 1855.1, and 1892.0 cm^{-1} ; (2) 2462.6, 2480.9, and 2497.4 cm^{-1} ; (3) 3085.8, 3104.1, and 3141.4 cm^{-1} . All these lines are assigned and given in Tables I and III. The analysis of phosphorescence of \underline{d}_4 in \underline{h}_6 is given in Table V.

The parallelism between \underline{h}_4 in \underline{h}_6 and \underline{h}_4 in \underline{d}_4 is very striking. Although the fundamental frequencies vary a lot, presumably because of crystal forces stronger than those met usually for, say, the pure hydrocarbons, the general vibrational pattern remains the same. This is strong justification for the assignments in the sense that it tends to rule out extraneous emission caused by impurities or defects in the two types of crystals.

Although the first overtone of ν_{6b} is strong in both \underline{h}_4 in \underline{h}_6 and \underline{h}_4 in \underline{d}_4 , it is not observed in \underline{d}_4 in \underline{h}_6 . Instead, a 1291.4 cm^{-1} band, tentatively assigned as $\nu_5 + \nu_{6b}$ is observed. An accurate Raman value of ν_{6b} is not available in the literature. In fact the only reported value of 516 cm^{-1} by Lord *et al.*¹⁵ has never been confirmed by other workers.^{16,17} Normal coordinate analysis of Scrocco *et al.*¹⁸ predicted 641 and 620 cm^{-1} for \underline{h}_4 and \underline{d}_4 , respectively. These values seem to compare well with our values of 615 (\underline{h}_4 in \underline{h}_6) and 571.7 cm^{-1}

(\underline{d}_4 in \underline{h}_6). The present assignments of the 1207.0 (\underline{h}_4 in \underline{h}_6) and 1231.2 cm^{-1} (\underline{h}_4 in \underline{d}_4) bands are mainly based on the following grounds:

1. The ν_{6a} and ν_{6b} vibrations are correlated with the ν_6 vibration of benzene (606 cm^{-1} , e_{2g}). Their frequencies should be quite similar. Although the ν_{6b} fundamental is forbidden by symmetry (according to the crystal site symmetry and spin-orbit vibronic coupling routes to be discussed later), the first overtone is allowed. In particular, for the pyrazine- \underline{h}_4 molecule, the $2\nu_{6b}$ vibration comes so close to $2\nu_{6a}$ and ν_{9a} that appreciable interactions among them are expected (Fermi resonance). This explains why $2\nu_{6b}$ is strong in \underline{h}_4 spectra but missing in the \underline{d}_4 spectrum. The assignment of the 1291.4 cm^{-1} band in the \underline{d}_4 spectrum to $\nu_5 + \nu_{6b}$ is also consistent with selection rules. With an overall symmetry of b_{1g} , this transition is allowed in a crystal site of C_{2h} or lower symmetry (benzene crystal has a site symmetry of C_i , however, the effective site symmetry is close to C_{2h} ¹⁹).
2. The Raman spectra of crystalline pyrazine has been taken at room temperature using a neon-helium laser (Model: Cary 81). Preliminary results²⁰ locate two weak lines at 610 and 1225 cm^{-1} , which might correlate with the vibronic bands assigned here.
3. This is one of the few combinations of the ground state vibrations, observed or predicted, having the right frequency and the right symmetry. Other possibilities are: $\nu_{6b} + \nu_4$ (b_{1g}), $\nu_{11} + \nu_{16b}$ (a_{1g}),

ν_3 (b_{3g}), and $\nu_{6b} + \nu_{6a}$ (b_{3g}) with frequencies 1334, 1221, 1368, and 1247 cm^{-1} , respectively.²¹ Based on 1 and 2, we chose the present assignment as the most reasonable one.

In addition to the totally symmetric vibrations mentioned above, all the non-totally symmetric vibrations of b_{1g} and b_{2g} symmetry are observed in the emission spectra (see Tables I, III, and V). For \underline{h}_4 in \underline{d}_4 system, the site symmetry is C_{2h} ²² and b_{1g} vibrations become allowed through crystal perturbations. The striking resemblance between the \underline{h}_4 in \underline{d}_4 and \underline{h}_4 in \underline{h}_6 spectra suggests that the \underline{h}_4 in \underline{h}_6 system probably has the same site symmetry. The N-N axis of the pyrazine molecule will have to coincide with the C_2 axis just like the \underline{h}_4 in \underline{d}_4 system (in benzene crystal, the C_2 axis in question is roughly parallel to the crystallographic \underline{b} -axis²³). A site symmetry of C_{2h} in the \underline{d}_4 in \underline{h}_6 crystal also explains the large intensity enhancement of the ν_{10a} band (590.9 cm^{-1}) through the so-called "crystal-induced Fermi resonance"¹¹ with the ν_{6a} (577.6 cm^{-1}) band. As to the b_{2g} vibrations, spin-orbital-vibronic coupling must be invoked. It is known from the theoretical analysis of Sidman²⁴ and experimental results of Krishna and Goodman²⁵ that the first-order spin-orbital coupling with the ${}^1B_{1u}$ state provides most of the ${}^3B_{3u} \leftarrow {}^1A_{1g}$ transition intensity. It is also known that the ${}^1B_{3u}$ state is coupled vibronically with the ${}^1B_{1u}$ state⁴ and vice versa. Based on these facts, a satisfactory spin-orbital-vibronic coupling scheme can be obtained. The ${}^3B_{3u}$ state is first coupled to the ${}^1B_{1u}$ state spin-orbitally and then coupled to the ${}^1B_{3u}$ state vibronically, thus activating the b_{2g} vibrations. Notice that

an alternative route can also be written simply by reversing the order of spin-orbital and vibronic couplings. The final state is still the ${}^1B_{3u}$ state whereas the intermediate state is now the ${}^3B_{1u}$ state. This state was predicted by McWeeny and Peacock²⁶ to lie at 3.5 eV above the ground state and yet unconfirmed experimentally. The latter mechanism was proposed by El-Sayed²⁷ in his discussion of the radiationless path in pyrazine. Quantum mechanically these two routes are indistinguishable.

All the ground-state fundamentals observed in this work are given in Table VII, together with the Raman data by several other workers. The only overtone of an ungerade vibration observed in our spectra, namely $2\nu_{16b}$, is not included. However, its frequency is also in good agreement with the infrared data of Califano et al.¹⁸

In the recent paper by Moomaw and El-Sayed,¹³ vibrational analyses of pyrazine in cyclohexane and pure crystal emission spectra were given. Because of the high efficiency of excitation trapping by a minute amount of impurity in pure crystals, the authors have carefully analyzed their spectra to establish the point that it is genuine pyrazine emission. However, when we compare their analysis with our \underline{h}_4 in \underline{d}_4 spectrum, some discrepancies are found.

1. ν_1 , which is found to be 1011.6 cm^{-1} in our case, is reported to be 1022 cm^{-1} by Moomaw and El-Sayed. 10 cm^{-1} difference is considered to be too large considering the high resolution involved in our spectra and theirs.

2. ν_{9a} , which is one of the most intense lines of the whole phosphorescence spectrum, is found by Moomaw and El-Sayed to be 1255 cm^{-1} compared to our 1249.4 cm^{-1} . The discrepancy, again, is considered to be too large.
3. The 1231.2 cm^{-1} vibration is not found by Moomaw and El-Sayed, nor is its combination with ν_{6a} and ν_{9a} at 1837.9 , 2480.9 and 3085.8 cm^{-1} . These are very strong indeed in our spectrum.
4. The overtone of ν_1 at 2044 cm^{-1} is not found by Moomaw and El-Sayed, and the overtone of ν_{10a} observed by us to be 1513.8 cm^{-1} was reported by them to be 1523 cm^{-1} .

The ring mode ν_1 , which was reported by Ito and Shigeoka¹⁷ to be 1012 cm^{-1} at 77° K is undoubtedly the 1011.6 cm^{-1} band we observed at 4° K . This is further evidenced by the presence of the 1009.3 cm^{-1} band in fluorescence. The C-H bending mode, although reported by Ito to be 1254 cm^{-1} at 77° K and claimed by Moomaw and El-Sayed to be 1255 cm^{-1} , must be the 1249.7 cm^{-1} band observed in both phosphorescence and fluorescence at 4° K . The consistency of our assignment is very convincing, whereas Moomaw and El-Sayed have to resort to some kind of vibronic-phonon interaction in order to account for the inconsistency in almost all the overtones and combinations involving this particular vibration.

Moomaw and El-Sayed's analyses of the emission spectra of pyrazine in cyclohexane and the pyrazine pure crystal did not include the $2\nu_{6b}$ band observed by us. This band is observed in both the

phosphorescence and fluorescence spectra of \underline{h}_4 in \underline{d}_4 and \underline{h}_4 in \underline{h}_6 . For the pyrazine in cyclohexane system, the impurity problems are not too serious but the presence of the $2\nu_{6b}$ band might be masked by the $2\nu_{6a}$ and ν_{9a} bands associated with other sites (four sites are reported by Moomaw and El-Sayed). The absence of this band in the pure crystal spectrum could be a result of the wrong assignment. It could also mean that the emitting molecule is really not pyrazine itself.

In conclusion, we feel that impurity problems are less serious in mixed crystals. Weak emission from pure crystals, unless purity is guaranteed, is likely attributable to impurities. The emission observed by Moomaw and El-Sayed is definitely not triplet exciton emission. Azumi and Nakano's allegations¹⁴ that it is due to the chemical impurity perturbed pyrazine emission is only convincing, not conclusive. Intermolecular interactions in molecular crystals are generally small. A shift of 102 cm^{-1} seems too large to be attributed to such interactions, especially for the triplet state where only exchange interactions are important.²⁸ Chemical impurities in molecular crystals normally have very similar properties as the bulk. It is quite possible that these impurities exhibit similar vibronic structures. Furthermore, due to the complexity of the crystal phosphorescence spectrum, "complete vibrational analysis is quite a difficult task, if not impossible."²⁹ Any conclusion drawn from such an analysis must be taken with caution. Our analysis does show some disagreement with that of Moomaw and El-Sayed. Unless reassignment of the crystal spectrum shows otherwise, whether the crystal emission is, indeed, due to pyrazine still remains open.

B. Singlet-Singlet System

The only low temperature work on the singlet-singlet absorption of pyrazine is that of El-Sayed and Robinson.³ They interpreted their spectra in terms of two electronic transitions as suggested by Ito *et al.*¹ in their analysis of gas phase spectra. They claimed to have identified the origin of the ${}^1B_{2g}$ state at about 457 cm^{-1} to the red of the allowed ${}^1B_{3u}$ state.

Innes *et al.*⁴ have analyzed the polarization of the diffuse band reported by Ito *et al.*¹ to be forbidden ${}^1B_{2g}$ transition. With the use of the Deslandres Tables, they illustrated that these diffuse bands can be interpreted as a forbidden vibronic transition of the same ${}^1B_{3u}$ state involving the ground state vibration of 918.5 cm^{-1} (ν_5) and excited state vibration of 383.4 cm^{-1} . Deuterium substitution changes these frequencies to 721.1 and 291.8 cm^{-1} , respectively. Since ν_5 is of b_{2g} symmetry, the vibronic band has to steal intensity from the ${}^1B_{1u} \leftarrow {}^1A_{1g}$ transition through the vibronic coupling.

The key to this controversy seems to lie in the analysis of the fluorescence spectra. It is known that at low temperatures internal conversions are very fast and emission normally originates from the lowest excited states.³⁰ Vibrational analysis of the fluorescence spectrum would be a means of telling whether the lowest state is allowed or forbidden. El-Sayed and Robinson reported no fluorescence emissions from all the diazines in rare gas matrices. Recently Logan and Ross³¹ reported the fluorescence emission of pyrazine in the gas phase and in frozen hydrocarbon media, however, their spectra do not have

the required resolution to allow a detailed analysis. Hochstrasser and Marzzacco³² also reported the fluorescence spectrum of \underline{h}_4 in \underline{h}_6 in connection with their discussions of interactions between electronic states. No discussions on the ordering of the allowed and forbidden components were made. In the present work, we have observed the fluorescence spectra of both pyrazine \underline{h}_4 and \underline{d}_4 .

The absorption spectra were also taken for comparison. The pyrazine crystal has a site symmetry of C_{2h} . In the pyrazine in benzene system, if pyrazine molecule occupies the substitutional site, the site symmetry would be C_i . In both cases, the origin of the forbidden ${}^1B_{2g}$ state, even if it is there, is not expected to be observed.³³ In fact, no absorption to the red of the allowed 0-0 was observed. The absorption spectra of pyrazine in benzene also show the Shpol'skii³⁴ effect similar to that of the phosphorescence discussed before, two weak lines with 81.6 and 153.7 cm^{-1} to the blue of the strong 0-0 were observed. The nature of these defect sites is not known.

The absorption spectrum of \underline{h}_4 in \underline{h}_6 shows relatively short progressions. Between the first strong vibronic band ν_{6a} (found to be 585.2 cm^{-1}) and the 0-0, only one band at 429.9 cm^{-1} was observed. This is assigned to ν_5 observed by Innes *et al.*⁴ to be 383.4 cm^{-1} in the gas phase. The next group occurs at 900 ~ 1300 cm^{-1} region. It is very complicated and seems to include some impurity absorptions. No analysis was made. The absorption spectra of \underline{d}_4 in \underline{h}_6 shows more regularity in vibronic spacings and less contamination by impurity absorptions. More complete analysis was made and is shown in Table

VIII. It can be seen that ν_5 is also observed at 331.4 cm^{-1} compared to the gas phase value of 291.8 cm^{-1} by Innes et al. From the analysis of Table VIII, it seems very unlikely that the absorption spectrum is a superposition of two electronic transitions as proposed by Ito et al. The analysis of fluorescence spectrum also disagrees with the proposition that the lowest state is of $^1B_{2g}$ symmetry.

For allowed transitions, the 0-0 band in emission is usually missing due to reabsorption. Our fluorescence spectra were analyzed taking the 0-0 of absorption as the origin. The analysis is given in Tables II, IV, and VI.

In all three cases, it can be seen that essentially the same ground state vibrations observed in phosphorescence are also observed in fluorescence. The ground state vibration of ν_5 (B_{2g}) is found to be 930.2 cm^{-1} in \underline{h}_4 in \underline{h}_6 ; 946.8 cm^{-1} in \underline{h}_4 in \underline{d}_4 (918.5 cm^{-1} in gas phase), and 725.3 cm^{-1} in \underline{d}_4 in \underline{h}_6 (721.1 cm^{-1} in gas phase). The presence of non-totally symmetric vibrations is interpreted as follows: The b_{1g} vibrations are active due to the crystal site symmetry of C_{2h} and the b_{2g} vibrations are active because of the vibronic coupling with the $^1B_{1u}$ state.

In view of the coincidence of the 0-0 in absorption and emission and the consistency with the analysis of Innes et al., we concluded that the lowest singlet state is an allowed one. This contradicts the predictions of both the exciton and the crude MO theory of the $n \rightarrow \pi^*$ transitions.³⁵ However, recently Clementi³⁶ calculated the all-electron SCF wavefunctions for the ground state of pyrazine and

concluded that the A_{1g} and B_{1g} σ -orbitals (N^+ and N^- orbitals in the language of the crude MO theory) actually delocalize to the rest of the molecule. The concept of a non-bonding orbital is apparently inadequate in describing the electronic structure of pyrazine molecules. Furthermore, his calculations show that A_{1g} orbital lies 0.09150 a. u. (or 20,081.9 cm^{-1}) above the B_{1u} orbital. Since the π^* orbital is of the B_{3u} system,³⁷ the electronic transition ${}^1B_{3u} \leftarrow A_{1g}$ will be the lowest one, with the ${}^1B_{2g} \leftarrow A_{1g}$ lying much higher than previously predicted. Therefore, as far as our experimental results and theoretical calculations compare, the agreement is satisfactory.

Different views were expressed by Cohen and Goodman.³⁷ They measured the quantum yields of phosphorescence, fluorescence and intersystem crossing and concluded that the fast internal conversion rate is responsible for the depletion of the ${}^1B_{3u}$ state. Since the internal conversion rate ($\sim 10^9 \text{ sec}^{-1}$) is thought to be too large for an energy gap of $\sim 30,000 \text{ cm}^{-1}$ (between the ${}^1B_{3u}$ state and the ${}^1A_{1g}$ state), the experimental results of El-Sayed and Robinson were used to explain the low fluorescence yield. Refined calculations of the radiationless transition rate are, at this stage, very difficult. Only some of the most studied molecules, such as benzene, have recently been subjected to such detailed analysis.³⁸ In our opinion, a 10^9 sec^{-1} internal conversion rate is quite possible. Furthermore, heterocyclic compounds are more susceptible to photochemical reactions that may also contribute to the large radiationless transitions observed experimentally.

Finally, it can be noted that the fluorescence and phosphorescence spectra are very similar. The $^1B_{3u}$ and $^3B_{3u}$ states must have very similar geometry. This is consistent with the fact that these two states have the same MO occupations.

REFERENCES

1. M. Ito, R. Shimada, T. Kuraishi, and W. Mizushima, *J. Chem. Phys.* 26, 1508 (1957).
2. The notations used here are the same as those in Ref. 3. See Ref. 3 for a compilation of different notations by different workers.
3. M. A. El-Sayed and G. W. Robinson, *Mol. Phys.* 4, 273 (1961).
4. K. K. Innes, J. D. Simmons, and S. G. Tilford, *J. Mol. Spectry.* 11, 257 (1963).
5. L. Goodman and M. Kasha, *J. Mol. Spectry.* 2, 58 (1958).
6. G. Castro and G. W. Robinson, *J. Chem. Phys.* 50, 1159 (1969).
7. M. Kasha, *J. Opt. Soc. Am.* 38, 929 (1948).
8. S. D. Colson, Ph. D. Thesis, California Institute of Technology, (1967).
9. H. Sternlicht, G. C. Nieman, and G. W. Robinson, *J. Chem. Phys.* 38 1326 (1963).
10. R. Shimada, *Spectrochim. Acta* 17, 14 (1961).
11. E. R. Bernstein, S. D. Colson, D. S. Tinti, and G. W. Robinson, *J. Chem. Phys.* 48, 4632 (1968).
12. The origin of phosphorescence spectrum of \underline{h}_4 in \underline{d}_4 also shows multiple structure. This phenomenon has been attributed to site effects by D. S. McClure and E. F. Zalewski [see Molecular Luminescence, E. C. Lim, Ed. (W. A. Benjamin, Inc., New York, 1969), p. 739]. The 0-0 used in the analysis of Table III is the monomer line of a very dilute \underline{h}_4 in \underline{d}_4 mixed crystal.

Further investigation concerning the nature of the multiple structure is now in progress.

13. W. R. Moomaw and M. A. El-Sayed, J. Chem. Phys. 45, 3890 (1966); *ibid.* 48, 2502 (1968).
14. Moomaw and El-Sayed later withdrew their interpretations and attributed their spectra to defect emissions; see D. S. Tinti, W. R. Moomaw, and M. A. El-Sayed, J. Chem. Phys. 50, 1035 (1969). However, they still entertain that the emissions are genuine pyrazine emissions. Further investigation by T. Azumi and Y. Nakano firmly established the fact that several upper states are involved by lifetime studies [see Technical Reports of ISSP, Series A, No. 336 (1968)]. The latter attributed the spectrum to chemical impurity-induced pyrazine emission. Since all the arguments presented by the latter for their interpretation can be equally applied for impurity emissions it is imperative that the vibronic structures be reexamined and compared with our \underline{h}_4 in \underline{d}_4 spectrum. Moomaw and El-Sayed's analysis does not agree completely with our analysis. Unless a more careful analysis of crystal phosphorescence spectrum shows better agreement, the question of whether they are indeed pyrazine emissions still, in our opinion, remains open.
15. R. C. Lord, A. L. Marston, and F. A. Miller, Spectrochim. Acta 9, 113 (1957).
16. J. D. Simmons, K. K. Innes, and G. M. Begun, J. Mol. Spectry. 14, 190 (1964).

17. M. Ito and T. Shigeoka, *J. Chem. Phys.* 44, 1001 (1966).
18. M. Scrocco, C. di Lauro, and S. Califano, *Spectrochim. Acta* 21, 571 (1965).
19. G. C. Nieman and D. S. Tinti, *J. Chem. Phys.* 46, 1432 (1967).
20. H. K. Hong (unpublished work).
21. The frequencies of ν_{16b} and ν_{11} are known to be 417 and 804 cm^{-1} [S. Califano, G. Adembri, and G. Sbrana, *Spectrochim. Acta* 20, 385 (1964)]. The frequencies of ν_{6b} and ν_3 are calculated by Scrocco *et al.*¹⁸ to be 641 and 1368 cm^{-1} , respectively. The frequencies of ν_4 and ν_{6a} are taken from Table VII (\underline{h}_4 in \underline{d}_4).
22. P. J. Wheatley, *Acta Cryst.* 10, 182 (1957).
23. E. G. Cox, D. W. J. Cruickshank, and J. A. S. Smith, *Proc. Roy. Soc. (London)* 247A, 1 (1958).
24. J. W. Sidman, *J. Mol. Spectry.* 2, 333 (1958).
25. V. G. Krishma and L. Goodman, *J. Chem. Phys.* 36, 2217 (1962).
26. R. McWeeny and T. Peacock, *Proc. Phys. Soc. (London)* B70, 47 (1957).
27. M. A. El-Sayed, Molecular Luminescence, E. C. Lim, Ed. (W. A. Benjamin, Inc., New York, 1969), p. 715.
28. G. C. Nieman and G. W. Robinson, *J. Chem. Phys.* 39, 1298 (1963).
29. The analysis of Azumi and Nakano¹⁴ is incomplete. They listed vibrations of 605, 763, 958, 1013, and 1255 cm^{-1} as fundamentals. The 958 and 1255 cm^{-1} bands again differ from our values of 947.7

and 1249.4 cm^{-1} . Both our measurements and theirs are accurate to within 1 cm^{-1} .

30. G. W. Robinson and R. P. Frosch, *J. Chem. Phys.* 37, 1962 (1962); *ibid.* 38, 1187 (1963).
31. L. M. Logan and I. G. Ross, *J. Chem. Phys.* 43 2903 (1965).
32. R. M. Hochstrasser and C. A. Marzzacco, Molecular Luminescence, E. C. Lim, Ed. (W. A. Benjamin, Inc., New York, 1969), p. 631.
33. El-Sayed and Robinson³ claimed to observe the forbidden component in crystalline pyrazine. This is not supported by the group theoretical argument presented here.
34. E. Shopl'skii and L. Klimova, *Opt. Spectrosc.* 7, 499 (1959).
35. For a discussion on the exciton and MO theories of $n \rightarrow \pi^*$ transitions, see D. R. Kearns and M. A. El-Bayoumi, *J. Chem. Phys.* 38, 1508 (1963).
36. E. Clementi, *J. Chem. Phys.* 46, 4737 (1967).
37. B. J. Cohen and L. Goodman, *J. Chem. Phys.* 46, 713 (1967).
38. D. M. Burland and G. W. Robinson, *J. Chem. Phys.* 51 0000 (1969), "Calculated Radiationless Transition Rates for Benzene and Deuterobenzene."

TABLE I. Phosphorescence of pyrazine-h₄ in benzene.

$\bar{\nu}(\text{cm}^{-1})$	$\Delta\bar{\nu}(\text{cm}^{-1})$	Intensity	Assignment	Symmetry
25,996.0	0	vs	0-0	A _{1g}
25,399.8	596.2	s	ν_{6a}	A _{1g}
25,303.6	692.4	w	ν_4	B _{2g}
25,240.3	755.7	mw	ν_{10a}	B _{1g}
25,163.0	833.0	w	$2\nu_{16b}$	A _{1g}
25,066.3	929.7	w	ν_5	B _{2g}
24,986.3	1009.7	m	ν_1	A _{1g}
24,804.1	1191.9	m	$2\nu_{6a}$ $2 \times 596.2 = 1192.4$	A _{1g}
24,789.0	1207.0	s	$(2\nu_{6b})$ $2 \times 603.5 = 1207.0$	A _{1g}
24,767.5	1228.5	s	$\nu_9 a$	A _{1g}
24,710.4	1285.6	w	$\nu_4 + \nu_{6a}$ $692.4 + 596.2 = 1288.6$	B _{2g}
24,644.8	1351.2	w	$\nu_{10a} + \nu_{6a}$ $755.7 + 596.2 = 1351.9$	B _{1g}
24,570.2	1425.8	w	$2\nu_{16b} + \nu_{6a}$ $833.0 + 596.2 = 1429.2$	A _{1g}
24,485.5	1510.5	m	$2\nu_{10a}$ $2 \times 755.7 = 1511.4$	A _{1g}
24,473.0	1523.0	w	$\nu_5 + \nu_{6a}$ $929.7 + 596.2 = 1525.9$	B _{2g}

TABLE I. (continued)

$\bar{\nu}(\text{cm}^{-1})$	$\Delta\bar{\nu}(\text{cm}^{-1})$	Intensity	Assignment	Symmetry
24,425.1	1570.9	w	$\nu_8 \text{ a}$	A_{1g}
24,389.9	1606.1	m	$\nu_1 + \nu_{6a}$ $1009.7 + 596.2 = 1605.9$	A_{1g}
24,191.6	1804.4	m	$(2\nu_{6b}) + \nu_{6a}$ $1207.0 + 596.2 = 1803.2$	A_{1g}
24,170.8	1825.4	s	$\nu_{6a} + \nu_{9a}$ $596.2 + 1228.5 = 1824.7$	A_{1g}
24,138.4	1857.6	s	$2\nu_5$ $2 \times 929.7 = 1859.4$	A_{1g}
24,076.5	1919.5	w	$\nu_4 + \nu_{9a}$ $692.4 + 1228.5 = 1920.9$	B_{2g}
24,011.5	1984.5	w	$\nu_{10a} + \nu_{9a}$ $755.7 = 1228.5 = 1984.2$	B_{1g}
23,962.0	2034.0	w	$2\nu_1$ $1009.7 \times 2 = 2019.4$	A_{1g}
23,891.7	2104.3	w	$2\nu_{10a} + \nu_{6a}$ $1511.4 + 596.2 = 2107.6$	A_{1g}
23,838.3	2157.7	w	$\nu_5 + \nu_{9a}$ $929.7 + 1228.5 = 2158.2$	B_{2g}
23,798.0	2198.0	vw	$2\nu_{6a} + \nu_1$ $1191.9 + 1009.7 = 2201.6$	A_{1g}
23,778.4	2217.6	vw	$(2\nu_{6b}) + \nu_1$ $1207.0 + 1009.7 = 2216.7$	A_{1g}
23,757.7	2238.3	vw	$\nu_{9a} + \nu_1$ $1228.5 + 1009.7 = 2238.2$	A_{1g}
23,730.8	2265.2	vvw	$3\nu_{10a}$ $3 \times 755.7 = 2267.1$	B_{1g}
23,573.8	2422.3	w	$2\nu_{6a} + \nu_{9a}$ $1191.9 + 1228.5 = 2420.4$	A_{1g}

TABLE I. (continued)

$\bar{\nu}(\text{cm}^{-1})$	$\Delta\bar{\nu}(\text{cm}^{-1})$	Intensity	Assignment	Symmetry
23,559.1	2436.9	m	$(2\nu_{6b}) + \nu_{9a}$ 1207.0 + 1228.5 = 2435.5	A_{1g}
23,542.4	2453.6	m	$2\nu_5 + \nu_{6a}$ 1857.6 + 596.2 = 2453.8	A_{1g}
23,536.1	2459.9	m	$2\nu_{9a}$ 1228.5 \times 2 = 2457.0	A_{1g}
23,369.	2627.0	vw	$2\nu_1 + \nu_{6a}$ 2034.0 + 596.2 = 2630.2	A_{1g}
23,274.5	2721.5	w	$(2\nu_{6b}) + 2\nu_{10a}$ 1207.0 + 1510.5 = 2717.5	A_{1g}
23,255.5	2740.5	w	$\nu_{9a} + 2\nu_{10a}$ 1228.5 + 1510.5 = 2739.0	A_{1g}
22,961.5	3034.5	mw	$(2\nu_{6b}) + \nu_{6a} + \nu_{9a}$ 1207.0 + 596.2 + 1228.5 = 3033.9	A_{1g}
22,939.1	3056.9	mw	$\nu_{6a} + 2\nu_{9a}$ 596.2 + 2 \times 1228.5 = 3053.2	A_{1g}
22,911.7	3084.3	mw	$2\nu_5 + \nu_{9a}$ 1857.6 + 1228.5 = 3086.1	A_{1g}

TABLE II. Fluorescence of pyrazine-h₄ in benzene.

$\bar{\nu}(\text{cm}^{-1})$	$\Delta\bar{\nu}(\text{cm}^{-1})$	Intensity	Assignment	Symmetry
29,894.8	0		0-0	
29,299.1	595.7	s	ν_{6a}	A _{1g}
29,200.2	694.6	vw	ν_4	B _{2g}
29,140.1	754.7	vw	ν_{10a}	B _{1g}
28,964.6	930.2	mw	ν_5	B _{2g}
28,887.5	1007.3	w	ν_1	A _{1g}
28,702.7	1192.1	m	$2\nu_{6a}$ $2 \times 595.7 = 1191.4$	A _{1g}
28,687.0	1207.8	mw	($2\nu_{6b}$)	
28,665.7	1229.1	s	$\nu_9 a$	A _{1g}
28,323.8	1571.0	w	$\nu_8 a$	A _{1g}
28,090.6	1804.2	m	($2\nu_{6b} + \nu_{6a}$) $1207.8 + 595.7 = 1803.5$	
28,069.3	1825.5	mw	$\nu_{9a} + \nu_{6a}$ $1229.1 + 595.7 = 1824.8$	A _{1g}
28,037.0	1857.8	mw	$2\nu_5$ $930.2 \times 2 = 1860.4$	A _{1g}

TABLE II. (continued)

$\bar{\nu}(\text{cm}^{-1})$	$\Delta\bar{\nu}(\text{cm}^{-1})$	Intensity	Assignment	Symmetry
27,457.9	2436.9	vw	$(2\nu_{6b} + \nu_{9a})$ 1207.8 + 1229.1 = 2436.8	
27,442.1	2452.7	vw	$2\nu_5 + \nu_{6a}$ 1857.8 + 595.7 = 2435.5	A_{1g}
27,435.3	2459.5	vw	$2\nu_{9a}$ $2 \times 1229.1 = 2458.2$	A_{1g}

TABLE III. Phosphorescence of pyrazine-h₄ in pyrazine-d₄.

$\bar{\nu}(\text{cm}^{-1})$	$\Delta\bar{\nu}(\text{cm}^{-1})$	Intensity	Assignment	Symmetry
26,258.6	0	vs	0-0	A _{1g}
25,653.6	605.0	s	ν_{6a}	A _{1g}
25,544.7	713.9	w	ν_4	B _{2g}
25,497.0	761.6	w	ν_{10a}	B _{1g}
25,425.8	832.8	vw	$2\nu_{16b}$	A _{1g}
25,310.9	947.7	m	ν_5	B _{2g}
25,247.0	1011.6	m	ν_1	A _{1g}
25,047.1	1211.5	m	$2\nu_{6a}$ $2 \times 605.0 = 1210.0$	A _{1g}
25,027.4	1231.2	s	$(2\nu_{6b})$ $2 \times 615.6 = 1231.2$	A _{1g}
25,009.2	1249.4	s	ν_{9a}	A _{1g}
24,939.6	1319.0	w	$\nu_4 + \nu_{6a}$ $713.9 + 605.0 = 1318.9$	B _{2g}
24,893.1	1365.5	w	$\nu_{10a} + \nu_{6a}$ $761.6 + 605.0 = 1366.6$	B _{1g}
24,820.6	1438.0	w	$2\nu_{16b} + \nu_{6a}$ $832.8 + 605.0 = 1437.8$	A _{1g}
24,744.8	1513.8	m	$2\nu_{10a}$ $761.6 \times 2 = 1523.2$	A _{1g}
24,706.5	1552.1	m	$\nu_5 + \nu_{6a}$ $947.7 + 605.0 = 1552.7$	B _{2g}

TABLE III. (continued)

$\bar{\nu}(\text{cm}^{-1})$	$\Delta\bar{\nu}(\text{cm}^{-1})$	Intensity	Assignment	Symmetry
24,675.6	1583.0	vw	ν_{8a}	A_{1g}
24,640.3	1618.3	w	$\nu_1 + \nu_{6a}$ $1011.6 + 605.0 = 1616.6$	A_{1g}
24,420.7	1837.9	m	$(2\nu_{6b}) + \nu_{6a}$ $1231.2 + 605.0 = 1836.2$	A_{1g}
24,403.5	1855.1	s	$\nu_{9a} + \nu_{6a}$ $1249.4 + 605.0 = 1854.4$	A_{1g}
24,366.6	1892.0	s	$2\nu_5$ $947.7 \times 2 = 1895.4$	A_{1g}
24,294.6	1964.0	vw	$\nu_{9a} + \nu_4$ $1249.4 + 713.9 = 1963.3$	B_{2g}
24,248.1	2010.5	vw	$\nu_{9a} + \nu_{10a}$ $1249.4 + 761.6 = 2011.0$	B_{1g}
24,214.6	2044.0	w	$2\nu_1$ $2 \times 1011.6 = 2023.2$	A_{1g}
24,139.8	2118.8	w	$2\nu_{10a} + \nu_{6a}$ $1513.8 + 605.0 = 2118.8$	A_{1g}
24,064.4	2194.2	w	$\nu_5 + \nu_{9a}$ $947.7 + 1249.4 = 2197.1$	B_{2g}
24,036.2	2222.4	vw	$\nu_1 + 2\nu_{6a}$ $1011.6 + 1211.5 = 2223.1$	A_{1g}
24,016.7	2241.9	vw	$\nu_1 + 2\nu_{6b}$ $1011.6 + 1231.2 = 2242.8$	A_{1g}
23,997.1	2261.5	vw	$\nu_1 + \nu_{9a}$ $1011.6 + 1249.4 = 2261.0$	A_{1g}
23,796.0	2462.6	w	$2\nu_{6a} + \nu_{9a}$ $2 \times 605.0 + 1249.4 = 2461.4$	A_{1g}
23,777.7	2480.9	m	$(2\nu_{6b}) + \nu_{9a}$ $1231.2 + 1249.4 = 2480.6$	A_{1g}

TABLE III. (continued)

$\bar{\nu}(\text{cm}^{-1})$	$\Delta\bar{\nu}(\text{cm}^{-1})$	Intensity	Assignment	Symmetry
23,761.2	2497.4	m	$2\nu_{9a}$ $2 \times 1249.4 = 2498.8$	A_{1g}
23,425.0	2833.6	vw	$\nu_{8a} + \nu_{9a}$ $1583.0 + 1249.4 = 2832.4$	A_{1g}
23,172.8	3085.8	vw	$(2\nu_{6b}) + \nu_{6a} + \nu_{9a}$ $1231.2 + 605.0 + 1249.4 = 3085.6$	A_{1g}
23,154.5	3104.1	vw	$\nu_{6a} + 2\nu_{9a}$ $605.0 + 2 \times 1249.4 = 3103.8$	A_{1g}
23,117.2	3141.4	w	$2\nu_5 + \nu_{9a}$ $1892.0 + 1249.4 = 3141.4$	A_{1g}

TABLE IV. Fluorescence of pyrazine-h₄ in pyrazine-d₄.

$\bar{\nu}(\text{cm}^{-1})$	$\Delta\bar{\nu}(\text{cm}^{-1})$	Intensity	Assignment	Symmetry
30,049.7	0		0-0	A _{1g}
29,444.9	604.8	s	ν_{6a}	A _{1g}
29,102.9	946.8	w	ν_5	B _{2g}
29,040.4	1009.3	w	ν_1	A _{1g}
28,839.5	1210.2	m	$2\nu_{6a}$ $2 \times 604.8 = 1209.6$	A _{1g}
28,820.5	1229.2	m	$(2\nu_{6b})$	A _{1g}
28,801.6	1248.1	m	ν_{9a}	A _{1g}
28,497.6	1552.1	w	$\nu_5 + \nu_{6a}$ $946.8 + 604.8 = 1551.6$	B _{2g}
28,196.2	1853.5	w	$\nu_{9a} + \nu_{6a}$ $1248.1 + 604.8 = 1852.9$	A _{1g}
28,158.9	1890.8	w	$2\nu_5$ $2 \times 946.8 = 1893.6$	A _{1g}

TABLE V. Phosphorescence of pyrazine-d₄ in benzene.

$\bar{\nu}(\text{cm}^{-1})$	$\Delta\bar{\nu}(\text{cm}^{-1})$	Intensity	Assignment	Symmetry
26,144.1	0	s	0-0	A _{1g}
25,566.6	577.6	s	ν_{6a}	A _{1g}
25,553.2	590.9	s	ν_{10a}	B _{1g}
25,468.1	676.0	w	ν_4	B _{2g}
25,417.8	726.3	w	ν_5	B _{2g}
25,349.4	794.1	w	$2\nu_{16b}$	A _{1g}
25,263.0	881.1	s	ν_{9a}	A _{1g}
25,146.6	997.5	s	ν_1	A _{1g}
24,992.9	1151.2	w	$2\nu_{6a}$ $2 \times 590.9 = 1181.8$	A _{1g}
24,978.5	1165.6	m	$\nu_{6a} + \nu_{10a}$ $577.6 + 590.9 = 1168.5$	B _{1g}
24,958.6	1185.5	w	$2\nu_{10a}$ $577.6 \times 2 = 1155.2$	A _{1g}
24,852.7	1291.4	m	$(\nu_5 + \nu_{6b})$ $726.3 + 565.1 = 1291.4$	B _{1g}
24,691.1	1453.0	m	$2\nu_5$ $726.3 \times 2 = 1452.6$	A _{1g}
24,685.1	1459.0	m	$\nu_{6a} + \nu_{9a}$ $577.6 + 881.1 = 1458.7$	A _{1g}
24,672.7	1471.4	m	$\nu_{10a} + \nu_{9a}$ $590.9 + 881.1 = 1472.0$	B _{1g}

TABLE V. (Continued)

$\bar{\nu}(\text{cm}^{-1})$	$\Delta\bar{\nu}(\text{cm}^{-1})$	Intensity	Assignment	Symmetry
24,568.7	1575.4	m	$\nu_{6a} + \nu_1$ 577.6 + 997.5 = 1575.1	A _{1g}
24,555.5	1588.6	m	$\nu_{10a} + \nu_1$ 590.9 + 997.5 = 1588.4	B _{1g}
24,470.1	1674.0	w	$\nu_{9a} + 2\nu_{16b}$ 881.1 + 794.7 = 1675.8	A _{1g}
24,381.8	1762.3	mw	$2\nu_{9a}$ 881.1 × 2 = 1762.2	A _{1g}
24,352.1	1792.0	w	$\nu_1 + 2\nu_{16b}$ 997.5 + 794.7 = 1792.2	A _{1g}
24,265.1	1879.0	mw	$\nu_{9a} + \nu_1$ 881.1 + 997.5 = 1878.6	A _{1g}
24,150.2	1993.9	m	$2\nu_1$ 2 × 997.5 = 1995.0	A _{1g}
24,098.0	2046.1	w	$\nu_{6a} + \nu_{10a} + \nu_{9a}$ 1165.6 + 881.1 = 2046.7	B _{1g}
23,972.7	2171.4	w	$(\nu_5 + \nu_{6b}) + \nu_{9a}$ 1291.4 + 881.8 = 2172.5	B _{1g}
23,855.0	2289.1	w	$(\nu_5 + \nu_{6b}) + \nu_1$ 1291.4 + 997.5 = 2288.9	B _{1g}
23,810.0	2334.1	w	$2\nu_5 + \nu_{9a}$ 1453.0 + 881.1 = 2334.1	A _{1g}
23,804.7	2339.4	w	$\nu_{6a} + 2\nu_{9a}$ 577.6 + 2 × 881.1 = 2339.8	A _{1g}
23,791.1	2353.0	w	$\nu_{10a} + 2\nu_{9a}$ 590.9 + 2 × 881.1 = 2353.1	B _{1g}
23,694.1	2450.0	w	$2\nu_5 + \nu_1$ 1453.0 + 997.5 = 2450.5	A _{1g}
23,687.9	2456.2	w	$\nu_{6a} + \nu_{9a} + \nu_1$ 577.6 + 881.1 + 997.5 = 2456.2	A _{1g}
23,675.3	2468.8	w	$\nu_{10a} + \nu_{9a} + \nu_1$ 590.9 + 881.1 + 997.5 = 2469.5	B _{1g}

TABLE VI. Fluorescence of pyrazine-d₄ in benzene.

$\bar{\nu}(\text{cm}^{-1})$	$\Delta\bar{\nu}(\text{cm}^{-1})$	Intensity	Assignment	Symmetry
30,046.7	0		0-0	A _{1g}
29,470.1	576.6	s	ν_{6a}	A _{1g}
29,457.1	589.6	s	ν_{10a}	B _{1g}
29,321.4	725.3	m	ν_5	B _{2g}
29,254.7	792.0	vw	$2\nu_{16b}$	A _{1g}
29,167.5	879.2	s	ν_{9a}	A _{1g}
29,050.5	996.2	s	ν_1	A _{1g}
28,882.6	1164.1	w	$\nu_{6a} + \nu_{10a}$ 576.6 + 589.6 = 1166.2	B _{1g}
28,596.0	1450.7	w	$2\nu_5$ 725.3 × 2 = 1450.6	A _{1g}
28,590.2	1456.5	m	$\nu_{6a} + \nu_{9a}$ 576.6 + 879.2 = 1455.8	A _{1g}
28,577.2	1469.5	m	$\nu_{10a} + \nu_{9a}$ 589.6 + 879.2 = 1468.8	B _{1g}
28,473.0	1573.7	mw	$\nu_{6a} + \nu_1$ 576.6 + 996.2 = 1573.2	A _{1g}
28,460.0	1586.7	mw	$\nu_{10a} + \nu_1$ 589.6 + 996.2 = 1585.8	B _{1g}

TABLE VI. (continued)

$\bar{\nu}(\text{cm}^{-1})$	$\Delta\bar{\nu}(\text{cm}^{-1})$	Intensity	Assignment	Symmetry
28,285.3	1761.7	w	$2\nu_{9a}$ $2 \times 879.2 = 1758.4$	A_{1g}
28,170.5	1876.2	w	$\nu_{9a} + \nu_1$ $879.2 + 996.2 = 1875.4$	A_{1g}
28,053.5	1993.2	w	$2\nu_1$ $2 \times 996.2 = 1992.4$	A_{1g}
28,002.5	2044.2	w	$\nu_{6a} + \nu_{6a} + \nu_{9a}$ $576.6 + 589.6 + 879.2 = 2045.4$	A_{1g}

TABLE VII. Observed gerade vibrations of pyrazine in the ground state.

Sym- metry	Vibra- tion	pyrazine- <u>h</u> ₄					pyrazine- <u>d</u> ₄	
		LMM ^a	IS ^b	SIB ^c	<u>h</u> ₄ / <u>d</u> ₄ ^d	<u>h</u> ₄ / <u>h</u> ₆	SIB ^c	<u>d</u> ₄ / <u>h</u> ₆ ^d
a _{1g}	ν_2	3060	3043	3054	--	--	2274	--
	ν_{8a}	1584	1583	1578	1583.0	1570	1536	--
	ν_{9a}	1232	1254	1230	1249.4	1228.5	882.5	881.1
	ν_1	1015	1012	1015	1011.6	1009.7	1005.6	997.5
	ν_{6a}	609	600	596.1	605.0	596.2	586.0	577.6
b _{1g}	ν_{10a}	753	754	757	761.6	755.7	580 ^f	590.9
b _{2g}	ν_5	703	950	918.6	947.7	929.7	721.1	726.3
	ν_4	641	697	703	713.9	692.4	678	676.0
b _{3g}	ν_7	3045	3029	3041	--	--	2274	--
	ν_{8b}	1523	1521	1524	--	--	1505	--
	ν_3	1118	--	--	--	--	--	--
	ν_{6b}	516	--	--	615.6 ^e	603.5 ^e	--	571.7 ^e

TABLE VII. (continued)

^aReference 15.

^bReference 17.

^cReference 16.

^dThis work.

^eCalculated from overtones or combinations; see text.

^fEstimated by Simmons et al. from the product ratio.

TABLE VIII. Absorption spectrum of pyrazine-d₄ in benzene.

$\bar{\nu}(\text{cm}^{-1})$	$\Delta\bar{\nu}(\text{cm}^{-1})$	Intensity	Assignment	Symmetry
30,046.7	0	vs	0-0	A _{1g}
30,378.1	331.4	w	ν_5	B _{2g}
30,528.4	481.7	vw	?	?
30,617.2	570.5	s	ν_{6a}	A _{1g}
30,873.4	826.7	s	ν_{9a}	A _{1g}
31,021.9	975.2	m	ν_1	A _{1g}
31,034.4	987.7	m	?	?
31,185.5	1138.8	m	$2\nu_{6a}$ $2 \times 570.5 = 1141.0$	A _{1g}
31,203.0	1156.3	w	$\nu_5 + \nu_{9a}$ $331.4 + 826.7 = 1158.1$	B _{2g}
31,440.4	1393.7	m	$\nu_{6a} + \nu_{9a}$ $570.5 + 826.7 = 1397.2$	A _{1g}
31,589.5	1542.8	mw	$\nu_{6a} + \nu_1$ $570.5 + 975.2 = 1545.7$	A _{1g}
31,696.6	1649.9	w	$2\nu_{9a}$ $2 \times 826.7 = 1653.4$	A _{1g}
31,848.1	1801.4	mw	$\nu_{9a} + \nu_1$ $826.7 + 975.2 = 1801.9$	A _{1g}
32,011.2	1964.5	w	$2\nu_{6a} + \nu_{9a}$ $2 \times 570.5 + 826.7 = 1967.7$	A _{1g}

TABLE VIII. (continued)

$\bar{\nu}(\text{cm}^{-1})$	$\Delta\bar{\nu}(\text{cm}^{-1})$	Intensity	Assignment	Symmetry
32,156.4	2109.7	w	$2\nu_{6a} + \nu_1$ $2 \times 570.5 + 975.2 = 2116.2$	A_{1g}
32,261.2	2214.5	w	$2\nu_{9a} + \nu_{6a}$ $1649.9 + 570.5 = 2220.4$	A_{1g}
32,410.8	2364.1	w	$\nu_{6a} + \nu_{9a} + \nu_1$ $570.5 + 826.7 + 975.2 = 2372.4$	A_{1g}
32,574.6	2527.9	w	$\nu_{6a} + 2\nu_1$ $570.5 + 2 \times 975.2 = 2520.9$	A_{1g}
32,675.6	2628.9	w	$2\nu_{9a} + \nu_1$ $1649.9 + 975.2 = 2625.1$	A_{1g}
32,826.9	2780.2	w	$\nu_{9a} + 2\nu_1$ $826.7 + 2 \times 975.2 = 2777.1$	A_{1g}

FIG. 1. The phosphorescence spectrum of pyrazine-h₄ in benzene mixed crystal.

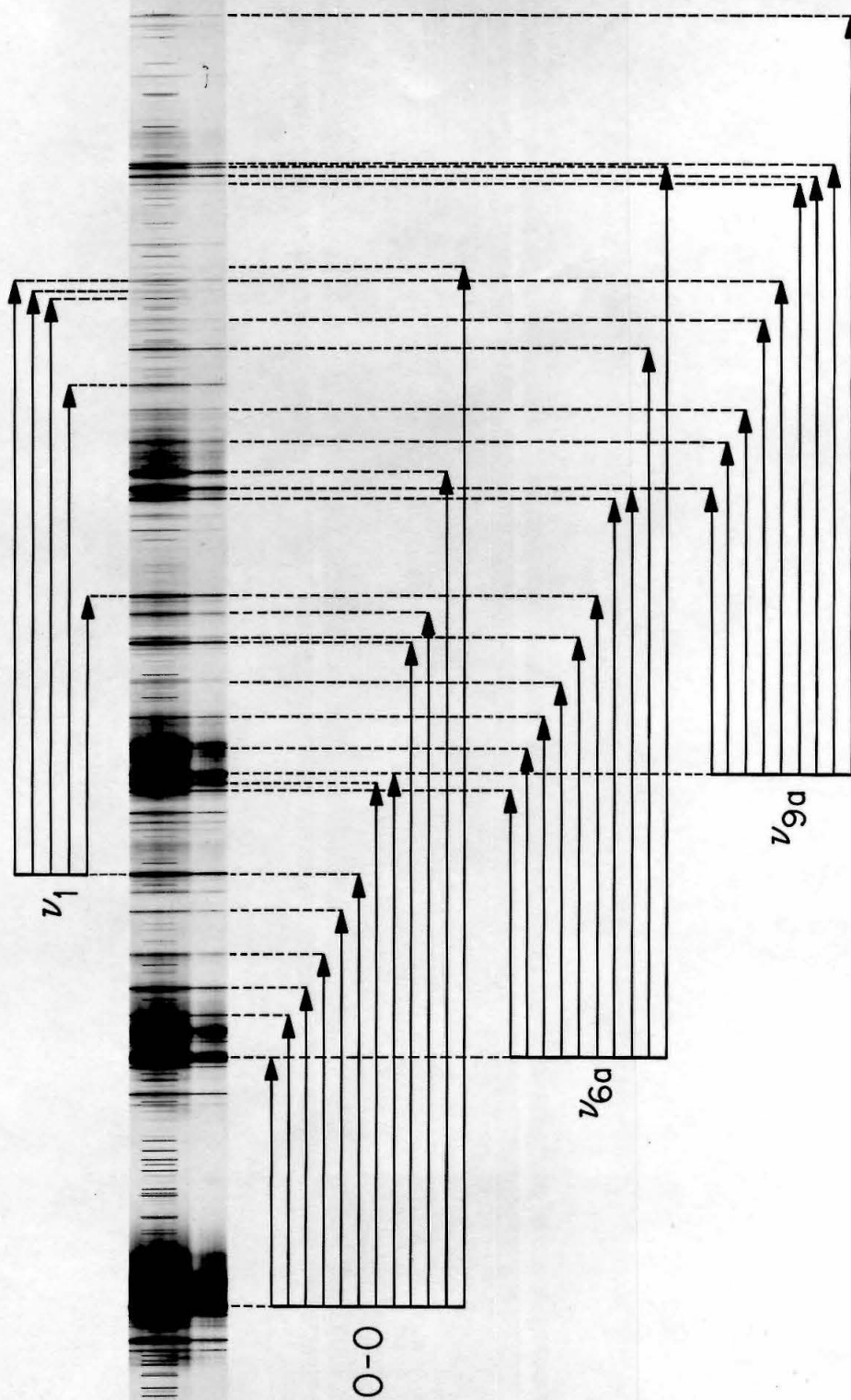


FIG. 2. The phosphorescence spectrum of pyrazine- \underline{h}_4 in \underline{d}_4 mixed crystal.

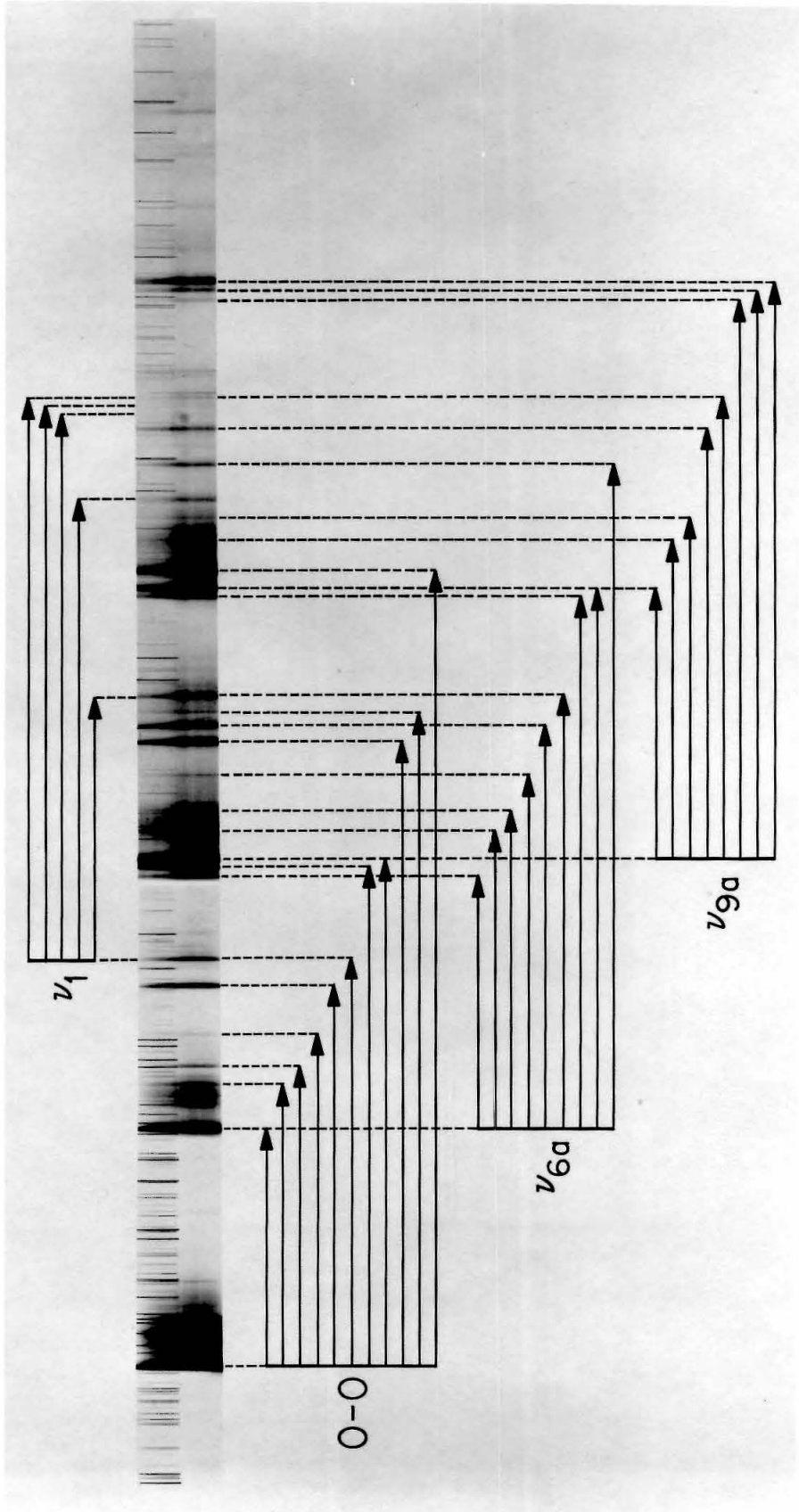
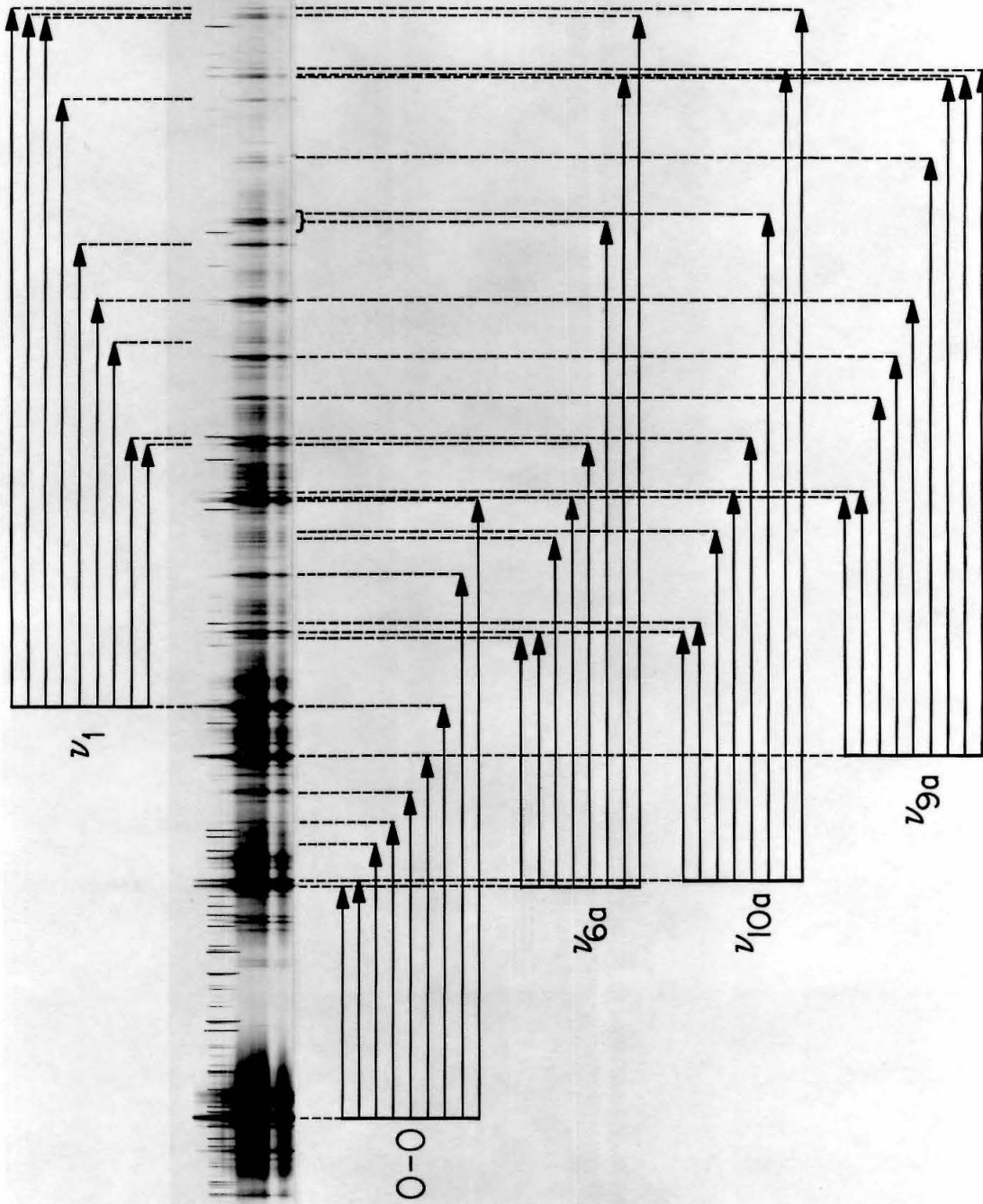


FIG. 3. The phosphorescence spectrum of pyrazine-d₄ in benzene mixed crystal.



PROPOSITION I

It is proposed that the substituent effect on the triplet excited states of aromatics can be studied by electron paramagnetic studies. Simple systems of di-halo naphthalenes in a solid matrix are suggested. By observing the change of the principal magnetic axes and hyperfine interactions, the perturbation caused by substitution on the spin density can be elucidated. Furthermore, these investigations may also shed some light on the nature of the internal heavy atom effect.

Substituent effect on the electronic structures of molecules is normally studied by molecular spectroscopy.¹ These studies are generally difficult to interpret and less informative due to the fact that both the ground and excited states of the parent molecules are subjected to substituent perturbations. On the other hand, the observation of the paramagnetic resonance absorption of molecules in their phosphorescent states by Hutchison and Mangum² provides vital information concerning the excited state wavefunctions of an aromatic and yet has not been applied to the study of substituent effect. Since comparisons can be made between the excited states of the substituted and parent molecules, interpretations of the e. p. r. results are straightforward.

The theoretical treatment of the paramagnetic resonance absorption of photoexcited molecules has been done by Hutchison and Mangum² and also by van der Waals and de Groot.³ They used the Hamiltonian which includes the magnetic interactions of the two

unpaired electrons with each other and with the constant magnetic field \underline{H} ,

$$\mathcal{H} = g\beta_e \underline{H} \cdot \underline{S} + 4\beta_e^2 \left\{ \frac{\underline{S}_1 \cdot \underline{S}_2}{r^3} - \frac{3(\underline{r} \cdot \underline{S}_1)(\underline{r} \cdot \underline{S}_2)}{r^5} \right\} \quad (1)$$

where \underline{r} is the interelectronic distance and β_e is the electronic magneton. Using the zero order spin functions suggested by Hamerka and Oosterhoff⁴

$$\begin{aligned} T_x(1, 2) &= \frac{1}{\sqrt{2}} (\beta_1\beta_2 - \alpha_1\alpha_2) \\ T_y(1, 2) &= \frac{1}{\sqrt{2}} i(\beta_1\beta_2 + \alpha_1\alpha_2) \\ T_z(1, 2) &= \frac{1}{\sqrt{2}} (\alpha_1\beta_2 + \beta_1\alpha_2) \end{aligned} \quad (2)$$

van der Waals and de Groot obtained the Hamiltonian matrix as,

$$\begin{pmatrix} 2\beta_e^2 \langle X^2 \rangle & -ig\beta_e H_z & ig\beta_e H_y \\ ig\beta_e H_z & 2\beta_e^2 \langle Y^2 \rangle & -ig\beta_e H_x \\ -ig\beta_e H_y & ig\beta_e H_x & 2\beta_e^2 \langle Z^2 \rangle \end{pmatrix} \quad (3)$$

where $\langle X^2 \rangle = \langle \Psi(1, 2) | \frac{3x^2}{r^5} - \frac{1}{r^3} | \Psi(1, 2) \rangle$ and $\langle Y^2 \rangle$, $\langle Z^2 \rangle$ are similar quantities.

It must be pointed out that, in using Eq. (3), the quantities $\langle X^2 \rangle$, $\langle Y^2 \rangle$ and $\langle Z^2 \rangle$ which measure the relative separations of the two electrons must be referred to the principal magnetic axes (vide infra). A more elaborate derivation is given as follows:

Consider a 4-dimensional vector space spanned by $\alpha_1\alpha_2$, $\alpha_1\beta_2$, $\beta_1\alpha_2$ and $\beta_1\beta_2$. In this vector space, four orthonormal vectors T_x , T_y , T_z and T_0 can be written as:

$$T_x = \frac{1}{\sqrt{2}} \begin{pmatrix} -1 \\ 0 \\ 0 \\ 1 \end{pmatrix} \quad T_y = \frac{1}{\sqrt{2}} \begin{pmatrix} i \\ 0 \\ 0 \\ i \end{pmatrix} \quad T_z = \frac{1}{\sqrt{2}} \begin{pmatrix} 0 \\ 1 \\ 1 \\ 0 \end{pmatrix} \quad T_0 = \frac{1}{\sqrt{2}} \begin{pmatrix} 0 \\ 1 \\ -1 \\ 0 \end{pmatrix}$$

where T_x , T_y and T_z are just the spin functions of Eq. (2) and T_0 is clearly a singlet.

The representation of the Hamiltonian in this space can be constructed by the method of product representation⁵ from the representations of the Hamiltonian in the α_1 , β_1 space and the α_2 , β_2 space. The representation of the Hamiltonian in the T_x , T_y , T_z and T_0 space can, then, be obtained by a unitary transformation.

The spin-spin interaction is calculated to be

$$2\beta_e^2 \begin{pmatrix} \langle X^2 \rangle & \langle XY \rangle & \langle XZ \rangle & 0 \\ \langle XY \rangle & \langle Y^2 \rangle & \langle YZ \rangle & 0 \\ \langle XZ \rangle & \langle YZ \rangle & \langle Z^2 \rangle & 0 \\ 0 & 0 & 0 & 0 \end{pmatrix} \quad (4)$$

where $\langle XY \rangle = \langle \Psi(1, 2) | \frac{3XY}{r^5} | \Psi(1, 2) \rangle$, etc. and the Zeeman term is

$$ig\beta_e \begin{pmatrix} 0 & -H_z & H_y & 0 \\ H_z & 0 & -H_x & 0 \\ -H_y & H_x & 0 & 0 \\ 0 & 0 & 0 & 0 \end{pmatrix} \quad (5)$$

It can be seen that for singlet, there is no interactions between the spins themselves and no interaction with the magnetic field.

The principal magnetic axes can thus be defined as the axes with respect to which the spin-spin interaction in Eq. (4) has a diagonal representation. That is

$$\langle XY \rangle = \langle YZ \rangle = \langle XZ \rangle = 0 \quad .$$

If all the quantities in the spin-spin interaction are referred to these principal axes, Eq. (4) plus Eq. (5) is reduced to Eq. (3).

Alternatively, the Hamiltonian can be written in a form suggested by Hutchison and Mangum,²

$$\begin{aligned} \mathcal{H} &= g\beta_e \vec{H} \cdot \vec{S} + DS_x^2 + E(S_y^2 - S_z^2) \\ D &= \frac{1}{2}[\langle Y^2 \rangle + \langle Z^2 \rangle] - \langle X^2 \rangle \\ E &= \frac{1}{2}[\langle Z^2 \rangle - \langle Y^2 \rangle] \end{aligned} \quad (6)$$

where S_x , S_y and S_z are, of course, referred to the principal magnetic axes.

For molecules having more than two reflection planes (such as those belonging to the D_{2h} or C_{2v} group, almost all the molecules previously studied belong to this category), the location of the principal axes are apparent. For example, for naphthalene molecule, the three axes $\hat{x}\hat{y}\hat{z}$ are: the normal to the molecular plane, the long axis and the short axis, respectively. However, if substituents are introduced at 1, 5 positions or 2, 6 positions, the symmetry becomes C_{2h} . The operator $3yz/r^5$ now belongs to the totally symmetric representation of the group and is clearly nonvanishing. The magnitude of its matrix element reflects the strength of the substituent perturbation. The new axes are obtained by rotating the old axes on the y, z plane through an angle θ given by

$$\theta = \frac{1}{2} \tan^{-1} \left[\frac{2\langle YZ \rangle}{\langle Y^2 \rangle - \langle Z^2 \rangle} \right] = \frac{1}{2} \tan^{-1} \left[\frac{-\langle YZ \rangle}{E} \right]$$

E is very small for naphthalene triplet. This is because the electron density is more concentrated on the α -position and the \hat{y} and \hat{z} axes are almost physically indistinguishable. A small perturbation would result in a large change of principal axes.

For mixed crystals with known guest orientation, it is experimentally feasible to observe such perturbation. Theoretically, it is interesting to see to what extent the π -system is distorted from D_{2h} to C_{2h} by substitution.

Detailed information of the spin density distribution can also be determined if hyperfine interactions with either proton or

substituents are observed. McConnell⁶ has shown that the hyperfine interaction can be expressed as

$$A_n = \delta_n K ,$$

where δ_n is the spin density on the adjacent carbon atom normalized to 1 for the entire molecule, $K = \{A^2\alpha^2 + B^2\beta^2 + C^2\gamma^2\}^{\frac{1}{2}}$ α , β , γ are the direction cosines of \underline{H} with respect to (i) the C-H bond direction (A-axis), (ii) the normal to the molecular plane (B-axis), and (iii) a third axis (C-axis) normal to both A and B. For naphthalene, Hutchison and Mangum² have shown that $|A| \sim 30$ Mc, $|B| \sim 76$ Mc and $|C| \sim 115$ Mc. These values can be used to evaluate the spin density distribution in our substituted naphthalenes.

In naphthalene-durene system, the α positions are less crowded, it is possible to introduce halogens which have small radii into the α positions and still obtain a good mixed crystal. Di-halo substitution is preferred in view of the fact that the site symmetry is C_i .⁷ Mono-substituted naphthalene would probably not go into the substitutional sites.

For β substituted naphthalene, it is proposed to use normal naphthalene as host. Mixed crystal of β -substituted naphthalene in naphthalene is possible;⁸ the triplet energy of the guest is lower than the host;⁹ and the intersystem crossing rate is faster than normal naphthalene.¹⁰

Finally, an important aspect of the halo-substituent effect is

the intensity enhancement of T - S absorption. This effect, known as internal heavy atom effect, has been discussed by Robinson¹¹ within the framework of perturbation theory. In Robinson's terminology, this intensity enhancement is due to the second order multiplicity covariant interaction. This interaction results in a migration of triplet spin from the π -system to the halogen atoms. Therefore, paramagnetic resonance study of halo-substituted naphthalenes can verify this mechanism. A large hyperfine interaction with halo-substituent would probably indicate some delocalization of triplet excitation to the halogen atom.

REFERENCES

1. See, for example, Chapters 9 and 10 in The Theory of the Electronic Spectra of Organic Molecules by J. N. Murrell (John Wiley & Sons, Inc., New York, 1963).
2. C. A. Hutchison and B. W. Mangum, *J. Chem. Phys.* 29, 952 (1958); *ibid.* 32, 1261 (1958); *ibid.* 34, 908 (1961).
3. M. S. de Groot and J. H. van der Waals, *Mol. Phys.* 6, 545 (1963).
4. H. F. Hamerka and L. J. Oosterhoff, *Mol. Phys.* 1, 358 (1958).
5. M. Hamermesh, Group Theory (Addison Wesley Pub. Co., Reading, Mass, 1962).
6. H. M. McConnell, *J. Chem. Phys.* 24, 764 (1956).
7. J. M. Robertson, *Proc. Roy. Soc. (London)* A141, 594 (1933); *ibid.* A142, 659 (1933).
8. A. I. Kitaigoroskii, Organic Chemical Crystallography, Consultants Bureau, New York (1961), p. 163.
9. D. S. McClure, *J. Chem. Phys.* 17, 905 (1949).
10. D. S. McClure, *ibid.* 22, 255 (1954).
11. G. W. Robinson, *J. Chem. Phys.* 46, 572 (1967).

PROPOSITION II

It is proposed that the exciton dispersion relation can be obtained by studying the "isolated" cluster states such as dimers and trimers with various energy gaps. Exact formula for these states are given and an iteration method is suggested. Such study not only yields information concerning the most fundamental parameters of Frenkel excitons but also serves to check the validity of the approximation of nearest neighbor interactions.

The energy states of molecular crystals such as crystalline benzene and naphthalene are frequently described within the framework of neutral Frenkel exciton theory.¹ Investigations done in this group² have shown that the neutral exciton description is indeed a very high approximation. Efforts have been made to describe the level splittings, the band structures, the impurity states, the excitation migrations, etc. in terms of more fundamental parameters, namely, the pairwise intermolecular interactions. These interactions also determine the exciton dispersion relations which can be written as,³

$$E^\alpha(\underline{K}) = \epsilon + D + \sum_{\underline{l} \neq \underline{p}} M_{lp}^{eq} e^{i\underline{K} \cdot (\underline{l} - \underline{p})} + \sum_{\underline{m}} A_m^\alpha(\underline{K}) M_{mp}^{ineq} e^{i\underline{K} \cdot (\underline{m} - \underline{p})} \quad (1)$$

where ϵ is the gas phase transition energy and D accounts for the difference in van der Waals' interactions in the ground and excited states

(also known as the site shift⁴). $M_{\ell p}^{\text{eq}}$ and $M_{\underline{m} \underline{p}}^{\text{ineq}}$ are pairwise interactions between translationally equivalent sites $\underline{\ell}$ and \underline{p} and translationally inequivalent sites \underline{m} and \underline{p} , respectively. $A_m^\alpha(\underline{K})$ is a coefficient derived from the diagonalization of the submatrix characterized by wavevector \underline{K} .

For the ${}^1B_{2u}$ states of benzene and naphthalene, the interactions are short range⁵ and the lattice sums converge rapidly. The nearest neighbor approximation seems appropriate. In this "restricted" Frenkel limit the dispersion relation has an especially simple form. It can be shown that for benzene,⁶

$$\begin{aligned}
 E^\alpha(\underline{K}) = & \epsilon + D + 2M_a \cos(k_a \cdot a) + 2M_b \cos(k_b \cdot b) + 2M_c \cos(k_c \cdot c) \\
 & + 4 A_{\text{II}}^\alpha M_{12} \cos(k_a \cdot \frac{1}{2} a) \cos(k_b \cdot \frac{1}{2} b) \\
 & + 4 A_{\text{III}}^\alpha M_{13} \cos(k_b \cdot \frac{1}{2} b) \cos(k_c \cdot \frac{1}{2} c) \\
 & + 4 A_{\text{IV}}^\alpha M_{14} \cos(k_c \cdot \frac{1}{2} c) \cos(k_a \cdot \frac{1}{2} a) , \quad (2)
 \end{aligned}$$

where A_{II}^α , A_{III}^α , A_{IV}^α are, respectively, +1, +1, +1, for $\alpha = A$; +1, -1, -1, for $\alpha = B_1$; -1, +1, -1, for $\alpha = B_2$; -1, -1, =1, for $\alpha = B_3$ (A_{I}^α always equals to +1, since molecule I is the reference. The rest of the interchange equivalent molecules in the unit cell have different phase factors according to interchange representations). Similarly for naphthalene,

$$\begin{aligned}
 E^\alpha(\underline{K}) = & \epsilon + D + 2M_a \cos(k_a \cdot a) + 2M_b \cos(k_b \cdot b) \\
 & + 2M_c \cos(k_c \cdot c) + 4A_{\text{II}}^\alpha M_{12} \cos(k_a \cdot \frac{1}{2} a) \cos(k_b \cdot \frac{1}{2} b) , \quad (3)
 \end{aligned}$$

where A_{II}^{α} equals to +1 for $\alpha = Au$ and -1 for $\alpha = Bu$.

On the other hand, formula for "isolated" dimer states have been derived by Craig and Philpott⁷ and also by Hong and Robinson.⁸ These authors stressed the difference between the secular equations for translationally equivalent and inequivalent dimers. In general, an energy matrix of the following form can be written,

$$\begin{vmatrix} 1 - \left(\frac{\Delta}{N}\right) \sum_{\alpha} \sum_{\underline{K}} \frac{1}{E - E^{\alpha}(\underline{K})} & - \left(\frac{\Delta}{N}\right) \sum_{\alpha} \sum_{\underline{K}} \frac{A_{nm}^{\alpha} e^{i\underline{K} \cdot \underline{R}_{nm}}}{E - E^{\alpha}(\underline{K})} \\ - \left(\frac{\Delta}{N}\right) \sum_{\alpha} \sum_{\underline{K}} \frac{A_{nm}^{\alpha} e^{-i\underline{K} \cdot \underline{R}_{nm}}}{E - E^{\alpha}(\underline{K})} & 1 - \left(\frac{\Delta}{N}\right) \sum_{\alpha} \sum_{\underline{K}} \frac{1}{E - E^{\alpha}(\underline{K})} \end{vmatrix} = 0, \quad (4)$$

where $A_{nm}^{\alpha} = A_n^{\alpha} \cdot A_m^{\alpha}$, thus for translationally equivalent dimers $A_{nm}^{\alpha} = 1$, for all α whereas for translationally inequivalent dimers A_{nm}^{α} equals to +1 or -1 depending on representations. \underline{R}_{nm} is the separation between the sites. Δ is the energy gap and E is the dimer energy. Trimers are given by similar equations except that the dimension of the energy matrix becomes three and three roots can be found.

It is easily shown that when $\Delta \gg T$ (band width), Eq. (4) is reduced to,

$$\begin{vmatrix} \frac{1}{\Delta} (E_{nm} - E_1) & - \frac{M_{nm}}{\Delta} \\ - \frac{M_{nm}}{\Delta} & \frac{1}{\Delta} (E_{nm} - E_1) \end{vmatrix} = 0 \quad (5)$$

where E_1 is the "isolated" monomer state, so

$$E_{nm} = E_1 \pm M_{nm} \quad .$$

By observing the dimer states in this limit we have a direct means of evaluating the pairwise interactions and hence the dispersion relation. This is the technique Hanson⁹ used, however, a more elaborate method of approach would be to study the dimer state as a function of trap depth and extrapolate to infinite energy gap.

Notice that crystalline naphthalene is probably one of the molecule crystals whose dimer state cannot be treated by using Eq. (5). The band width is 160 cm^{-1} and the largest energy gap that can be attained by deuterium substitution is only 115 cm^{-1} (\underline{h}_8 in \underline{d}_8). The quasiresonance interactions with the host is appreciable even at this trap depth. For monomer state, this shift amounts of 13.0 cm^{-1} .¹⁰ At an energy $\sim 15 \text{ cm}^{-1}$ below the monomer state lies the dimer state. A rough estimate shows that the dimer state is subjected to a quasi-resonance shift of about 10 cm^{-1} . Thus the separation between the monomer state and the dimer state cannot be safely taken as M_{12} . The method suggested above will have to be used. The situations are better for benzene because the limit $\Delta \gg T$ can be easily reached by deuteration.

An alternative approach which involves successive iterations is also proposed. For simplicity, only naphthalene dimers are considered. It can be seen that four parameters are contained in Eq. (3), namely, M_a , M_b , M_c and M_{12} . Four different dimers are expected.

The energy states of each dimer are given by the corresponding matrix of the form of Eq. (4). For translationally equivalent dimers only one state is allowed; for translationally inequivalent dimers, two states can be observed.⁹ Crystalline naphthalene is centrosymmetric and the off-diagonal elements in Eq. (4) are real. Equation (4) can be further simplified and the energy of the plus state which is always allowed is simply given by

$$F(E, M_a, M_b, M_c, M_{12}) + G(E, M_a, M_b, M_c, M_{12}) = 0$$

where F and G are diagonal and off-diagonal matrix elements, respectively. If the dimer states are located at E_a , E_b , E_c and E_{12} , respectively, four equations of the following form can be obtained.

$$\begin{aligned} F(E_a, M_a, M_b, M_c, M_{12}) + G_a(E_a, M_a, M_b, M_c, M_{12}) &= 0 \\ F(E_b, M_a, M_b, M_c, M_{12}) + G_b(E_b, M_a, M_b, M_c, M_{12}) &= 0 \\ F(E_c, M_a, M_b, M_c, M_{12}) + G_c(E_c, M_a, M_b, M_c, M_{12}) &= 0 \\ F(E_{12}, M_a, M_b, M_c, M_{12}) + G_{12}(E_{12}, M_a, M_b, M_c, M_{12}) &= 0 \end{aligned} \tag{6}$$

Here we have four equations from which the four parameters M_a , M_b , M_c and M_{12} can be calculated by using Newton's iteration method. Furthermore, by varying the energy gap, we can check whether the same set of values also yields the dimer energy in agreement with experiments. This last step can be used to determine whether the nearest neighbor interaction approximation is indeed adequate.

From a purely physical point of view, we can argue that E_{nm}

depends primarily on M_{nm} . In this case, the iteration is simplified. To begin with, we solve the following equations,

$$\begin{aligned}
 F(E_a, M_a) + G_a(E_a, M_a) &= 0 \\
 F(E_b, M_b) + G_b(E_b, M_b) &= 0 \\
 F(E_c, M_c) + G_c(E_c, M_c) &= 0 \\
 F(E_{12}, M_{12}) + G_{12}(E_{12}, M_{12}) &= 0
 \end{aligned}
 \tag{7}$$

In each case, only one parameter is varied to obtain best fit with experiments while others are fixed at some arbitrary values. The resulting values can then be put together as a zero order approximation to be used in Eq. (6).

In the experimental aspect, a study similar to that of Hanson⁹ can be carried out. Dimer states of naphthalene βd_1 and αd_1 in d_8 are easy to observe. Other combinations of various deuterated naphthalenes and benzenes can also be included to cover a wide range of energy gaps. Before other techniques such as electron impact spectroscopy are fully developed to compete with optical measurements, such studies are, by far, the most direct way of studying the exciton dispersion relation.

REFERENCES

1. (a) A. S. Davydov, Theory of Molecular Excitons (McGraw Hill Book Co., New York, 1962); (b) D. P. Craig and S. H. Walmsley, in Physics and Chemistry of Organic Solid State, D. Fox. M. M. Labes and A. Weissberger, Eds. (Interscience Publishers Inc., New York, 1963), Vol. 1, Chap. 10.
2. See, for example, (a) D. M. Hanson, R. Kopelman and G. W. Robinson, J. Chem. Phys. 51, 212 (1969); (b) S. D. Colson, D. M. Hanson, R. Kopelman and G. W. Robinson, J. Chem. Phys. 48, 2215 (1968), etc.
3. See Ref. 1(b), p. 586 and references therein.
4. E. R. Bernstein, S. D. Colson, D. S. Tinti and G. W. Robinson, J. Chem. Phys. 48, 4632 (1968).
5. S. D. Colson, R. Kopelman and G. W. Robinson, J. Chem. Phys. 47, 27 (1967).
6. Taken from Ref. 2(b).
7. D. P. Craig and M. R. Philpott, Proc. Roy. Soc. (London) 290A, 583 (1966).
8. H. K. Hong and G. W. Robinson, J. Chem. Phys. 51, 0000 (1969). "The Electronic States of Heavily-Doped Molecular Crystals-- Naphthalene. I. Theoretical."
9. D. M. Hanson, Ph. D. Thesis, California Institute of Technology (1969). Hanson did not elaborate on whether the naphthalene $-h_s$ in d_s system actually corresponds to the $\Delta \gg T$ limit.
10. B. S. Sommer and J. Jortner, J. Chem. Phys. 50, 822 (1969).

PROPOSITION III

It has been suggested that $^1B_{2u}$ excitons are formed by β - or γ -ray radiolysis of crystalline benzene. However, evidence in support of this proposition is mainly of a chemical nature. It is thus proposed that low temperature radiolysis of benzene be carried out and fluorescence and phosphorescence from neat crystals and mixed crystals be monitored. Such study will aid our understanding of dynamic processes in organic solids.

Radiolysis of organic materials normally leads to the production of ions, radicals and molecular fragments¹ as the primary products. In the early 1950's, only reactions that involved ions and radicals were believed to be important in the radiolysis processes. Later investigations gradually unveiled the role of neutral molecular excited states, both singlet and triplet, in the secondary reactions. In the gas phase, these neutral excited states are usually formed as a result of a collision with a high energy particle, while in condensed systems, they are usually formed by charge neutralization. The involvement of excited molecules in the radiolysis process closed the gap between radiation chemistry and photochemistry. Radiation and photochemists soon adapted the same terminology. Terms such as "energy transfer," "sensitizer," "quantum yield," "quenching process," etc appear in both literatures.

The radiolysis of air-free liquid benzene has been investigated by several workers.²⁻⁴ Recently Cooper and Thomas⁵ investigated pulse radiolysis of liquid benzene in the nano second region. The benzene excited state is believed to be involved as shown by the appearance of fluorescence emission of suitable quenchers such as naphthalene and anthracene and also by absorption at 515 m μ tentatively assigned to the transition ${}^1E_{1u} - {}^1B_{2u}$ of benzene. However, the last interpretation is rather doubtful for the following reasons:

- (1) A u-u transition is forbidden by symmetry, whereas experimentally Cooper and Thomas found a moderate extinction coefficient of about 4300.
- (2) There is a 4000 cm⁻¹ difference between the observed maximum and other spectroscopic data. This difference appears to be too large to be attributed to a transition to higher vibronic levels of the ${}^1E_{1u}$ state.

Despite these discrepancies, I believe that benzene molecules in the ${}^1B_{2u}$ state are formed in the radiolysis.⁶ However, the kinetic information Cooper and Thomas obtained is probably not without uncertainties. On the other hand, it is also possible that triplet benzene is also formed in an appreciable amount since charge recombination in a homogeneous medium favors the formation of triplet excited states (3:1).⁷

Radiolysis data for solid organic materials are relatively rare. One reason is the inability of many organic crystals to act as satisfactory hosts for "radical scavengers." In the few cases where

observations have been made on dilute organic solutions^{8,9} at nitrogen temperature the neutral excited molecules are formed only by stimulation because of the immobility of the majority of primary species.

The stimulation normally takes the following forms:

- (i) The trapped electrons can be released by thermal means and become temporarily free to wander (thermostimulation).
- (ii) The trapped electrons can also be released by absorbing infrared radiation (photostimulation).

McCain and Albrecht,⁹ in particular, showed that in TMPD (N, N, N¹, N¹-tetramethyl paraphenylene diamine) the triplet and singlet states of TMPD have the same precursor, namely, the ion pair prior to recombination.

One interesting phenomenon was discovered by Collinson et al.¹⁰ in their study of β - and γ -ray radiolysis of liquid and crystalline benzene containing FeCl₃ as a radical scavenger. Collinson et al. found that the behavior of G(-FeCl₃) in benzene (which they classified as crystal type B; also included in this crystal type are phenetole, diphenyl ether, dimethyl aniline and diphenyl methane) is very different from that in diethyl ether or 1,4 dioxan (crystal type A).

Although the value of G(-FeCl₃) drops sharply on freezing diethyl ether to 77° K, it actually increases in type B crystals as temperature is lowered. Phase transition caused an abrupt decrease of G(-FeCl₃) in type A crystals but an abrupt increase of G(-FeCl₃) in type B crystals. The distinction was so striking that Collinson et al. proposed that an exciton must have been formed in type B crystals by

irradiation. The possibility of mobil electrons was ruled out because the value of $G(-\text{FeCl}_3)$ is too large compared with Ge^- and also because no color centers were observed. Further support of this mechanism comes from the observation that FeCl_3 can be reduced by light absorption and also that benzene excited states seem to be formed in the liquid state.

The evidence that Collinson et al. presented is basically chemical in nature. It would be of interest to seek some physical evidences. Several questions can also be raised: How is the exciton formed? Is it formed via charge neutralization or by some other process? Is the mobil entity a $^1\text{B}_{2\text{u}}$ exciton or a $^3\text{B}_{1\text{u}}$ exciton? Does the quality of the crystal (known to effect exciton states) also effect the reduction of FeCl_3 ? What is the effect of irradiation on the lattice? Is the effect large enough to alter the exciton energy or migration?¹¹ Are trapped electrons present? Can they be released by photo or thermo-stimulation? All these questions are important for an understanding of dynamic processes in organic solids.

My proposition is to study the same process at 4°K , with and without FeCl_3 . It is relatively easy to observe the fluorescence of $^1\text{B}_{2\text{u}}$ excitons. The introduction of isotopic impurities can also be employed to trap the $^3\text{B}_{1\text{u}}$ excitons. If the exciton is the mobil entity, trapping of excitation will decrease the value of $G(-\text{FeCl}_3)$. By examining the fluorescence spectra, we will also be able to see the difference between the exciton produced by radiolysis and that by photo

excitation. This knowledge will be helpful in understanding radiation damage in lattices. By comparing the intensities of fluorescence and phosphorescence emission from the trap, we can also obtain quantitative information about the relative populations of $^1B_{2u}$ and $^3B_{1u}$ excitons. Constant irradiation can be used as a first attempt. These investigations can further be augmented by pulse studies. E. P. R. studies will also be needed to identify the trapped electrons and their environments.

REFERENCES

1. See, for example, Annual Review of Physical Chemistry, H. Eyring, C. J. Christensen and H. S. Johnson, Eds. (Annual Review, Inc., Palo Alto, 1965, 1966) Vol. 16, p. 347; Vol. 17, p. 205.
2. J. P. Keene, T. J. Kemp and G. A. Salmon, Proc. Roy. Soc. 287A, 494 (1965).
3. W. N. Patrick and M. Burton, J. Amer. Chem. Soc. 76, 2626 (1954).
4. E. A. Cherniak, E. Collison and F. S. Dainton, Trans. Faraday Soc. 60, 1408 (1964).
5. R. Cooper and J. K. Thomas, J. Chem. Phys. 48, 5097 (1968).
6. P. Skarstad, R. Ma and S. Lipsky, Mol. Cryst. 4, 3 (1968).
7. B. Brocklehurst, G. Porter and J. M. Yates, J. Phys. Chem. 68, 203 (1964).
8. D. S. Skelly, W. H. Hamill, J. Chem. Phys. 43, 3497 (1965).
9. W. M. McCain, A. C. Albrecht, J. Chem. Phys. 43, 465 (1965).
10. E. Collinson, J. J. Conlay and F. S. Dainton, Disc. Faraday Soc. 36, 153 (1964).
11. S. D. Colson observed a change in exciton absorption spectrum due to strain. See J. Chem. Phys. 45, 4746 (1966).

PROPOSITION IV

It is proposed to study the Mössbauer effect in molecular crystals, specifically, molecular crystal of diiodobenzene. The feasibility of such a study is discussed and the information that can be obtained is also outlined.

Mössbauer spectroscopy is a useful tool for chemists. Although it was originally discovered by a physicist,¹ applications in solid state physics and chemistry soon dominated the field. The reason is clearly expressed in a statement by Frauenfelder:² The number of nuclear properties that can be investigated is limited, but the number of solid state parameters that can be varied and studied is very large. Here we will discuss the possibility of using this tool to study chemical bonding, the field gradient and the lattice dynamics of a molecular crystal. More specifically, we will discuss the Mössbauer effect in diiodobenzene with radioactive iodine.

The Mössbauer effect is essentially a recoilless nuclear resonance absorption of gamma radiation. The recoilless fraction is usually given by:³

$$f = \exp \left[- \frac{4\pi^2 \langle x^2 \rangle}{\lambda^2} \right]$$

where $\langle x^2 \rangle$ is the mean square amplitude of the vibration in the direction of emission of the gamma ray over an interval equal to the lifetime of the nuclear level involved in the gamma ray emission process.

It is often desirable to use the Debye approximation to express

the recoilless fraction in terms of more familiar quantities. If the crystal is represented by $3N$ oscillators of frequency w_j , the average energy associated with each oscillator is

$$(\bar{n}_j + \frac{1}{2}) \hbar w_j$$

where \bar{n}_j is given by the Planck distribution function

$$\bar{n}_j = \frac{1}{\exp(\hbar w_j / kT) - 1}$$

The energy of the crystal due to the j^{th} oscillator is

$$MNw_j^2 \langle r_j^2 \rangle = (\bar{n}_j + \frac{1}{2}) \hbar w_j$$

where r_j is the contribution to the displacement of the atoms due to the j^{th} oscillator. Summation over j yields:

$$\langle r^2 \rangle = \frac{\hbar}{MN} \sum \frac{(\bar{n}_j + \frac{1}{2})}{w_j}$$

Replace the summation with an integral and introducing the density of vibrational states $\rho(w)$, we obtain,

$$\langle r^2 \rangle = \frac{\hbar}{NM} \int_0^{w_{\max}} \left(\frac{1}{2} + \frac{1}{(e^{\hbar w / kT} - 1)} \right) \frac{\rho(w)}{w} dw \quad (1)$$

For a Debye solid, $\rho(w) = 9Nw^2/w_{\max}$ which is normalized so that

$$\int \rho(w) dw = 3N$$

Introducing this into (1) and defining the Debye temperature θ_D by $\hbar\omega_{\max} = k\theta_D$, we get,

$$\langle r^2 \rangle = \frac{9\hbar^2}{4Mk\theta_D} \left[1 + 4 \frac{T^2}{\theta_D^2} \int_0^{\theta_D/T} \frac{udu}{e^u - 1} \right].$$

For $T \ll \theta_D$, we take the upper limit as infinity and carry out the integration,

$$\langle r^2 \rangle_{T \ll \theta_D} = \frac{9\hbar^2}{4Mk\theta_D} \left[1 + \frac{2\pi^2 T^2}{3\theta_D^2} \right].$$

Therefore,

$$f = \exp \left\{ -\frac{4\pi^2 \langle x^2 \rangle}{\lambda^2} \right\} = \exp - \left\{ \frac{3}{2} \frac{E_R}{k\theta_D} \left[1 + \frac{2\pi^2}{3} \frac{T^2}{\theta_D^2} \right] \right\}, \quad (2)$$

where $E_R = E^2/2Mc^2$ is the recoil energy, and $\lambda = hc/E$. The final result is

$$f = \exp \left[-\frac{E_R}{k\theta_D} \left\{ \frac{3}{2} + \frac{\pi^2 T^2}{\theta_D^2} \right\} \right], \quad T \ll \theta_D,$$

which is the familiar form for the Debye-Waller factor.⁴

For molecular crystal, there are two types of phonons: acoustical phonons and optical phonons. The effect on the recoilless fraction provided by an optical phonon is readily evaluated by introducing the proper vibrational spectrum into Eq. (1). Consider an optical mode as having a single frequency, the spectrum can be

represented by a delta function,

$$\rho(w) = 3N \delta(w - w_0) \quad .$$

The required integral is now trivial and yields,

$$f = \exp \left[-\frac{E^2}{2Mc^2} \frac{\coth(\hbar w_0/2kT)}{\hbar w_0} \right] = \exp \left[-\frac{E_R}{\hbar w_0} \coth\left(\frac{\hbar w_0}{2kT}\right) \right]$$

If this expression is evaluated for a characteristic frequency and compared with that obtained from the Debye-Waller equation for $\theta_D = \hbar w_0/k$, it is found that the optical mode results in a much larger recoilless fraction. In general, the optical mode of high energy will result in little attenuation of the recoilless fraction.⁵ It is feasible to observe the Mössbauer spectrum in a molecular crystal.

As far as chemistry is concerned, Mössbauer spectroscopy measures 3 parameters: the isomer shift, the electric quadrupole coupling constant and the Debye-Waller factor.

The isomer shift δ is related to the s-electron density by the following expression²

$$\delta = \frac{2}{3} \pi Z e^2 \left[\langle r_B^2 \rangle - \langle r_A^2 \rangle \right] \left\{ |\psi_a(0)|^2 - |\psi_e(0)|^2 \right\}$$

where r_B , r_A are nuclear radii at excited state and ground state, respectively and $|\psi_a(0)|^2$, $|\psi_e(0)|^2$ are the s-electron densities at the nuclei for absorber and emitter. More accurate formulae, including those taking into account the relativistic effect⁶ are available. In any case, the isomer shift can be expressed as,⁷

$$\delta = F(Z) \left[\langle r_B^2 \rangle - \langle r_A^2 \rangle \right] \left\{ |\psi_a(0)|^2 - |\psi_e(0)|^2 \right\}$$

where $F(Z)$ is a complicated proportionality constant depending on Z , the nuclear charge.

The quadrupole coupling is given as:⁸

$$E(m_I) = e^2qQ \left[\frac{3m_I^2 - I(I+1)}{4I(2I-1)} \right]$$

where $m_I = I, I-1, \dots, -I$. Although the quantity e^2qQ can also be determined from N. Q. R (nuclear quadrupole resonance), the Mössbauer effect provides supplementary information.

Lattice dynamics can also be studied through the measurement of the temperature dependence of the recoilless fraction. If the phonon spectrum is not available, the Debye approximation can be used for theoretical calculations. If the phonon spectrum is available, the recoilless fraction can be obtained by integrating over the phonon spectrum and checking it with experiment.

Two known isotopes of iodine have been studied, I-127⁹ and I-129.¹⁰ The nuclear data are given in Table I. The chemical compounds investigated included: Alkali iodide, KIO_3 , NH_4IO_3 , KIO_4 , $Na_3H_2IO_6$, $KICl_4 \cdot H_2O$ and $KICl_2 \cdot H_2O$, etc. Much information was obtained by such study concerning chemical bonding. For example, KI was found to be predominantly ionic; in IO_4 , strong sp^3 hybridization was involved; and finally in IO_3 , covalency predominates.

N. Q. R. for diiodobenzene has been measured by Schawlow.¹¹ Using Townes and Dailey's theory,¹² he calculated the percentage of

covalency to be 82%, corresponding to a nuclear quadrupole resonance frequency of 280.243 Mc/sec.

The relationship between N. Q. R. and the Mössbauer effect is somewhat similar to the relationship between the vibrational spectrum and the vibronic spectrum. It is certainly true that more information can be obtained by doing Mössbauer spectroscopy.

Hafemeister¹⁰ has calculated all the nuclear parameters for I-129, for example, $\frac{\Delta R}{R} = 3 \times 10^{-5}$, $\delta = 6.69 \times 10^{-28}$ ($|\psi_a(0)|^2 - |\psi_e(0)|^2$), $Q_{\text{gnd}} = -0.55b$ and $Q_{26.8} = -0.68b$. These parameters would facilitate the evaluation of chemical parameter in diiodobenzene which we are interested in.

The phonon spectrum for molecular crystals is seldom available. A powerful technique is neutron inelastic scattering.¹³ It can be seen that the Debye-Waller factor can be calculated from the frequency spectrum of phonons. If the dispersion relation can be obtained experimentally, it would be possible to calculate the frequency spectrum¹⁴ and hence the Debye-Waller factor. This type of calculation can further be checked with the temperature-dependent behavior of the recoilless fraction. In view of the present lack of understanding about phonons in molecular crystals, experiments of this type seem desirable. The diiodobenzene crystal is of D_{2h}^{15} symmetry, with four molecules per unit cell.¹⁵ It is suitable for Mössbauer study as a prototype of many molecular crystals.

REFERENCES

1. R. L. Mössbauer, Z. Physik 151, 124 (1958).
2. Hans Frauenfelder, The Mössbauer Effect (W. A. Benjamin, Inc., New York, 1963).
3. G. K. Wertheim, Mössbauer Effect (Academic Press, New York, 1964).
4. P. P. Ewald, Handbuch der Physik (Springer, Berlin, 1933).
5. Yu Kagan, Soviet Phys., J. E. T. P., 14, 472 (1962).
6. G. Breit, Rev. Mod. Phys. 30, 507 (1958).
7. J. F. Duncan and R. M. Golding, Quarterly Rev. 19, 36 (1965).
8. G. K. Wertheim, Science 144, 253 (1964).
9. G. J. Perlow and S. L. Ruby, Phys. Letters 13, 198 (1964);
F. De. S. Barros, N. Ivantchev, S. Jha and K. R. Reddy, Phys. Letters 13, 142 (1964).
10. H. de Waard, G. De Pasquali and D. Hafemeister, Phys. Letters 5, 217 (1963); D. Hafemeister, G. De Pasquali and H. de Waard, Phys. Rev. 135, 1089 (1964).
11. A. L. Schawlow, J. Chem. Phys. 22, 1211 (1954).
12. C. H. Townes and B. P. Dailey, J. Chem. Phys. 17, 782 (1949).
13. J. M. Ziman, Electron and Phonon (Oxford Press, London, 1960) p. 38.
14. C. B. Walker, Phys. Rev. 103, 547 (1956).
15. L. Dun-choi and Yu T. Struchkov, Izvest. Akad. Nauk. S. S. S. R. OkhN 12, 2095 (1959).

TABLE I. Nuclear data for I-127 and I-129

	I-127	I-129
Source	ZnTe ^{127m}	ZnTe ^{129m}
Ray energy	57.6 keV	26.8 keV
Lifetime of excited state	1.8 nsec	18.5 nsec
Lifetime of ground state	stable	1.6×10^7 yr
Nuclear quadrupole		
ground state	-0.79 b	-0.55 b
excited state	-0.71 b	-0.68 b
Nuclear spin		
ground state	5/2	7/2
excited state	7/2	5/2

PROPOSITION V

It is proposed that triplet exciton behavior can be investigated by paramagnetic resonance of various isotopic mixed crystals. These investigations will yield information concerning the intermolecular exchange interactions in the excited triplet state of molecular crystals.

There are two groups of investigators working on the problem of organic triplet states: the spectroscopic and the magnetic resonance people. It is probably not an overstatement that the spectroscopists know about the importance of intermolecular interactions and yet frequently they have troubles in applying their techniques to the study of triplet excitons. On the other hand, the resonance people have the tools but often they overlook the importance of intermolecular interactions. For example, the beautiful experiments of Nieman and Robinson¹ were the first endeavor the spectroscopic ever made to study the triplet interactions. Later investigations, however, show that the quasiresonance shifts Nieman and Robinson observed are probably due to site shifts rather than interactions. Sommer and Jortner's² calculations also indicate that the variation of energy denominator method is not very useful in studying triplet interactions because the energy gaps are too big and the band widths are too small.

The band-to-band transition method,³ despite its success in studying singlet density-of-states function, has no place in the study of triplet interactions, again due to the narrow band width and broad

phosphorescence line width. The resonance pair spectrum⁴ is relatively easy to obtain for the singlet but not for the triplet. In the corresponding phosphorescence spectrum, pair states are barely separated from the monomer line and, furthermore, can not be verified by a concentration study.

The magnetic resonance people frequently used isotopic mixed crystals to trap the excitation. However, almost all the experiments are done in the limit of the oriented gas model. The concept of k -mixing and quasisonance shifts seems foreign to this group. Except for the recent experiments done in Wolf's group,⁵ no experiments were designed to illustrate the exciton behavior of the triplet state. Theoretically, the resonance spectrum of triplet exciton has been worked out by Sternlicht and McConnell⁶ but experimental attempts have been, so far, unsuccessful. The theory of e. p. r. spectral changes induced by exciton interactions between the host and the guest has not been worked out. Sommer and Jortner² recently applied Koster and Slater's theory⁷ to the triplet impurity state but no reference was made to its e. p. r. spectrum. From our research on singlet interactions, we can say qualitatively that the excitation is gradually delocalized as the trap depth is reduced and the e. p. r. spectrum will change from that of the isolated molecule to that of the pure crystal.

Sternlicht and McConnell's formulation for triplet excitons seems appropriate for crystals such as naphthalene and benzene. The exciton interactions in these crystals are larger than the spin-spin

interactions and hence the factor group symmetry classification can be made. This is called the strong spin coupling limit by Hochstrasser and Lin.⁸ In this limit, the intermolecular interactions are strong enough to ensure that triplet spins are quantized with respect to crystallographic axes.

The zero order exciton wavefunctions are constructed according to the irreducible representations of the interchange group.⁹ The matrix elements of the spin-spin interaction operator are then evaluated with these basis sets. The resulting matrix that shows no \underline{K} -dependence is found to be,

$$\begin{aligned} & \langle \underline{K}_\ell M | H' | \underline{K}_\ell M' \rangle \\ &= \frac{1}{L} \left(\langle M | [D(S_Z^2 - \frac{1}{3} S^2) + E(S_X^2 - S_Y^2)]_I | M' \rangle \right. \\ & \quad + \langle M | [D(S_Z^2 - \frac{1}{3} S^2) + E(S_X^2 - S_Y^2)]_{II} | M' \rangle \\ & \quad \left. + \dots \right) \end{aligned}$$

where \underline{K} and ℓ denote the translational and interchange symmetries, respectively, and M denotes the spin state. L is the number of molecules per unit cell. The summation is carried over all the interchange equivalent molecules. Using this formula, the spin-spin interactions for benzene and naphthalene are found to be,

$$H' = D[0.168(S_Z^2 - \frac{1}{3} S^2) - 0.228(S_X^2 - S_Y^2)]$$

where $D \approx 0.158 \text{ cm}^{-1}$ ¹⁰

and

$$H' = -0.00588(S_z^2 - \frac{1}{3}S^2) - 0.0345(S_x^2 - S_y^2) \\ + 0.0332(S_x S_y + S_y S_x) .$$

Here the \underline{x} , \underline{y} , \underline{z} axes for benzene coincide with \underline{b} , \underline{a} , \underline{c} , respectively and \underline{x} , \underline{y} , \underline{z} for naphthalene coincides with \underline{c}' , \underline{a} , \underline{b} , respectively. It is apparent that both the resonance absorptions and their angular dependence are quite different from that of isolated molecules.

Specifically, Sternlicht and McConnell calculated the zero field energies to be

for benzene: $E_+ = 0.284D$, $E_- = -0.172D$ and
 $E_0 = -0.112D$, compared with those of "isolated"
 molecule: $E_{+,-}^f = 0.333D$, $E_0^f = -0.667D$;

for naphthalene: $E_+ = 0.0458 \text{ cm}^{-1}$, $E_- = -0.0499 \text{ cm}^{-1}$ and
 $E_0 = 0.0039 \text{ cm}^{-1}$, compared with $E_+^f = 0.0471 \text{ cm}^{-1}$
 $E_-^f = 0.0195 \text{ cm}^{-1}$, and $E_0^f = -0.0671 \text{ cm}^{-1}$.

The e.p.r. spectra of isotopic mixed crystals will resemble that of the isolated molecule in the deep trap limit and that of the pure crystal in the low trap limit. Notice that this type of experiment differs from that of Schworer and Wolf.⁵ There an extra absorption line is observed when dimers are present, whereas a gradual change of the spectral response will be observed in the system proposed here.

It is proposed that, although the guest-host interactions are too small to observe in optical experiments, they should manifest

themselves in the e. p. r. spectrum. By varying the trap depth, this gradual change in the resonance absorptions should be observable. Coupled with a detailed calculation on the impurity spectrum, these experiments may be the only source of information concerning triplet exciton interactions.

REFERENCES

1. G. C. Nieman and G. W. Robinson, J. Chem. Phys. 39, 1298 (1963).
2. B. S. Sommer and J. Jortner, J. Chem. Phys. 50, 839 (1969).
3. S. D. Colson, D. M. Hanson, R. Kopelman and G. W. Robinson, J. Chem. Phys. 48, 2215 (1968).
4. D. M. Hanson, Ph. D. Thesis, California Institute of Technology (1969).
5. M. Schwoerer and H. C. Wolf, Mol. Cryst. 3, 177 (1967).
6. H. Sternlicht and H. M. McConnell, J. Chem. Phys. 35, 1793 (1961).
7. G. F. Koster and J. C. Slater, Phys. Rev. 95, 1167 (1954).
8. R. M. Hochstrasser and T. S. Lin, J. Chem. Phys. 49, 4929 (1968).
9. R. Kopelman, J. Chem. Phys. 47, 2631 (1967).
10. M. S. de Groot, I. A. M. Hesselmann and J. H. van der Waals, Mol. Phys. 13, 583 (1967).